

THE ELECTRICAL AND MAGNETIC PROPERTIES  
OF AMORPHOUS Pd-Cu-P ALLOYS

Thesis by  
Gregory Ligot Tangonan

In Partial Fulfillment of the Requirements  
For the Degree of  
Doctor of Philosophy

California Institute of Technology  
Pasadena, California

1976

(Submitted December 12, 1975)

## ACKNOWLEDGMENTS

The author wishes to express his deepest gratitude to Professor Pol Duwez for his constant advice and encouragement of this work. Professor Duwez's kindness and generosity is a characteristic certainly reflected by his group. The author is thankful for the many close friends he has made as a result of this association. He is especially indebted to S. Kotake for his excellent technical help on the cryomagnetic system. The assistance of J. Wysocki in preparing the alloys and assuring that liquid helium was always available is greatly appreciated. C. Geremia is thanked for his help in making fibers, baskets, etc. and the assistance in the electrical resistivity measurements of P. Lebrun, M. Ma, M. Yung and C. Thompson is gratefully acknowledged. The author is also grateful for the assistance of Mrs. Angela Bressan in typing manuscripts, reports, and the rough draft of this thesis, and to Mrs. Ruth Stratton for typing the final version.

The financial support of the Hughes Aircraft Company by Hughes Research Laboratories received by the author while at Caltech is gratefully acknowledged. As a Howard Hughes Fellow this association with the Hughes Research Laboratories has been extremely beneficial to the author and his family. The financial support of the U. S. Atomic Energy Commission is also recognized.

The encouragement of my wife Diana during these difficult days has been gratefully received.

ABSTRACT

The amorphous phases of the Pd-Cu-P system has been obtained using the technique of rapidly quenching from the liquid state. Broad maxima in the diffraction pattern were obtained in the X-ray diffraction studies which are indicative of a glass-like structure. The composition range over which the amorphous solid phase is retained for the Pd-Cu-P system is  $(\text{Pd}_{100-x}\text{Cu}_x)_{80}\text{P}_{20}$  with  $10 \leq x \leq 50$  and  $(\text{Pd}_{65}\text{Cu}_{35})_{100-y}\text{P}_y$  with  $15 \leq y \leq 24$  and  $(\text{Pd}_{60}\text{Cu}_{40})_{100-y}\text{P}_y$  with  $15 \leq y \leq 24$ .

The electrical resistivity for the Pd-Cu-P alloys decreases with temperature as  $T^2$  at low temperatures and as  $T$  at high temperatures up to the crystallization temperature. The structural scattering model of the resistivity proposed by Sinha and the spin-fluctuation resistivity model proposed by Hasegawa are re-examined in the light of the similarity of this result to the Pt-Ni-P and Pd-Ni-P systems. Objections are raised to these interpretations of the resistivity results and an alternate model is proposed consistent with the new results on Pd-Cu-P and the observation of similar effects in crystalline transition metal alloys. The observed negative temperature coefficients of resistivity in these amorphous alloys are thus interpreted as being due to the modification of the density of states with temperature through the electron-phonon interaction. The weak Pauli paramagnetism of the Pd-Cu-P, Pt-Ni-P and Pd-Ni-P alloys is interpreted as being modifications of the transition d-states as a result of the formation of strong transition metal-metalloid bonds rather than a

large transfer of electrons from the glass former atoms (P in this case) to the d-band of the transition metal in a rigid band picture.

TABLE OF CONTENTS

I	INTRODUCTION	1
II	EXPERIMENTAL PROCEDURES	3
	Alloy Preparation	3
	Quenching Technique	4
	Verification of the Amorphous Phase	4
	Composition Range of $(\text{Pd}_{100-x}\text{Cu}_x)_{100-y}\text{P}_y$ Alloys	5
	Electrical Resistivity Measurements	5
	Magnetic Susceptibility Measurements	6
	Main field and Gradient Field Coils	7
	Variable Temperature Insert	8
	The Microbalance	13
	Calibration	14
III	ELECTRICAL RESISTIVITY RESULTS AND DISCUSSION	15
	Electrical Resistivity Results	15
	$(\text{Ni}_x\text{Pt}_{1-x})_{75}\text{P}_{25}$ Alloys Studied by Sinha	46
	Spin Fluctuation Model for Amorphous Metals	53
	Comparison with Crystalline Transition Metal Alloys	62
	An Alternate Explanation of the Resistivity Behavior	70
	Magnitude of the Observed Resistivities	70
	Concentration Dependence of $\rho$	76
	Temperature Dependence of $\rho$	78
IV	THE MAGNETIC SUSCEPTIBILITY RESULTS AND DISCUSSION	83
V	SUMMARY AND CONCLUSIONS	90
	REFERENCES	91

## I. INTRODUCTION

The increased interest of solid state physicists and engineers in amorphous metals is a relatively recent occurrence. This rise in interest has been caused by the discoveries that bulk amorphous metals can exhibit ferromagnetism,<sup>(1)</sup> superconductivity,<sup>(2)</sup> useful mechanical properties,<sup>(3)</sup> and oftentimes demonstrate "anomalous" resistivity properties (like very low temperature coefficients of resistivity). The possibilities of practical application of these materials as well as the possibilities of testing the basic concepts of solid state physics for over-emphasis on the existence of long range crystalline order account for the recent increase of interest in these amorphous metals.

Direct attempts to obtain amorphous metals by drastic cooling from the liquid state<sup>(4)</sup> have been successful in yielding numerous amorphous systems. Glass forming in these rapidly quenched alloys seems to be closely related to the existence of deep eutectics as well as rather high viscosity in the liquid state. The existence of rather low eutectics in the binary transition metal phosphides (like Fe-P, Ni-P, and Pd-P) at about 20 atomic % is the reason that this particular class of compounds has been investigated in considerable detail. Of particular interest in this study is the formation of amorphous Pd-Cu-P alloys and a study of the effects on the electrical and magnetic properties of substituting for Pd in the metal matrix the noble metal copper.

Amorphous alloys have been obtained for the Pd-Cu-P system within the composition ranges  $(\text{Pd}_{100-x}\text{Cu}_x)_{80}\text{P}_{20}$  where  $10 \leq x \leq 50$  and  $(\text{Pd}_{65}\text{Cu}_{35})_{100-y}\text{P}_y$  and  $(\text{Pd}_{60}\text{Cu}_{40})_{100-y}\text{P}_y$  with  $15 \leq y \leq 24$ . The decrease of the electrical resistivity with temperature and the weak magnetic behavior of these alloys are the subjects of this study. It is shown that the decrease of the resistivity with temperature is similar to the behavior of Pd-Ni-P and Pt-Ni-P alloys and that this similarity of behavior necessitates a re-examination of previously proposed models for the electrical resistivity behavior. An alternate explanation is given for the electrical resistivity behavior as a result of the realization that this property is also common to disordered transition metal alloys in the crystalline state. The phonon modification of the density of states with temperature is suggested to be the cause of the observed negative temperature coefficients of resistivity in the Pd-Cu-P, Pd-Ni-P and Pt-Ni-P systems.

The level of the resistivity as well as the concentration dependence of the resistivity is explained in terms of the Evans, Greenwood and Lloyd formalism<sup>(32)</sup> for liquid transition metal alloys. The low magnetic susceptibilities of these alloys are interpreted as being due to the reduction of the spin-paramagnetism enhancement and orbital paramagnetism as a result of the formation of strong transition metal-metalloid bonds and not due to a large transfer of electrons from the glass-forming metalloid (in this case P) to the transition metal d-band in a rigid band model.

## II. EXPERIMENTAL PROCEDURES

### Alloy Preparation

The materials used in preparing the ternary alloys of Pd-Cu-P were 99.99% palladium powder from Engelhard Industries Inc., 99.9+% copper powder from Alcan Metal Powders, Inc., and red amorphous phosphorus from Allied Chemical Co. The copper powder was hydrogen reduced at 300°C and stored along with red phosphorus in a vacuum dessicator. Samples of 2g total mass were prepared from these powders.

Powder metallurgical methods involving reactive sintering were used for the alloy preparation. It is of critical importance to form stable phosphides and to avoid a large vapor pressure of phosphorus during this process. The powders were thoroughly mixed and then compacted under a pressure of 3.50 Kbar (50,000 psi) into 1/2 cm diameter and approximately 1 cm high briquets. The samples were sealed in pyrex tubes and then slowly heated up to 350°C and kept for two days at this temperature. At this temperature the reaction in the solid state proceeds fairly rapidly and the pure red phosphorus vapor pressure is still < 100 mm Hg. The pyrex tubes were subsequently opened, and the samples were placed in evacuated quartz tubes for higher temperature sintering. The tubes are heated up to ~ 800°C for two more days until completion of the sintering process. The sintered briquets are then placed in a quartz crucible in an argon gas atmosphere and completely melted using an induction furnace. The molten alloys are then cast into rods by sucking the liquid alloys into quartz tubes 2 mm in diameter.

### Quenching Technique

The "piston and anvil technique" was used to obtain the amorphous state from the melt of these alloys. The description given here follows those given previously.<sup>(5)</sup> A piece of the alloy was placed in a fused silica tube 3 mm in diameter with a small opening at the bottom. An induction furnace is used to melt the alloy with the aid of a susceptor (usually graphite). The liquid drop is forced out the small opening under the pressure of a helium blast. Quenching of the melt is achieved by squeezing the droplet between a fixed anvil and a moving piston. The motion of the piston is electronically timed using the passage of the droplet between a photocell and a light source as a time reference. At the appropriate moment the piston is released and accelerated under a 200 psi gas pressure. An estimate of the cooling rate is of the order of  $10^6$ °C/sec.<sup>(6)</sup>

The quenched foils obtained by this technique are about 2 cm in diameter and 30 to 50  $\mu$ m in thickness. The shape of the foil is by no means circular; there is a "lace-like" outer fringe of very thin dimensions. In fact, these areas can be used for transmission electron microscopy.

### Verification of the Amorphous Phase

Each foil obtained in the manner described above was checked by x-ray diffraction with  $\text{CuK}_{\alpha}$  radiation. A diffraction pattern was recorded with a Norelco diffractometer at  $2\theta$  angles between  $34^\circ$  and  $50^\circ$  and in angular steps of  $0.05^\circ$  (in  $2\theta$ ). Within this angular range the diffraction pattern of the quenched foil exhibits a very broad maximum

typical of a liquid structure. The presence of microcrystals in the foil can be detected by weak Bragg reflections superimposed on a broad maximum. The quenched foils which show any deviation from the liquid structure diffraction pattern were eliminated from further study.

#### Composition Range of $(\text{Pd}_{100-x}\text{Cu}_x)_{100-y}\text{P}_y$ Alloys

For  $(\text{Pd}_{100-x}\text{Cu}_x)_{100-y}\text{P}_y$  alloys the maximum variation of the Cu concentration  $x$  was found for  $y = 20$  and  $10 \leq x \leq 50$ . The maximum variation of the phosphorus concentration  $y$  was found for  $x = 35$  and  $x = 40$  and  $15 \leq y \leq 24$ . At the extrema of these composition ranges the yield of amorphous foils is quite low; for most of these quenched foils the presence of microcrystals is easily detected by the x-ray scan.

#### Electrical Resistivity Measurements

The electrical resistivity of Pd-Cu-P has been measured from 4.2°K to  $T_c$ , the crystallization temperature of the alloys ( $\sim 525^\circ\text{K}$ ). The temperature range was covered using two separate experimental apparatuses. An automated resistivity set-up was used for 4 to 300°K measurements and a high temperature resistivity apparatus for 300 to 525°K. Special care was taken to select areas of the quenched foils of fairly uniform thickness to limit the effect of the thickness variations due to non-uniform quenching rates. Still the uncertainty in the dimensions of the foil is dominated by these variations and is estimated to be  $\sim 20\%$ . The standard four-probe method was used with the leads being .0127 cm diameter Pt-10%Rh wire spot welded onto the specimen.

The automatic data acquisition system utilized for low temperature measurements is the same apparatus described by Chen.<sup>(7)</sup> The system consists of a micro-processor, a relay array, and ASR-33 teletype and a digital voltmeter. Analog channel selection is controlled by the micro-processor through the relay array. The selected analog signal is sent to the digital voltmeter and converted to parallel BCD data. The data are then fed back to the micro-processor, transcribed into ASCII characters there, and transmitted serially to the teletype unit. The data are recorded on punched paper tape for later computer data reduction.

The digital voltmeter used in the data acquisition system is a 7-1/2 digit Hewlett Packard 3462A digital voltmeter. The analog signal is amplified by a Keithley 150 AR micro-ammeter 1 amplifier before it is fed to the digital voltmeter. The constant current source used is a North Hill Model TC-1002 BR voltage/current reference source.

Of importance to this study of materials with small temperature coefficients of resistivity is the stability of the apparatus over the 12-hour duration it normally takes for a resistivity experiment. By measuring a sample with our apparatus at fixed temperature, a stability of the measured resistivity  $\pm 5 \times 10^{-4}$  was measured over 12 hours.

#### Magnetic Susceptibility Measurements

The magnetic susceptibility of the alloys has been measured over the temperature range of 4.2 to 300°K using a Faraday magnetic balance apparatus. The magnet system consists of a superconducting magnet, superconducting gradient coils, and a variable temperature insert

mounted in a helium dewar. The construction and design of the magnet system was done by Oxford Instrument Company, England. The vacuum microbalance system and the auxiliary vacuum system for the dewar and variable temperature insert were designed around the magnet system as delivered by Oxford Instruments. The necessary designing was done so as to utilize the high field and high field gradient capabilities of this magnet system for studying weakly magnetic alloys.

#### The Main Field and Gradient Field Coils

The main field is provided by a superconducting magnet made of NbTi filamentary wires. The bore was designed to be  $\approx 2.5$  cm, which is sufficiently large to permit measurements from 1°K to 300°K. The magnet remains immersed in liquid helium under normal operating conditions and a maximum field of 75 kG is attainable. The 2.5 cm bore allows for sufficient sample isolation from the helium bath so that room temperature measurements can be performed without large helium consumption. The effect of turning the gradient coils on and off does not quench the magnet when operating at 75 kG. The magnet can be operated in persistent mode by closing a superconducting path in parallel with the magnet. The opening and closing of the path, which is a superconducting wire, is controlled by a heater wound around this wire which raises the temperature of the wire above its critical temperature. By operating in persistent mode, measurements at fixed field and varying temperature can be made with low liquid He consumption.

The gradient coils are independent in operation from the main solenoid. The maximum field gradient of 1 kG/cm is attained at a

current of 47 A, with a linearity of 1% over 2 cm. The gradient field can be switched on and, with a constant voltage input, made to come to full value in 5 seconds. These coils are connected in series opposition. A homogeneous field gradient is obtained between two non-distributed coaxial wires when they are separated by a distance  $\sqrt{3} R$  when  $R$  is the radius of each coil, and the gradient is given by

$$\frac{\delta H_z(0)}{\delta z} = \frac{0.8058}{R^2} n I$$

where  $n$  = number of turns on each coil.

#### Variable Temperature Insert

The variable temperature insert provides a sample environment in which measurements from 1 to 300°K can be performed while the magnet system is kept at 4.2°K in an external helium bath. Samples are suspended down the center of the variable insert, which has a tail which fits into the solenoid bore. The description of this system is aided by referring to Figs. 1 and 2.

The sample is suspended in an inner sample tube chamber made of stainless steel. Near the bottom of the tube are three small holes through which helium gas can be admitted while changing samples at low temperatures. This gas flow prohibits air, which may cause a susceptibility run to be stopped, from condensing in the sample tube. Helium exchange gas is allowed into this tube during normal measuring conditions to equilibrate the sample temperature with the inner wall temperature of the variable temperature insert. The wall temperature of

Legend for Figure 1

1. Belljar
2. Mirror
3. Electro-Microbalance
4. Sapphire
5. Innertube Gas Purge
6. Liquid Helium Transfer Tube
7. Sample Tube
8. Inner Tube
9. Outer Vacuum Chamber
10. Liquid Nitrogen Chamber
11. Helium Pot Needle Valve
12. Inner Vacuum Chamber
13. Helium Pot
14. Specimen
15. Superconducting Magnet and Gradient Coils
16. Lamp

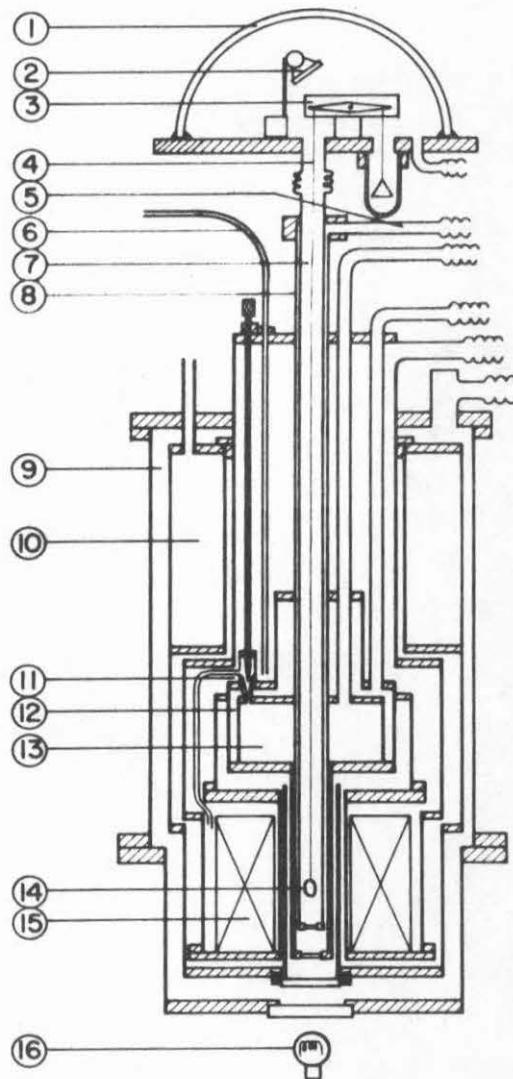


Fig. 1 Cryomagnetic system with microbalance.

Legend for Figure 2

1. Liquid Nitrogen Reservoir
2. Helium Pot Needle Valve
3. Helium Pot Chamber
4. Inner Vacuum Chamber
5. Liquid Helium Chamber
6. Outer Vacuum Chamber
7. Heater
8. Superconducting Magnet
9. Carbon Resistor
10. Specimen
11. Differential Thermocouple
12. Temperature Sensor
13. Radiation Shield
14. Sapphire Rod
15. Center Tube
16. Sample Tube
17. Helium Pot Pump-Out
18. Inner Vacuum Chamber Pump-Out

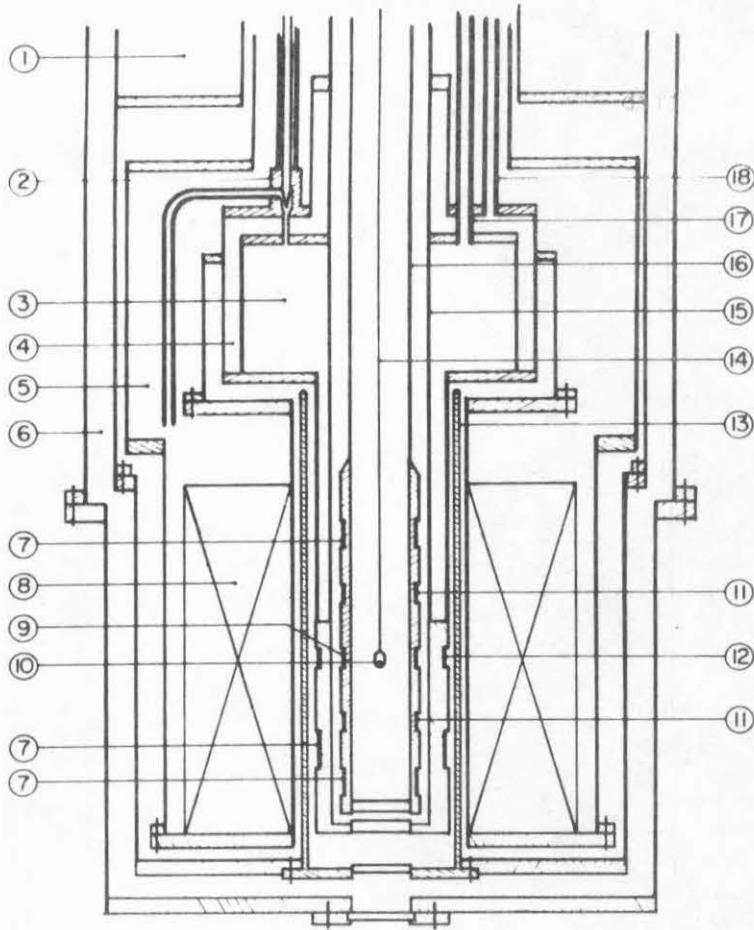


Fig. 2 Variable temperature insert of cryostat.

the insert is monitored by a Au-0.03 at.% Fe/chromel thermocouple which has its reference junction in the outer helium bath. The inside sample tube has wound on it, in the region of the sample position, a heater which is used to reduce the temperature gradients over the sample space. The gradients are measured by a differential thermocouple with junctions 3 cm above and below the correct sample position.

Liquid helium may be drawn into the helium pot through the needle valve from the helium bath. The system is operated down to 1°K by pumping on the liquid helium in the pot. By carefully choosing the inner vacuum chamber gas pressure as well as that of the helium pot, temperatures from 4°K up to 300°K can be maintained for extended periods using simple temperature control circuitry.

#### The Microbalance

The vacuum microbalance used for the sample weight measurements is a Cahn microbalance Model RG. This balance is designed expressly for use in high vacuum systems and in a controlled environment situation. The materials used in the construction are specially chosen to minimize outgassing. In the configuration used in this system, the balance capacity is 1 gram total weight of sample + suspension fiber with a sensitivity of 0.1  $\mu\text{g}$ . The sample weight can be continuously monitored on a digital voltmeter and the weight changes caused by switching the gradient coils on and off are directly measurable. In practice, the effects of sample motion, gas movement in the sample tube chamber and vibrations limit the sensitivity of the balance to .5  $\mu\text{g}$ . The sensitivity to vibration was minimized using vibration

isolation pads obtained from Acoustic Technology, Columbus, Ohio, and weighting down the balance table with lead bars.

#### Calibration

The apparatus, when finally made operational, was tested by measuring the susceptibility of palladium, platinum, and copper at various temperatures. These results agreed reasonably well with reported data for these materials. Using a mechanical movement controlled outside the bell jar, the sample could be positioned at the center of the magnetic's homogeneous region to within  $\pm 1$  mm by monitoring the effective weight of the sample with position. The correct positioning of the sample is perhaps the most important factor affecting accuracy and reproducibility of results. For paramagnetic samples the position of maximum weight with the gradient field on is determined, and the linearity of the weight change with field is checked as a further confirmation of correct centering of the sample with respect to the main solenoid and gradient coils. The sensitivity of this system is such that the easily detectable change of weight of  $1.0 \mu\text{g}$  of a sample of  $250 \text{ mg}$  studied at  $50 \text{ kG}$  and  $1 \text{ kG/cm}$  gradient corresponds to a susceptibility of  $2 \times 10^{-11} \text{ emu/gm}$ .

### III ELECTRICAL RESISTIVITY RESULTS AND DISCUSSION

#### Electrical Resistivity Results

The electrical resistivity of the amorphous alloys  $(\text{Pd}_{100-x}\text{Cu}_x)_{100-y}\text{P}_y$  was measured over the temperature range of 4°K to  $T_g$ , the crystallization temperature of the alloys ( $\sim 550^\circ\text{K}$ ). The measurements were performed in three parts. First, the room temperature resistivity of at least nine samples of each composition obtained from four or more different quenched foils was measured. In Fig. 3 and Fig. 4 the resistivity at room temperature for various concentrations of the amorphous phase is shown. It is clear that, despite the error ( $\pm 20\%$ ) due to thickness variations of the samples, a definite trend in the data is observable. The data point shown is the average of the measured resistivity for the different foils and the bars indicate the extent of the variation of the data points.

Secondly, the resistivity from room temperature to above the crystallization temperature of the alloys was measured. The resistivity data are plotted in Figs. 5 to 17. Of interest is the linear decrease of resistivity with temperature up to  $T_g$  ( $\sim 550^\circ\text{K}$ ) and the compositional dependence of the temperature coefficients of resistivity at the crystallization. The parameters of interest obtained by these high temperature measurements for alloys of different compositions are given in Table 1. The determination of the temperature coefficient of resistivity near  $T_g$  is complicated by the effects of inhomogeneity of the quenched samples. The amorphous samples do not crystallize uniformly at a given temperature  $T_g$ . Portions of the samples may crystallize at 20 to 30 degrees centigrade less than

the major portion of the sample. These crystallized portions provide low resistivity paths and may cause large errors in the estimated temperature coefficients. Nonetheless, clear trends are visible in the data. The temperature coefficients of resistivity decrease (become more negative) with increases of Cu concentration  $x$  or P concentration  $y$ , with  $y$  and  $x$  fixed respectively. The resistivity at  $T_g$  follows the same compositional trends observed at room temperature. For the crystallized samples, which contain phosphides of palladium and copper, as well as solid solutions of palladium and copper, the temperature coefficients of resistivity are positive and 5 to 30 times larger in magnitude than for the amorphous alloys. With  $x$  fixed, the effect of increasing the phosphorus concentration is to decrease the crystalline temperature coefficient of resistivity for both the  $(Pd_{65}Cu_{35})_{100-y}P_y$  and the  $(Pd_{60}Cu_{40})_{100-y}P_y$  series. For the  $(Pd_{100-x}Cu_x)_{80}P_{20}$  alloys a maximum in the measured  $\alpha$ 's occur in the  $x = 20$  to 35 range.

Lastly, the resistivity from 4.2°K to room temperature was measured using a computerized data acquisition system. The results of these measurements are shown in Figs. 18 to 26. The decrease of the resistivity with temperature observed for high temperatures is also seen at low temperatures. At very low temperature (4 to 15°K) a local resistivity minimum is observed and can be accounted for by the presence of up to 100 ppm Fe impurities which give rise to a "Kondo-like" minimum (a true Kondo minimum is impossible in the case of negative  $\alpha$ ). Further increases of temperature cause a  $T^2$  decrease of resistivity up

to  $\approx 120^\circ\text{K}$ . This is followed by a T decrease of resistivity which, as we have already seen, continues up to  $T_g$ . The effects of increasing the phosphorus and copper concentrations are to increase the resistivity and to make  $\alpha$  more negative. For all phosphorus concentrations studied with  $x = 35$  or  $40$ , the measured  $\alpha$ 's at room temperature are negative. By increasing the Cu concentration above  $x = 10\%$ , the room temperature slope can be made to change sign at around  $x = 15$ . For the alloys studied, the alloys  $(\text{Pd}_{65}\text{Cu}_{35})_{85}\text{P}_{15}$  and  $(\text{Pd}_{85}\text{Cu}_{15})_{80}\text{P}_{20}$  exhibit the least sensitive resistivity behavior to temperature. The experimental results are shown in Fig. 18 and Fig. 23. These curves serve to demonstrate the ability of the apparatus to measure the small variations in temperature without difficulty.

The temperature coefficients of resistivity measured at room temperature are shown for the series  $(\text{Pd}_{65}\text{Cu}_{35})_{100-y}\text{P}_y$  and  $(\text{Pd}_{100-x}\text{Cu}_x)_{80}\text{P}_{20}$  in Figs. 27 and 28, respectively. A clear trend of increasingly more negative  $\alpha$ 's with increasing Cu and P concentrations is observed.

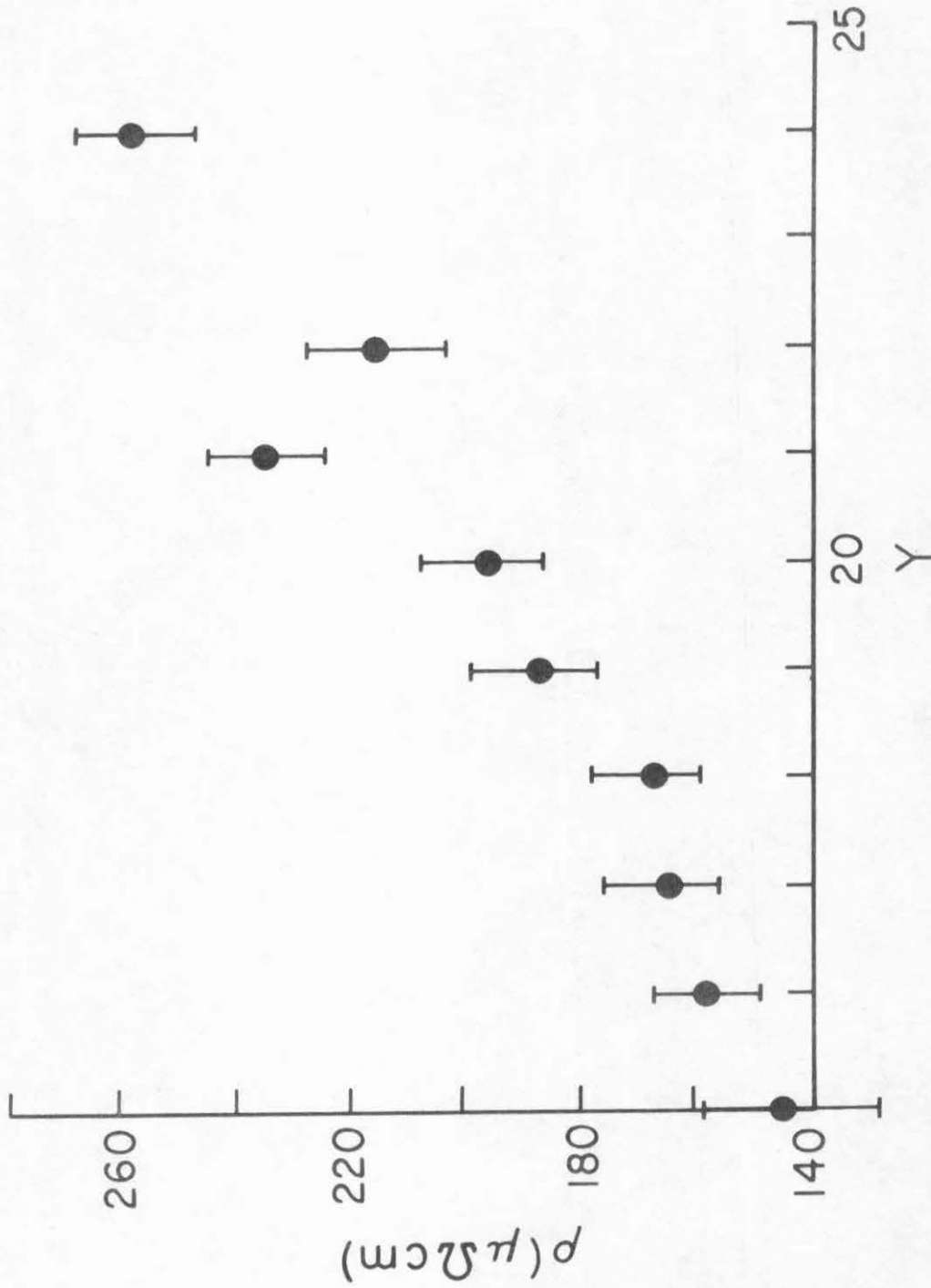


Fig. 3 Room Temperature Resistivity of  $(\text{Pd}_{65}\text{Cu}_{35})_{100-y}\text{P}_y$  Alloys

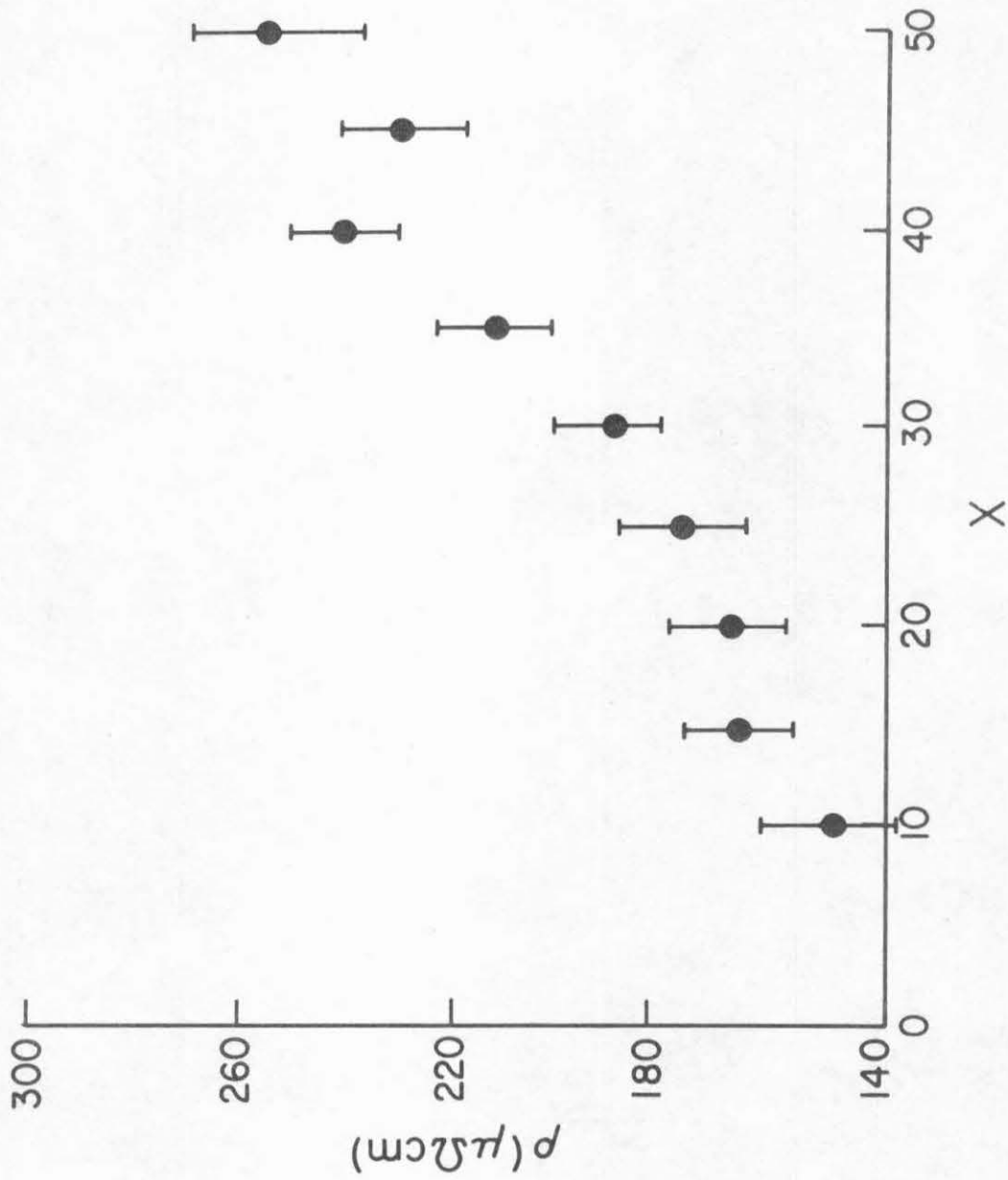


Fig. 4 Room Temperature Resistivity of  $(\text{Pd}_{100-x}\text{Cu}_x)_{80}\text{P}_{20}$  Alloys

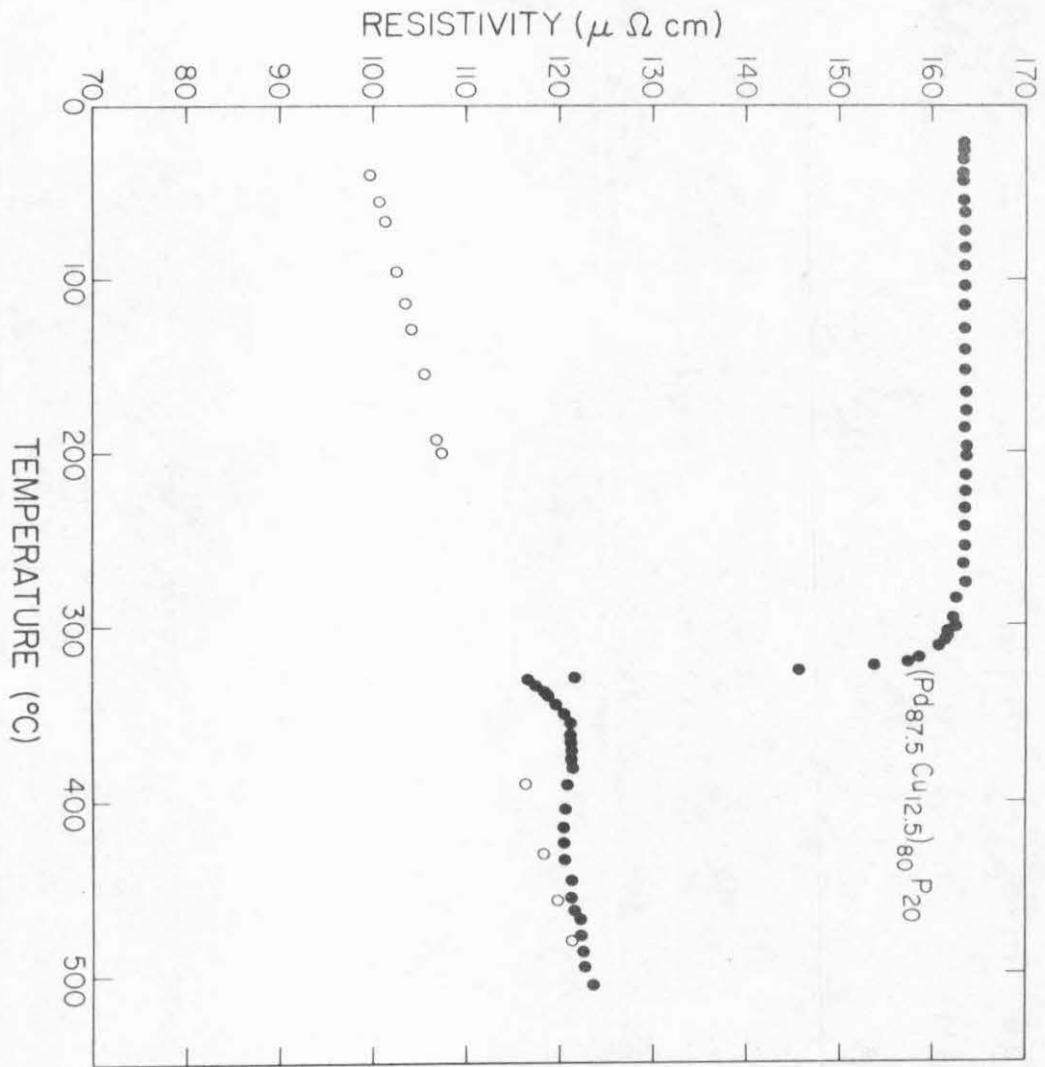


Fig. 5 High Temperature Resistivity of (Pd<sub>87.5</sub>Cu<sub>12.5</sub>)<sub>80</sub>P<sub>20</sub>

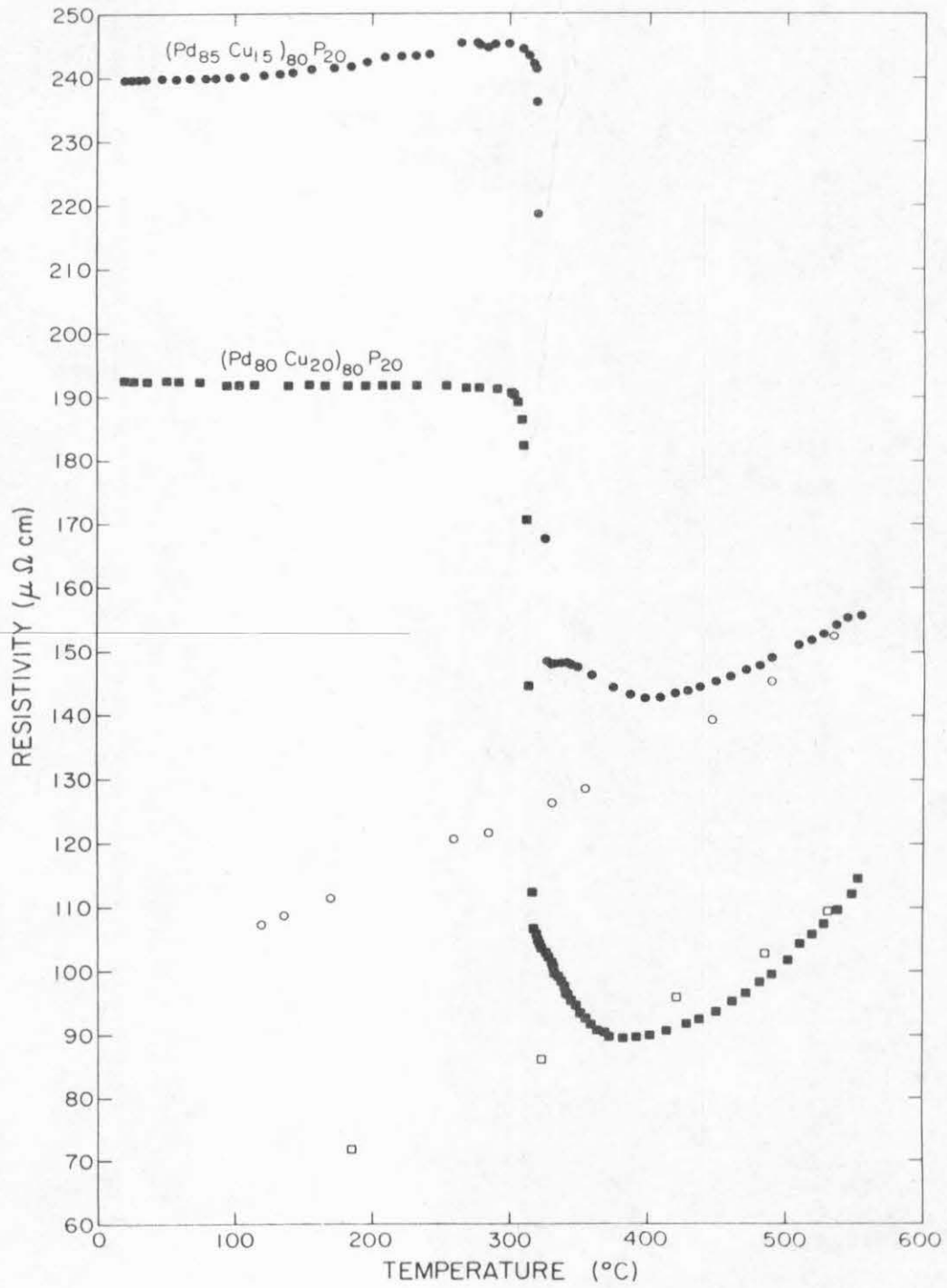


Fig. 6 High Temperature Resistivity of  $(\text{Pd}_{85}\text{Cu}_{15})_{80}\text{P}_{20}$  and  $(\text{Pd}_{80}\text{Cu}_{20})_{80}\text{P}_{20}$

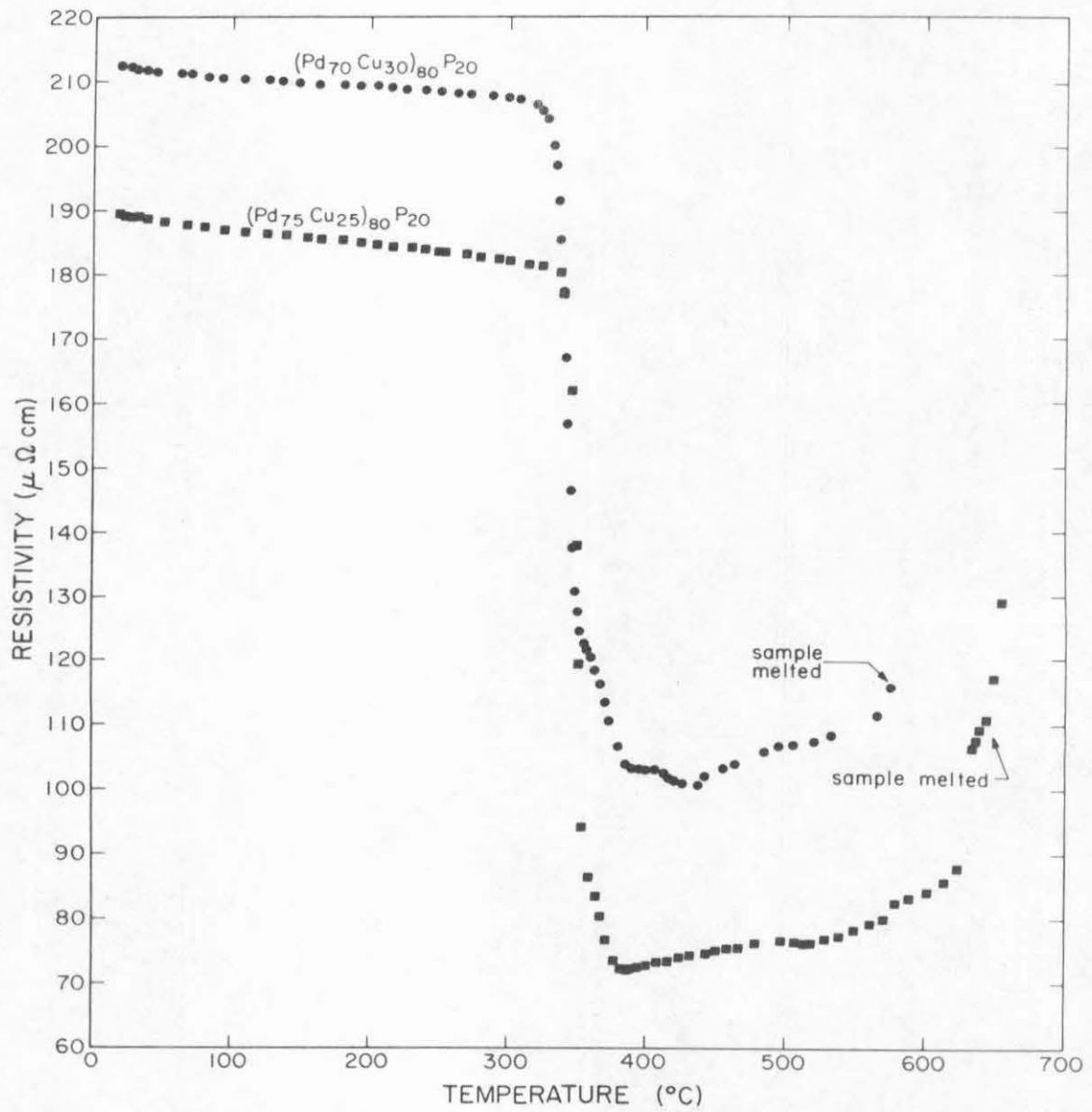


Fig. 7 High Temperature Resistivity of  $(\text{Pd}_{75}\text{Cu}_{25})_{80}\text{P}_{20}$  and  $(\text{Pd}_{70}\text{Cu}_{30})_{80}\text{P}_{20}$

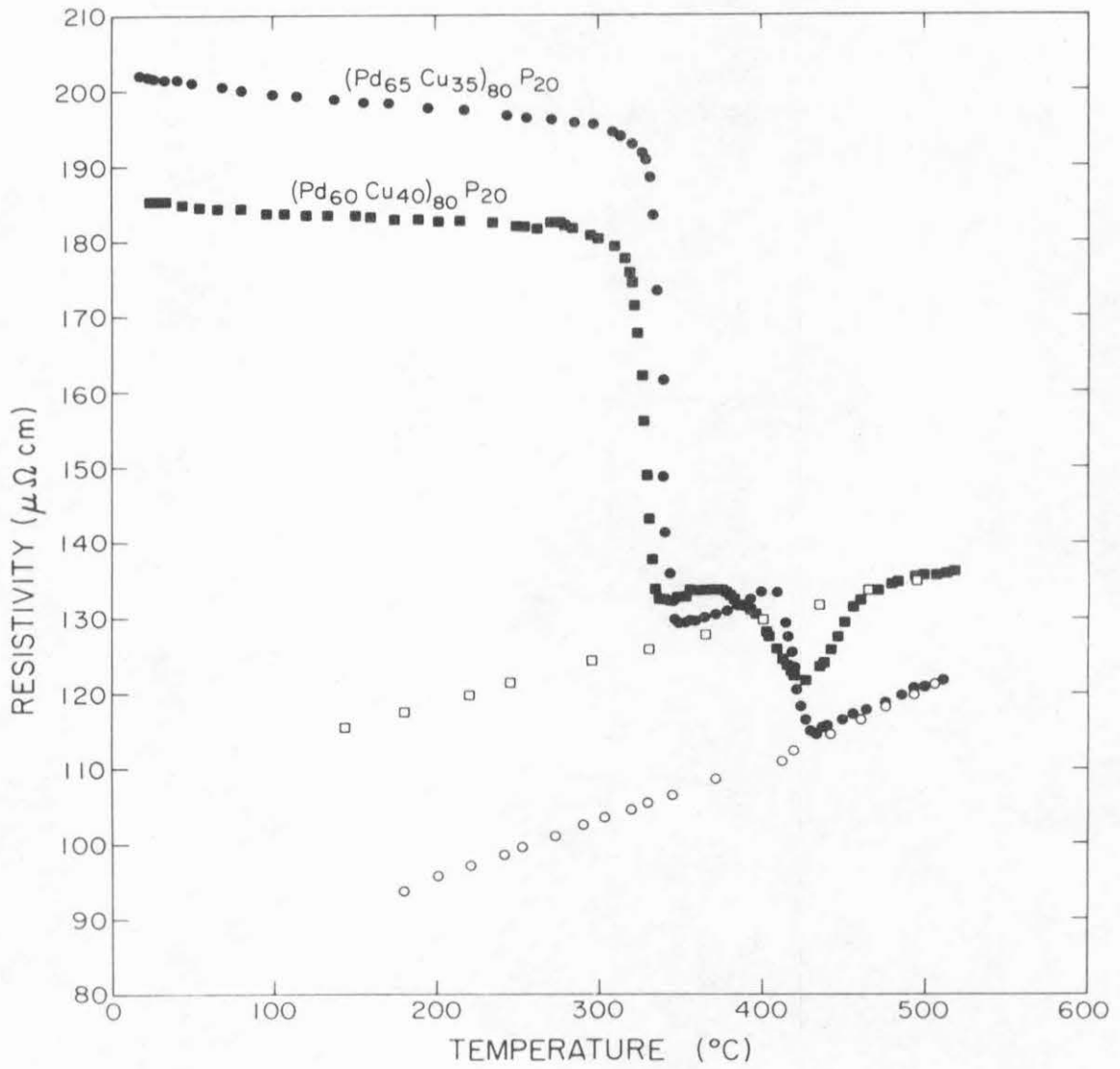


Fig. 8 High Temperature Resistivity of  $(\text{Pd}_{65}\text{Cu}_{35})_{80}\text{P}_{20}$  and  $(\text{Pd}_{60}\text{Cu}_{40})_{80}\text{P}_{20}$

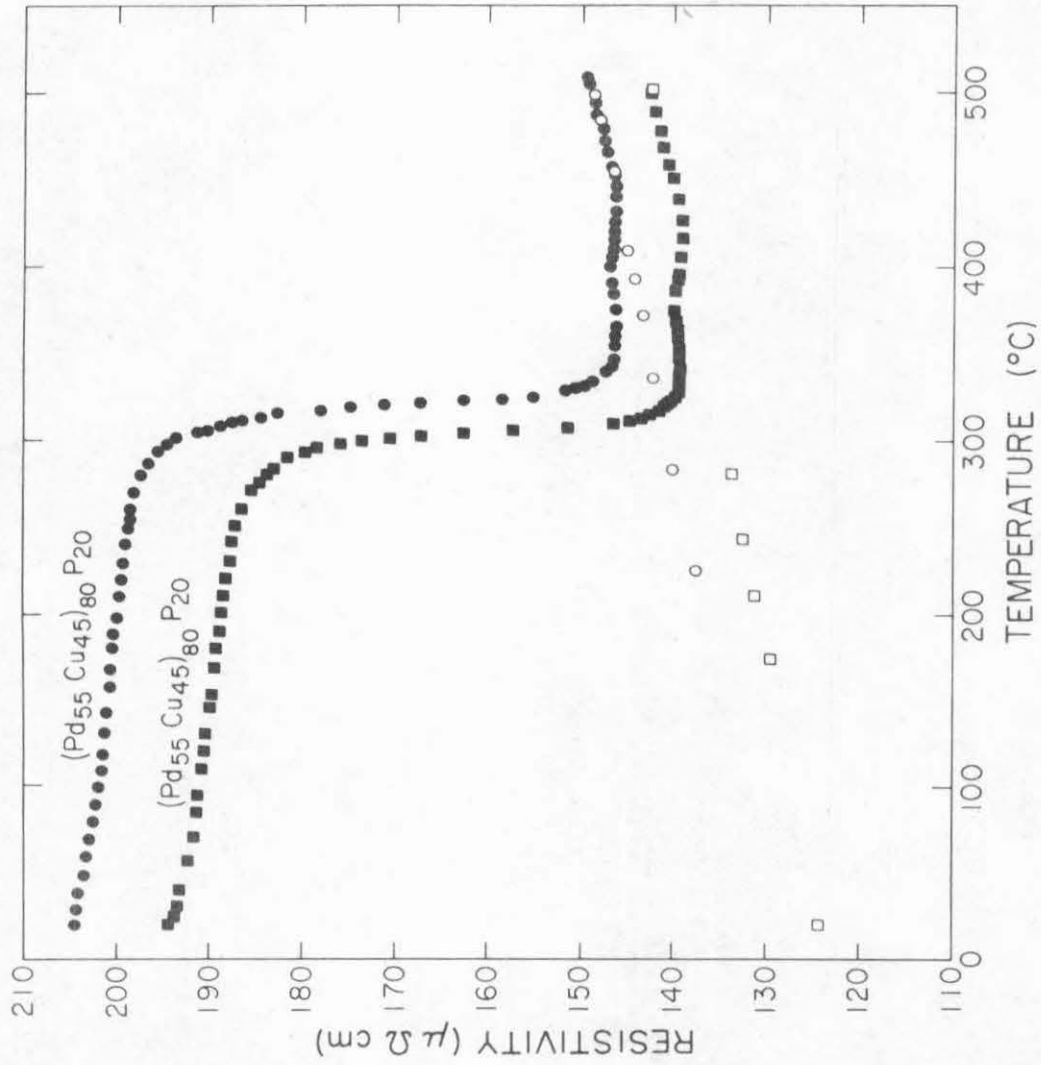


Fig. 9 High Temperature Resistivity of  $(\text{Pd}_{55}\text{Cu}_{45})_{80}\text{P}_{20}$

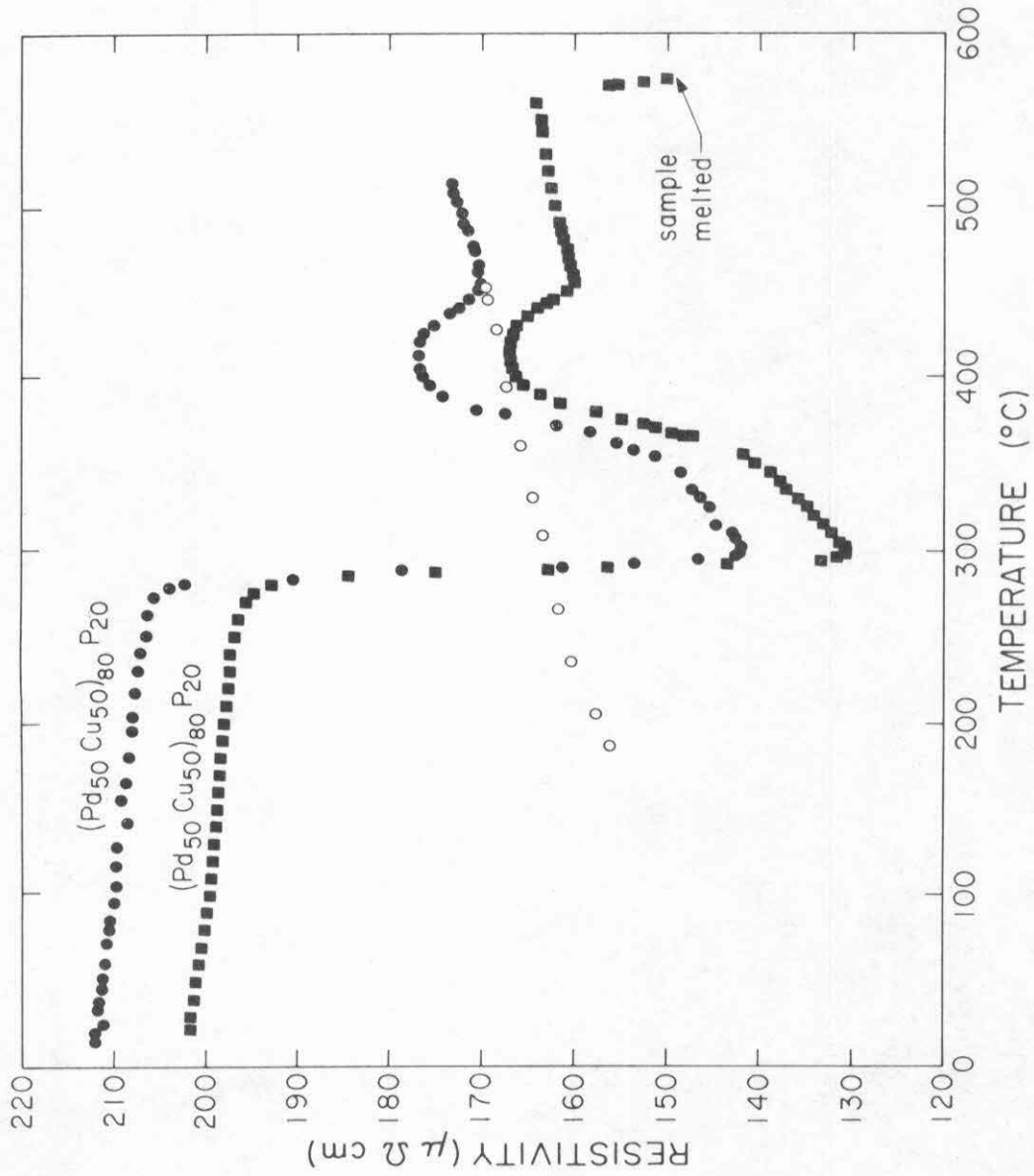


Fig. 10 High Temperature Resistivity of  $(Pd_{50}Cu_{50})_{80}P_{20}$

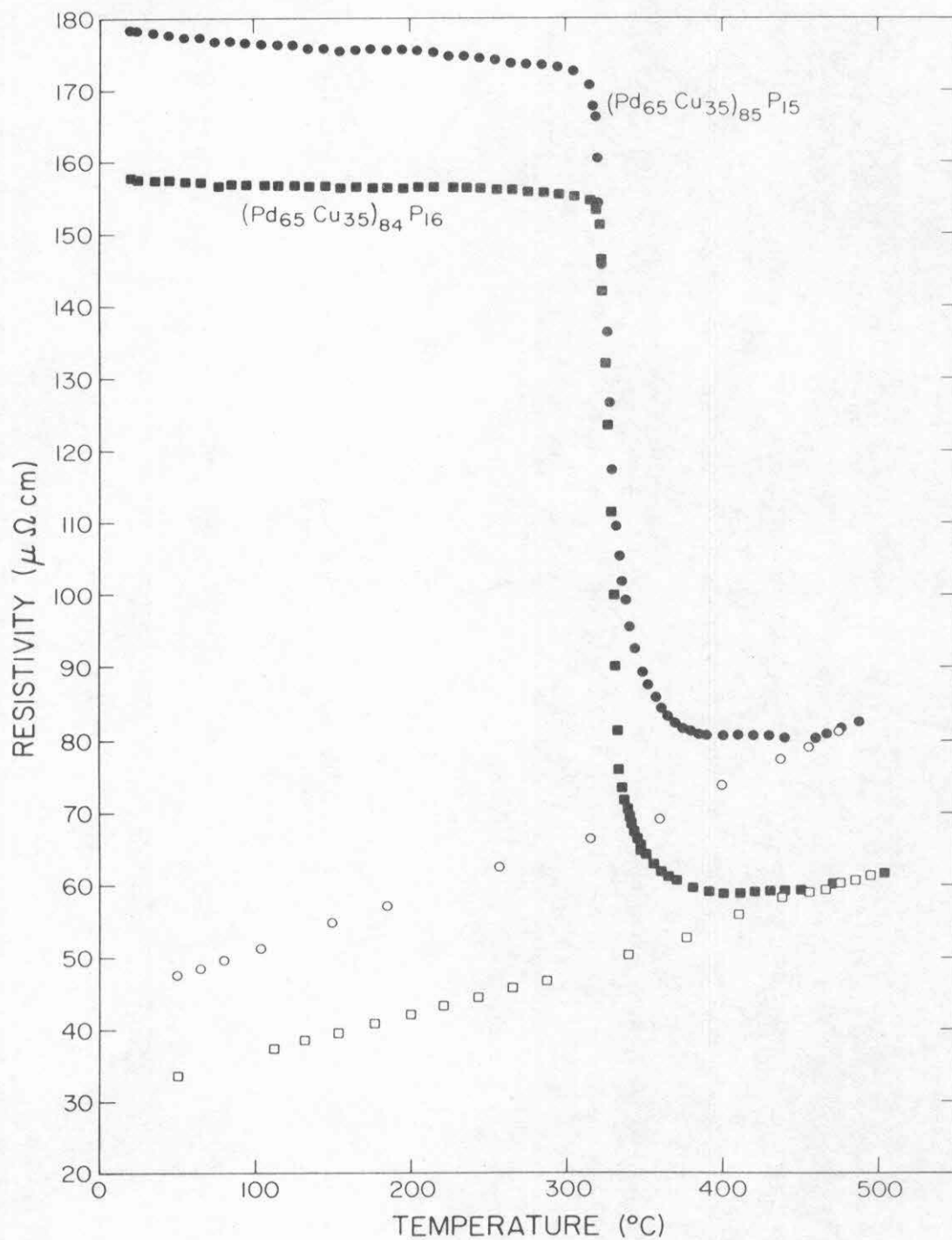


Fig. 11 High Temperature Resistivity of  $(\text{Pd}_{65}\text{Cu}_{35})_{85}\text{P}_{15}$  and  $(\text{Pd}_{65}\text{Cu}_{35})_{84}\text{P}_{16}$

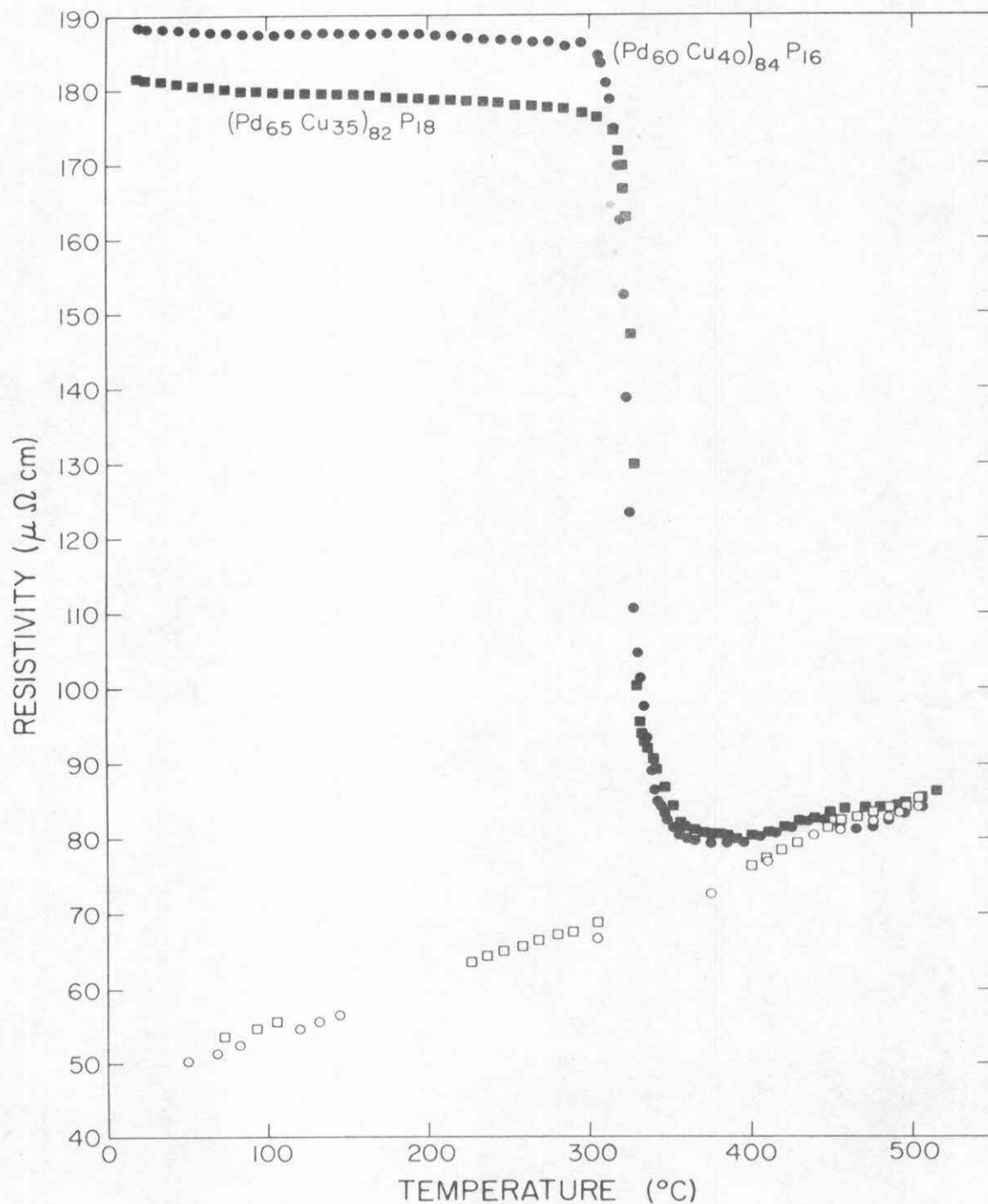


Fig. 12 High Temperature Resistivity of  $(\text{Pd}_{60}\text{Cu}_{40})_{84}\text{P}_{16}$  and  $(\text{Pd}_{65}\text{Cu}_{35})_{82}\text{P}_{18}$

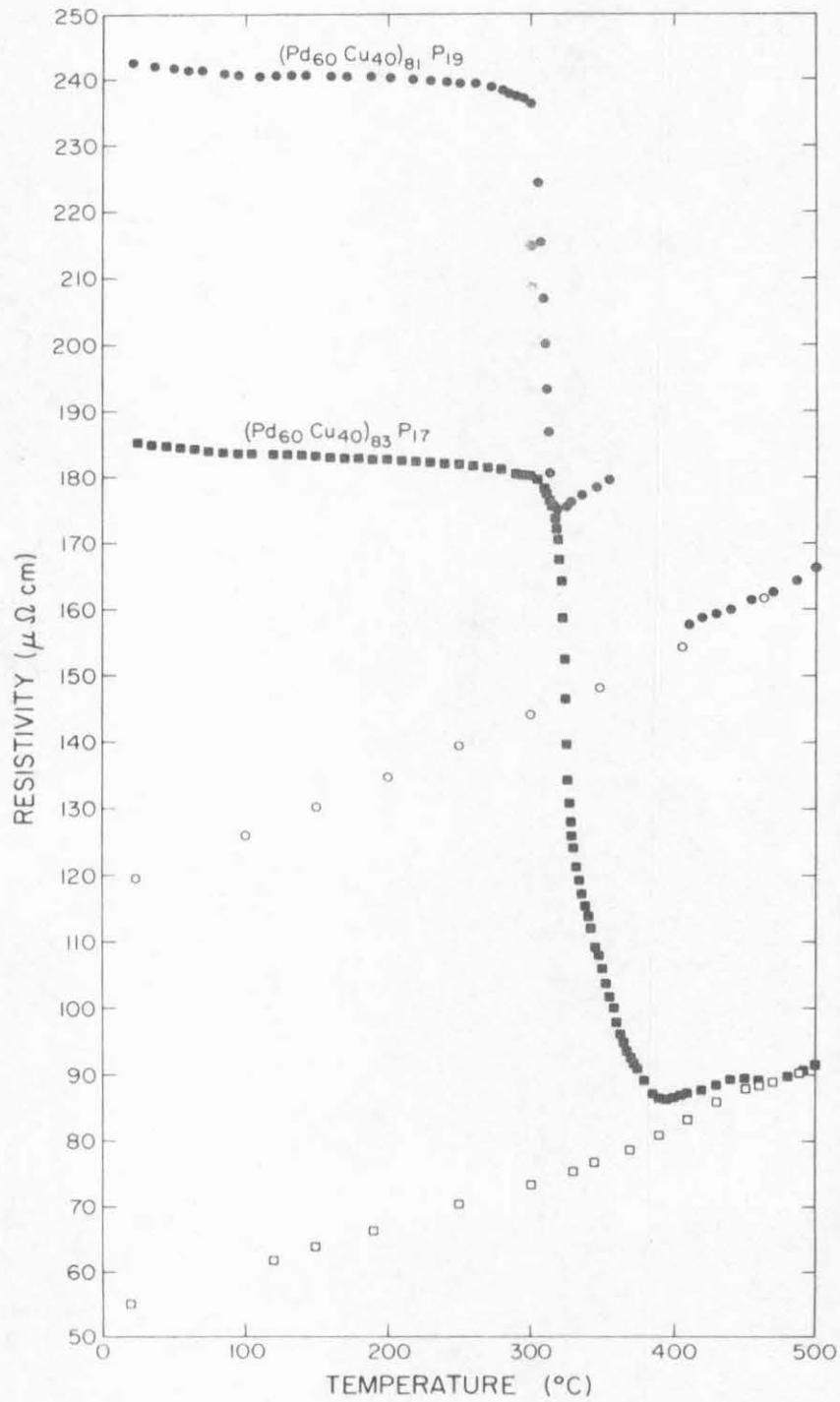


Fig. 13 High Temperature Resistivity of  $(\text{Pd}_{60}\text{Cu}_{40})_{83}\text{P}_{17}$  and  $(\text{Pd}_{60}\text{Cu}_{40})_{81}\text{P}_{19}$

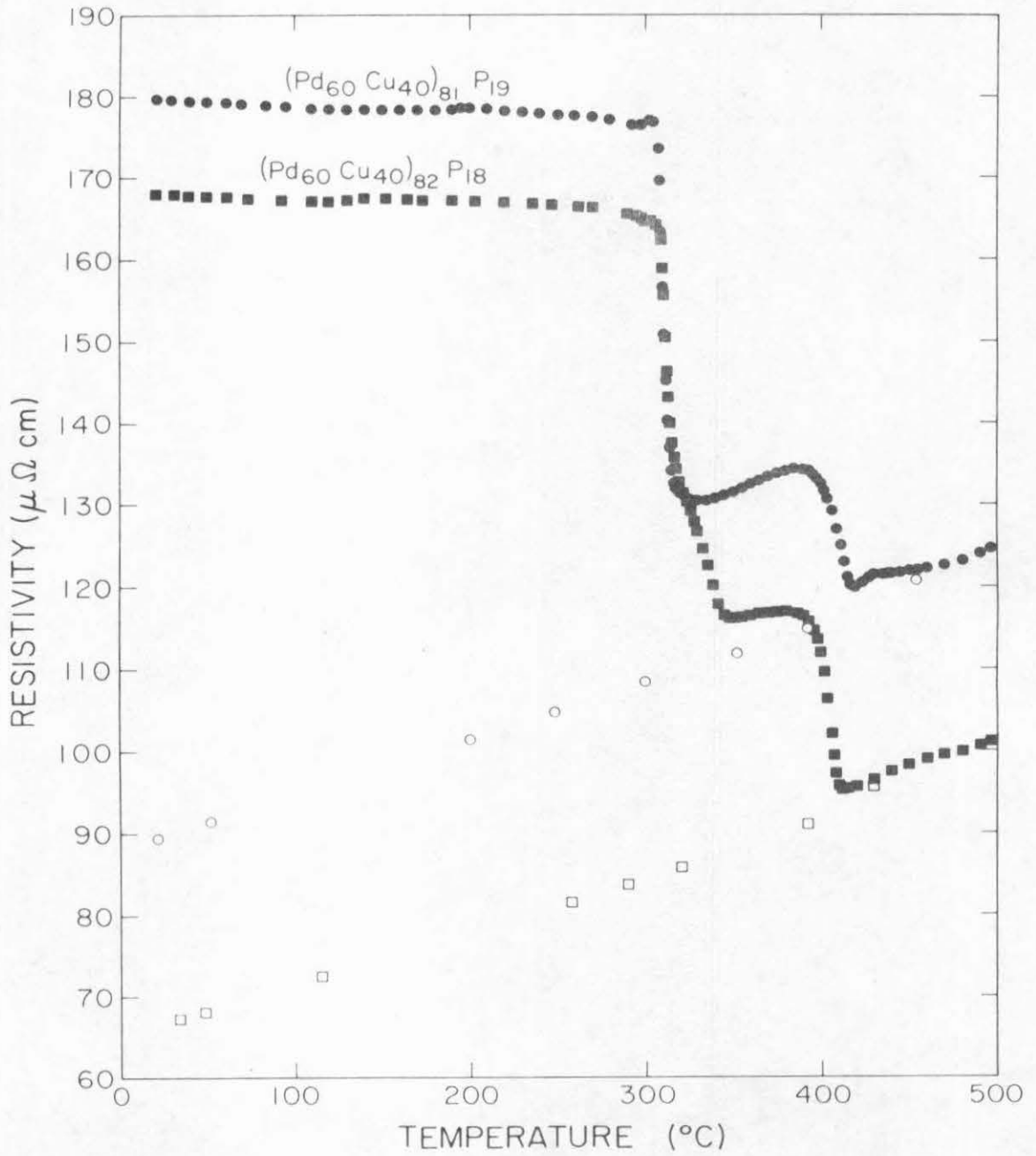


Fig. 14 High Temperature Resistivity of  $(\text{Pd}_{60}\text{Cu}_{40})_{82}\text{P}_{18}$  and  $(\text{Pd}_{60}\text{Cu}_{40})_{81}\text{P}_{19}$

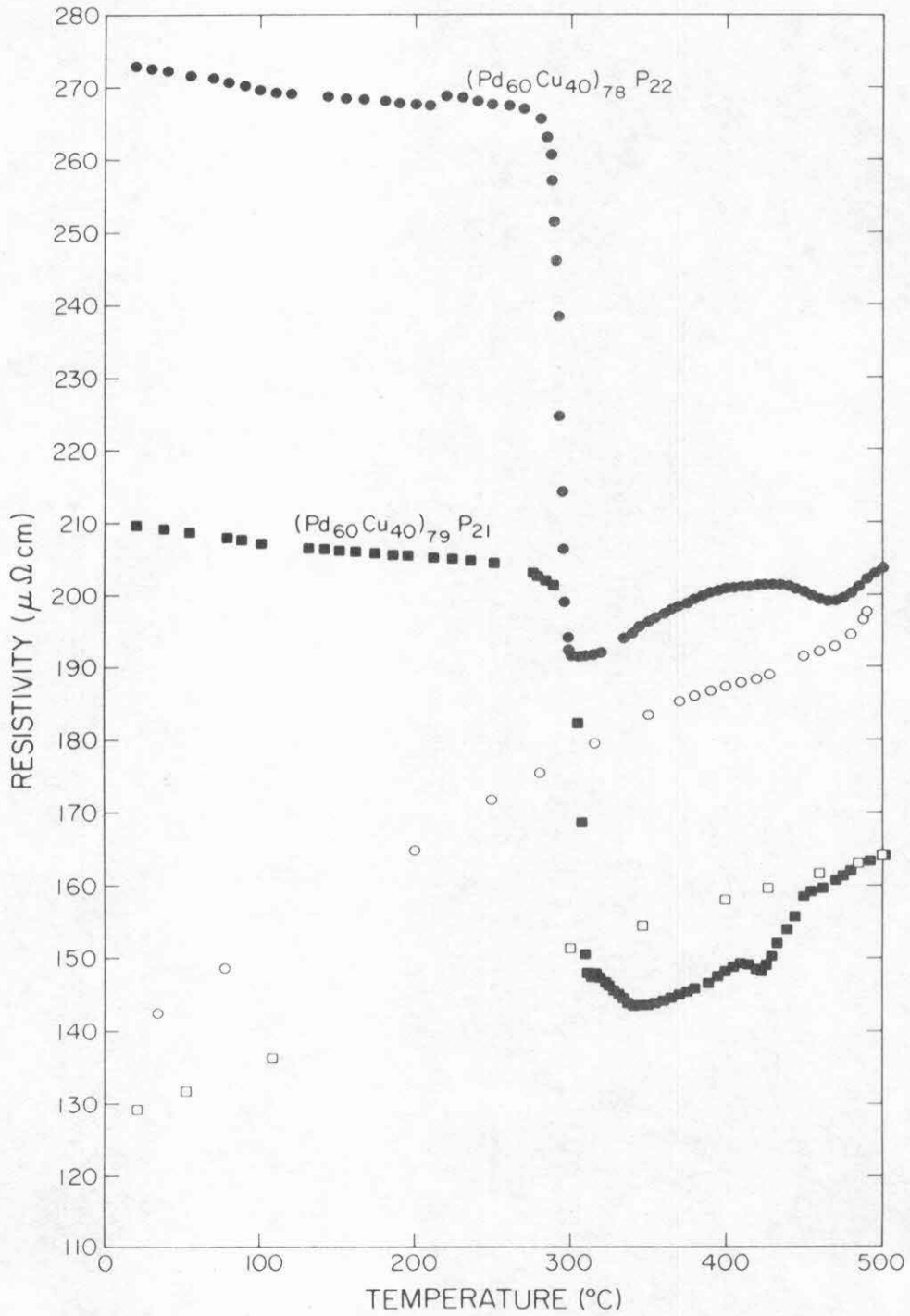


Fig. 15 High Temperature Resistivity of  $(\text{Pd}_{60}\text{Cu}_{40})_{79}\text{P}_{21}$  and  $(\text{Pd}_{60}\text{Cu}_{40})_{78}\text{P}_{22}$

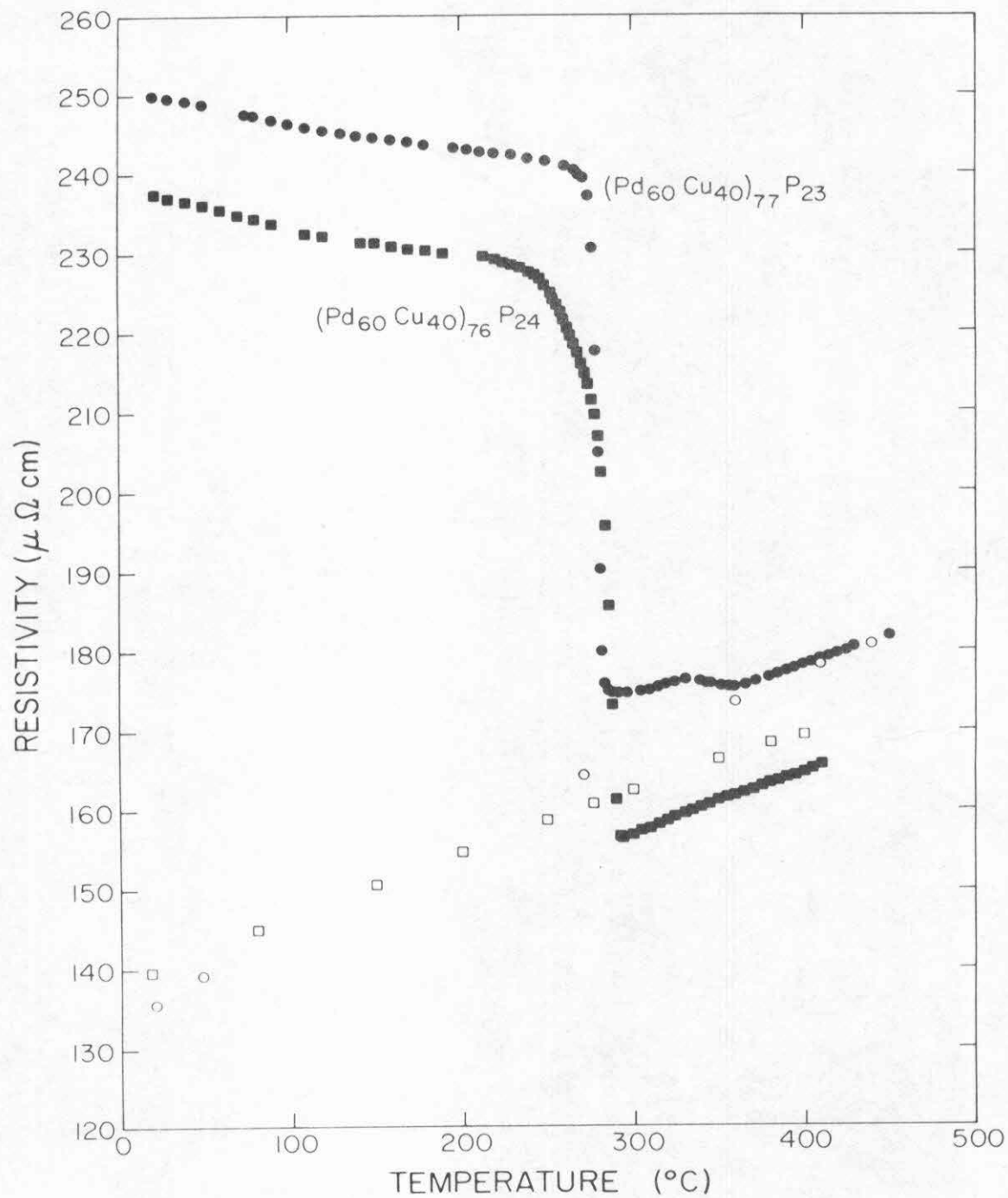


Fig. 16 High Temperature Resistivity of  $(\text{Pd}_{60}\text{Cu}_{40})_{77}\text{P}_{23}$  and  $(\text{Pd}_{60}\text{Cu}_{40})_{76}\text{P}_{24}$

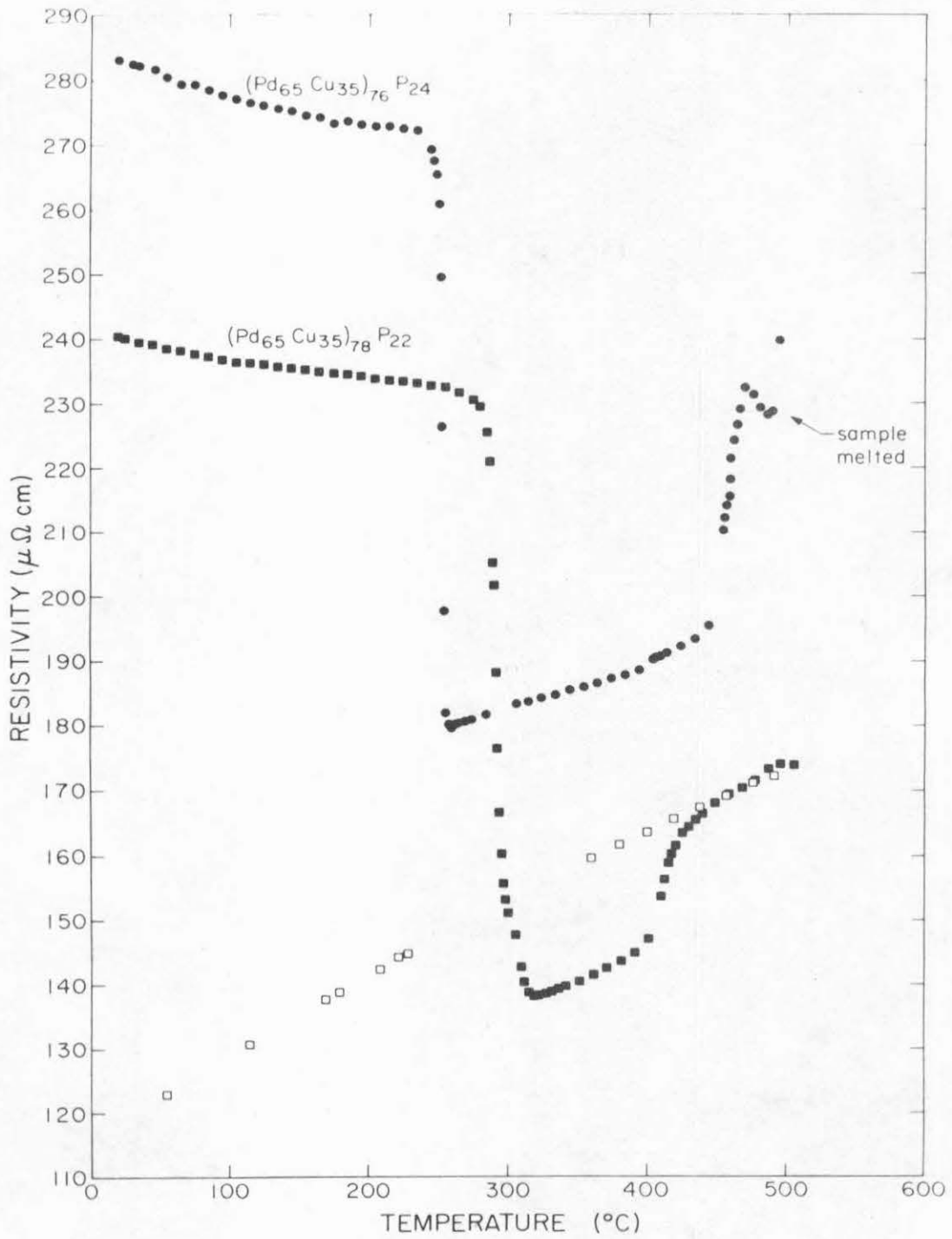


Fig. 17 High Temperature Resistivity of  $(\text{Pd}_{65}\text{Cu}_{35})_{78}\text{P}_{22}$  and  $(\text{Pd}_{65}\text{Cu}_{35})_{76}\text{P}_{24}$

Table 1. High Temperature Resistivity Parameters

	$T_g$ (°K) $\alpha_c$	$\rho_{\text{cryst.}}$ ( $\mu\Omega$ cm)	$\rho_{\text{amorph.}}$ ( $\mu\Omega$ cm)	$\alpha_{\text{cryst.}}$ ( $10^{-6} \circ\text{K}^{-1}$ )	$\alpha_{\text{amorph.}}$ ( $10^{-6} \circ\text{K}^{-1}$ )
(Pd <sub>87.5</sub> Cu <sub>12.5</sub> ) <sub>80</sub> P <sub>20</sub>	320	115	164	606	0
(Pd <sub>85</sub> Cu <sub>15</sub> ) <sub>80</sub> P <sub>20</sub>	320	125	240	705	-
(Pd <sub>80</sub> Cu <sub>20</sub> ) <sub>80</sub> P <sub>20</sub>	310	85	192	1406	-15
(Pd <sub>75</sub> Cu <sub>35</sub> ) <sub>80</sub> P <sub>20</sub>	350	72	182	761	-110
(Pd <sub>70</sub> Cu <sub>30</sub> ) <sub>80</sub> P <sub>20</sub>	340	-	205	-	-39
(Pd <sub>65</sub> Cu <sub>35</sub> ) <sub>80</sub> P <sub>20</sub>	380	109	195	781	-94
(Pd <sub>60</sub> Cu <sub>40</sub> ) <sub>80</sub> P <sub>20</sub>	350	125	185	461	-44
(Pd <sub>55</sub> Cu <sub>45</sub> ) <sub>80</sub> P <sub>20</sub>	300	135	188	307	-121
(Pd <sub>55</sub> Cu <sub>45</sub> ) <sub>80</sub> P <sub>20</sub>	320	142	198	300	-93
(Pd <sub>50</sub> Cu <sub>50</sub> ) <sub>80</sub> P <sub>20</sub>	290	162	208	306	-109
(Pd <sub>50</sub> Cu <sub>50</sub> ) <sub>80</sub> P <sub>20</sub>	290	130	195	-	-75
(Pd <sub>65</sub> Cu <sub>35</sub> ) <sub>85</sub> P <sub>15</sub>	320	75	175	1318	-50
(Pd <sub>65</sub> Cu <sub>35</sub> ) <sub>84</sub> P <sub>16</sub>	320	55	155	1000	-36
(Pd <sub>65</sub> Cu <sub>35</sub> ) <sub>72</sub> P <sub>18</sub>	320	75	175	1314	-76
(Pd <sub>65</sub> Cu <sub>35</sub> ) <sub>78</sub> P <sub>22</sub>	290	156	230	740	-109
(Pd <sub>60</sub> Cu <sub>40</sub> ) <sub>77</sub> P <sub>23</sub>	280	170	241	625	-122
(Pd <sub>65</sub> Cu <sub>35</sub> ) <sub>76</sub> P <sub>24</sub>	250	280	272	353	-158
(Pd <sub>60</sub> Cu <sub>40</sub> ) <sub>76</sub> P <sub>24</sub>	260	160	230	468	-126
(Pd <sub>60</sub> Cu <sub>40</sub> ) <sub>84</sub> P <sub>16</sub>	340	70	186	1045	-43
(Pd <sub>60</sub> Cu <sub>40</sub> ) <sub>83</sub> P <sub>17</sub>	320	75	180	1151	-46

Table 1 - continued

	$T_g$ (°K)	$\rho_{\text{cryst.}}$ ( $\mu\Omega$ cm)	$\rho_{\text{amorph.}}$ ( $\mu\Omega$ cm)	$\alpha_{\text{cryst.}}$ ( $10^{-6} \circ K^{-1}$ )	$\alpha_{\text{amorph.}}$ ( $10^{-6} \circ K^{-1}$ )
$(Pd_{60}Cu_{40})_{82}P_{18}$	310	85	168	931	-26
$(Pd_{60}Cu_{40})_{81}P_{19}$	310	110	179	671	-44
$(Pd_{60}Cu_{40})_{81}P_{19}$	310	150	240	535	-54
$(Pd_{60}Cu_{40})_{79}P_{21}$	300	150	204	466	-62
$(Pd_{60}Cu_{50})_{78}P_{22}$	290	176	268	764	-64

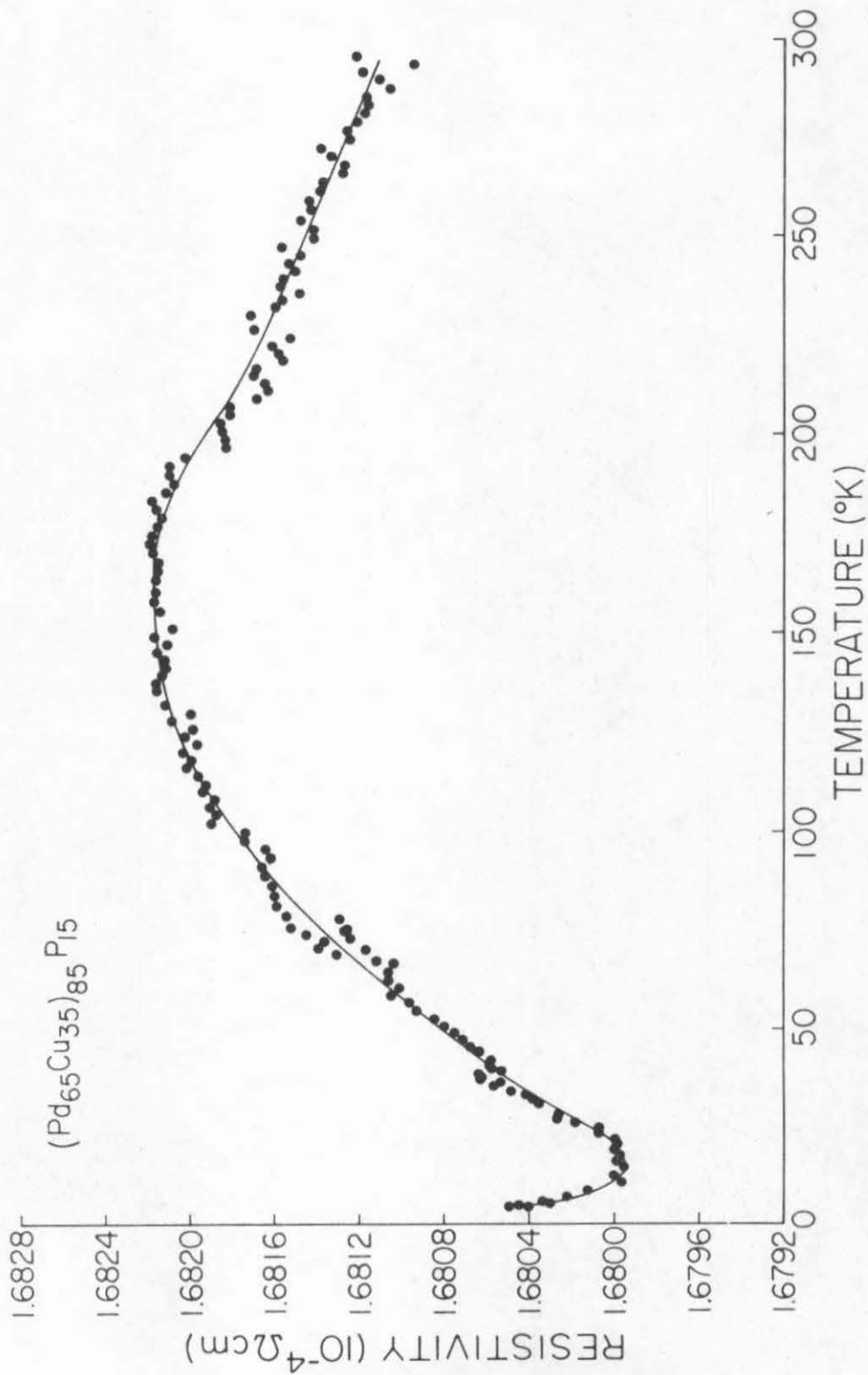


Fig. 18 Low Temperature Resistivity of  $(\text{Pd}_{65}\text{Cu}_{35})_{85}\text{P}_{15}$

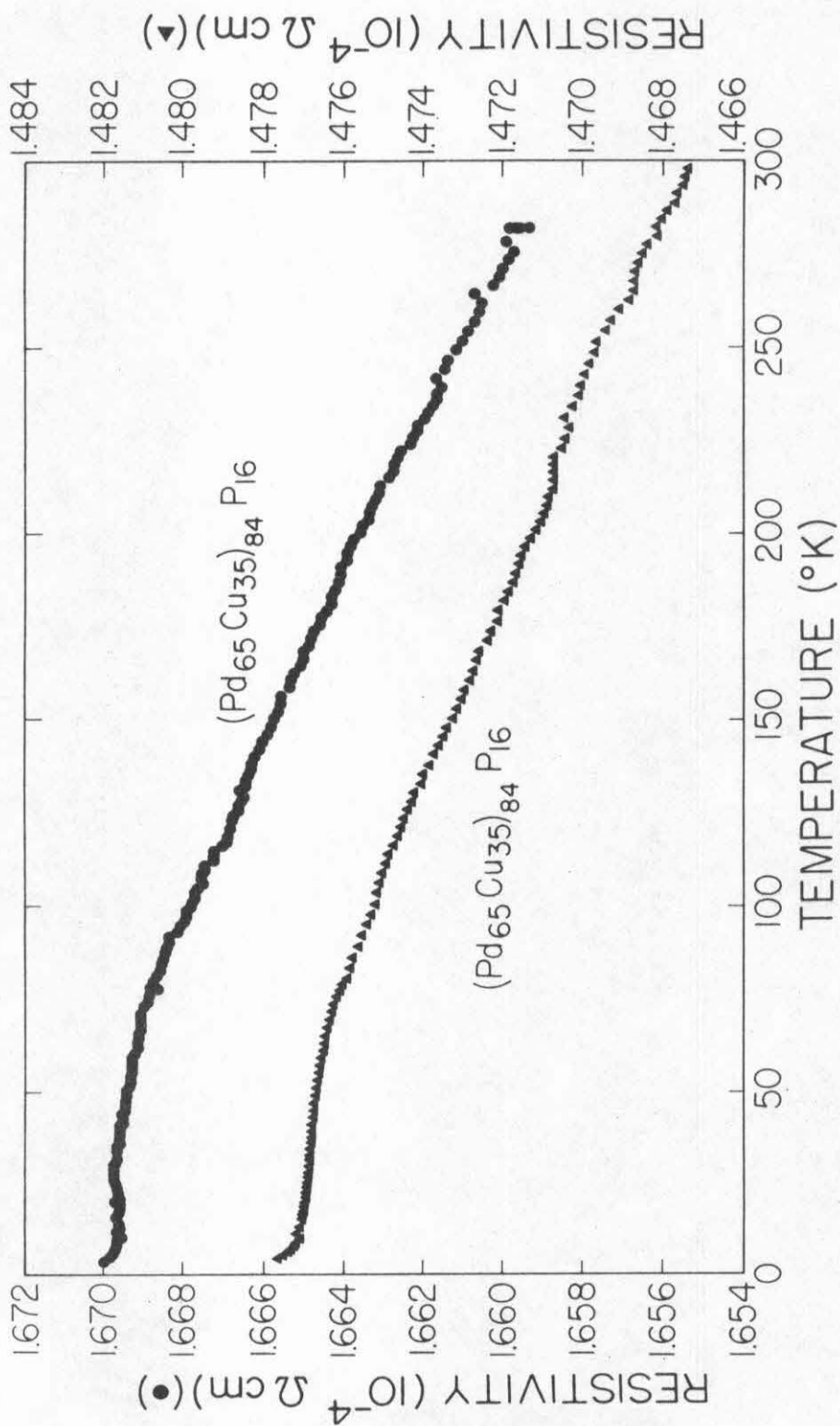


Fig. 19 Low Temperature Resistivity of (Pd<sub>65</sub>Cu<sub>35</sub>)<sub>84</sub>P<sub>16</sub>

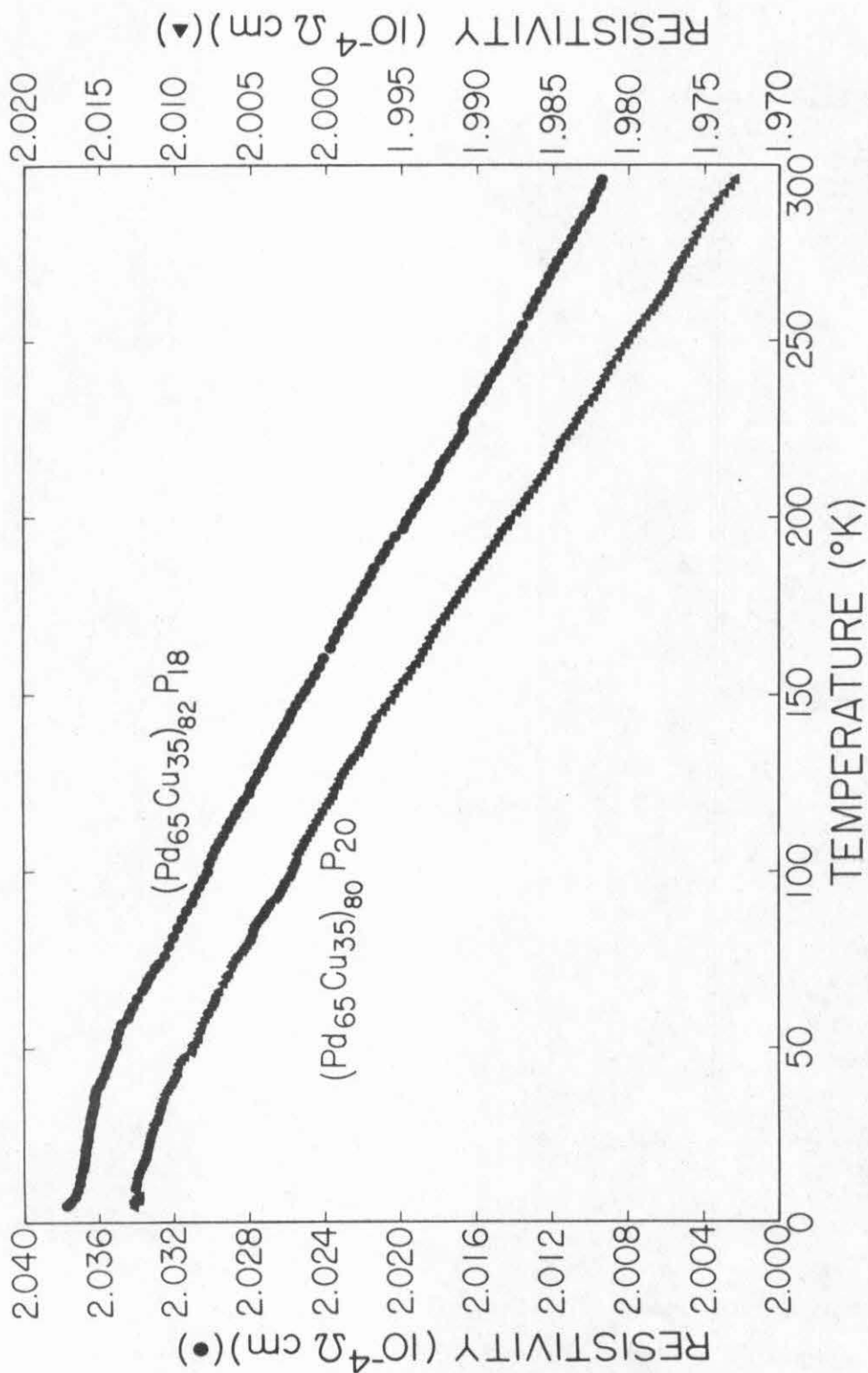


Fig. 20 Low Temperature Resistivity of  $(\text{Pd}_{65}\text{Cu}_{35})_{80}\text{P}_{20}$  and  $(\text{Pd}_{65}\text{Cu}_{35})_{82}\text{P}_{18}$

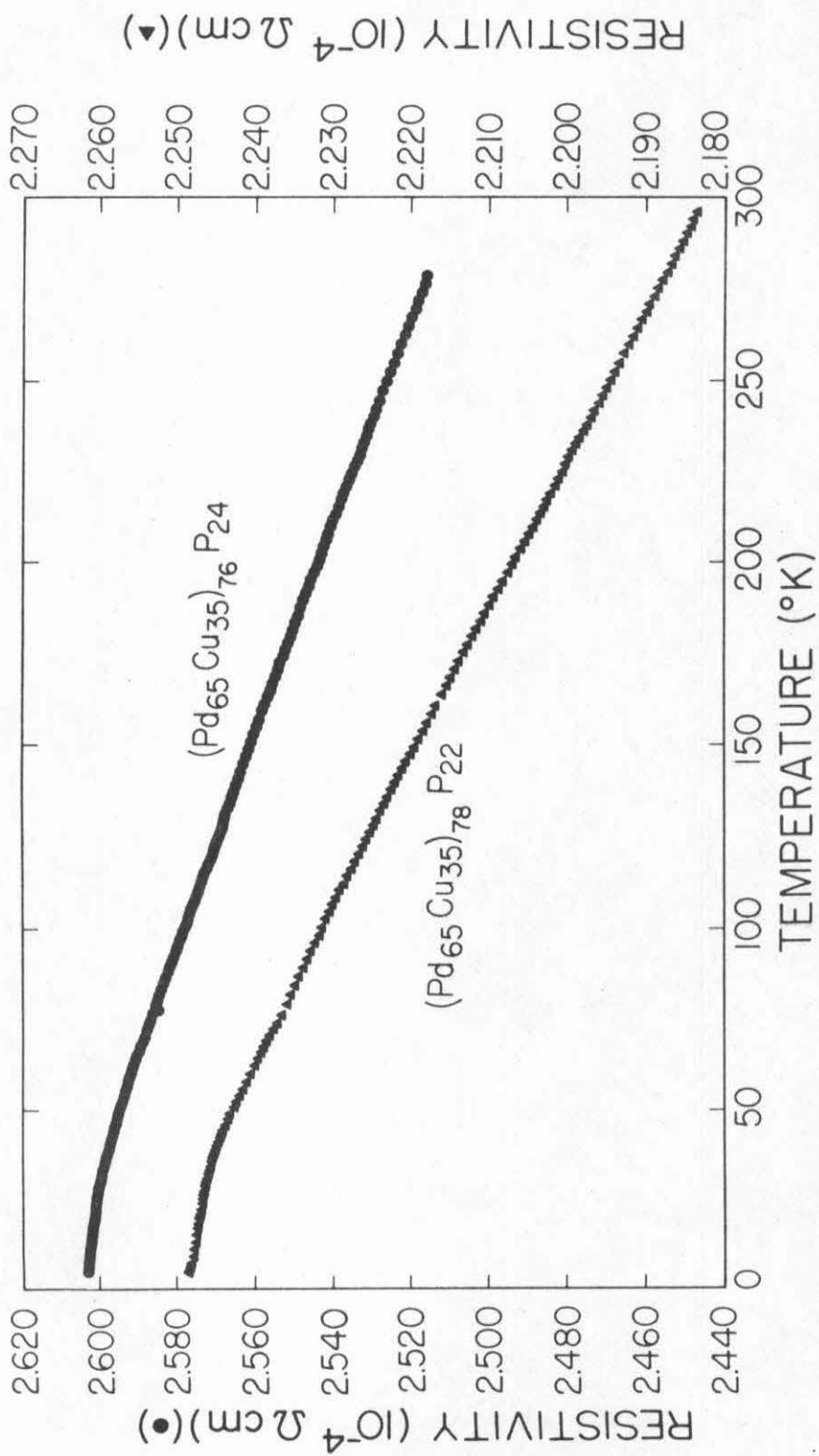


Fig. 21 Low Temperature Resistivity of (Pd<sub>65</sub>Cu<sub>35</sub>)<sub>78</sub>P<sub>22</sub> and (Pd<sub>65</sub>Cu<sub>35</sub>)<sub>76</sub>P<sub>24</sub>

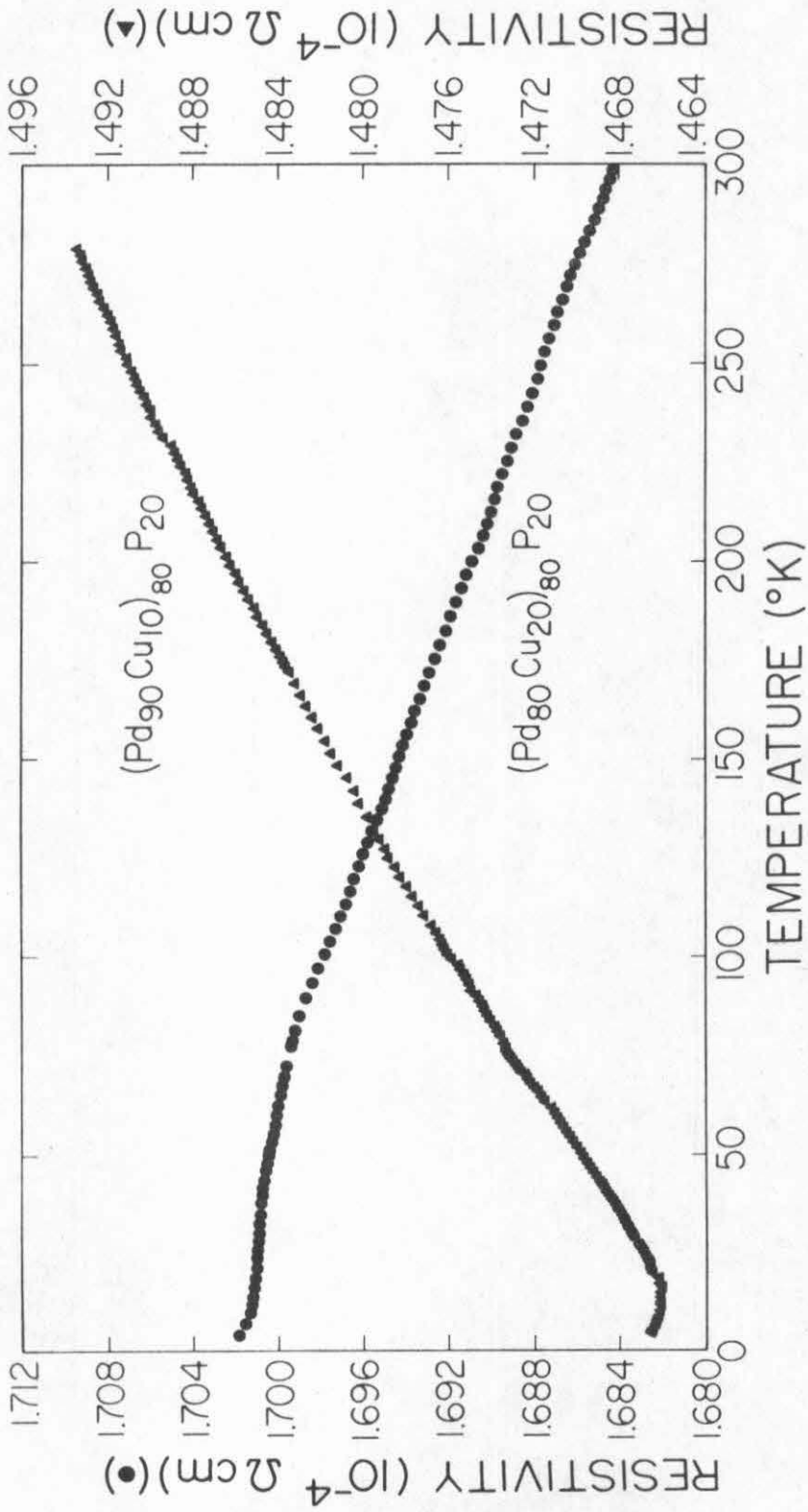


Fig. 22 Low Temperature Resistivity of  $(\text{Pd}_{90}\text{Cu}_{10})_{80}\text{P}_{20}$  and  $(\text{Pd}_{80}\text{Cu}_{20})_{80}\text{P}_{20}$

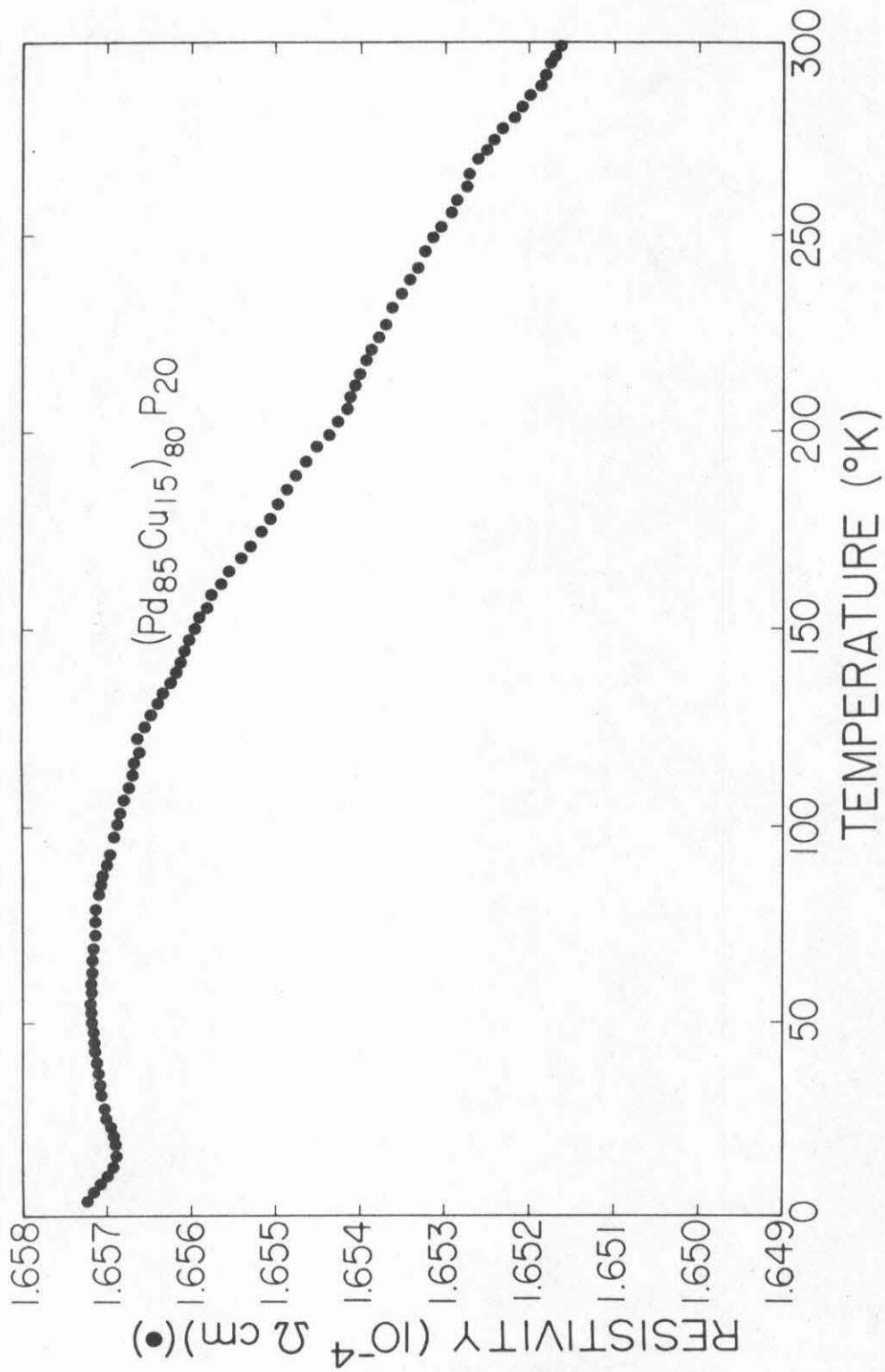


Fig. 23 Low Temperature Resistivity of (Pd<sub>85</sub>Cu<sub>15</sub>)<sub>80</sub>P<sub>20</sub>

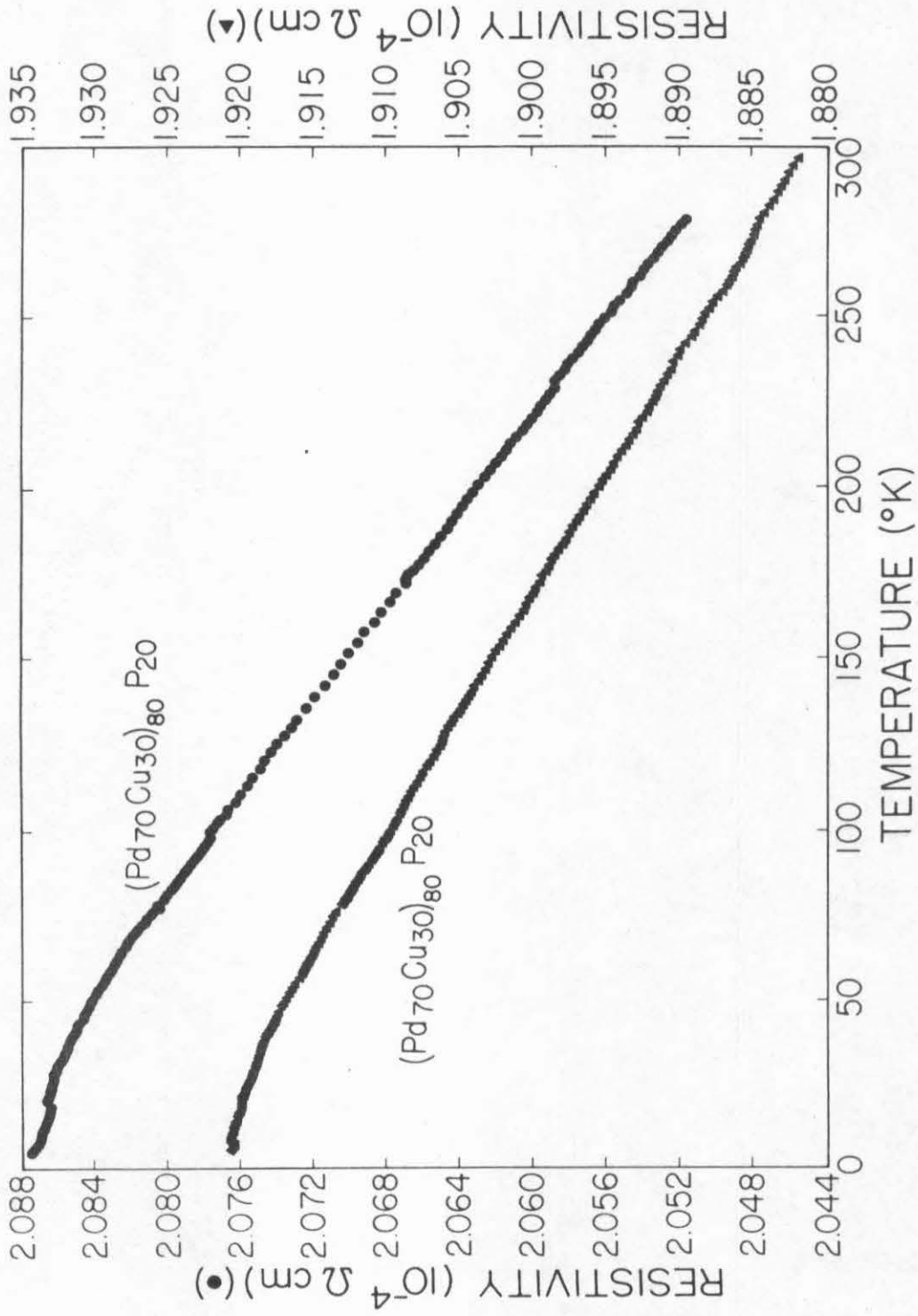


Fig. 24 Low Temperature Resistivity of (Pd<sub>70</sub>Cu<sub>30</sub>)<sub>80</sub>P<sub>20</sub>

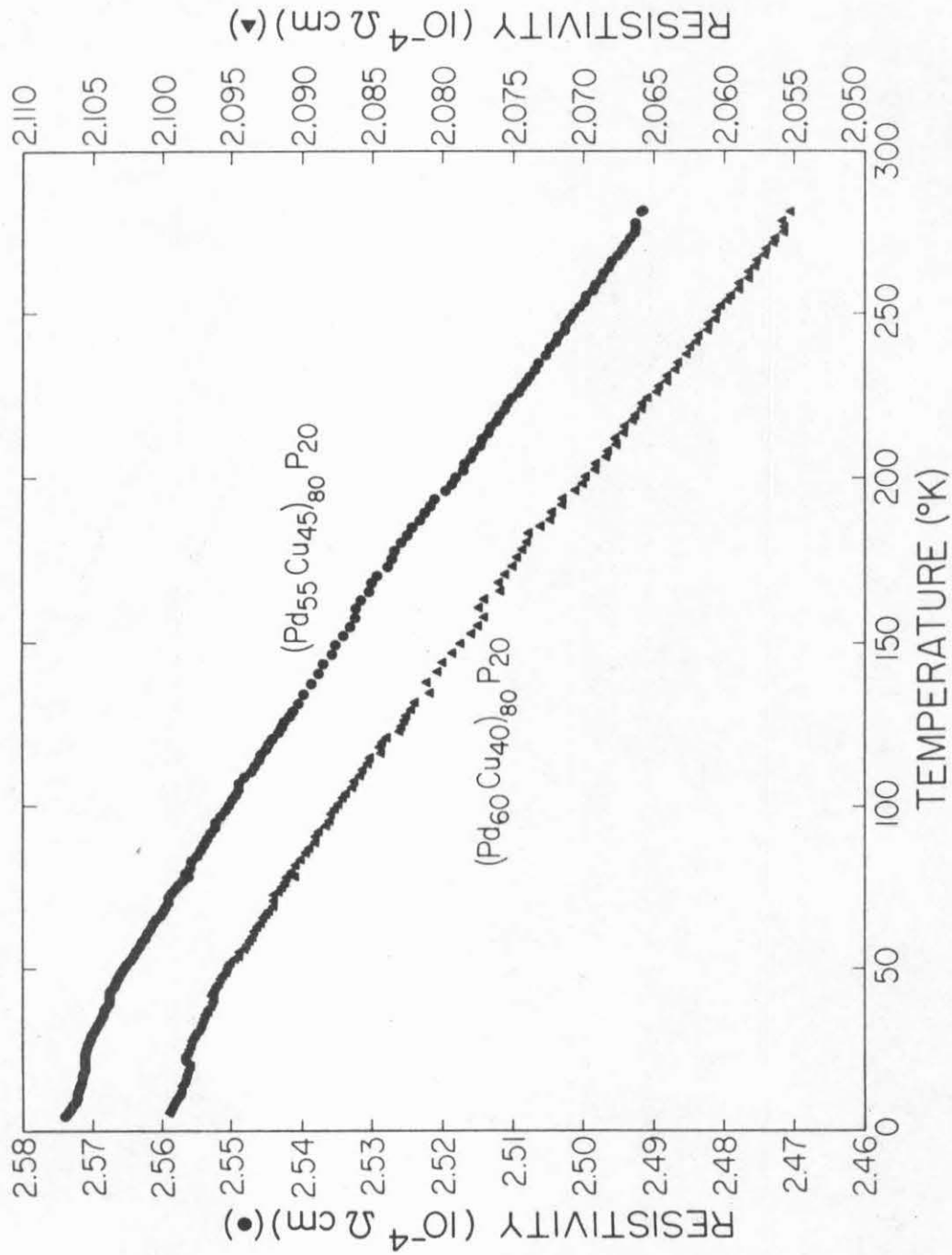


Fig. 25 Low Temperature Resistivity of  $(\text{Pd}_{60}\text{Cu}_{40})_{80}\text{P}_{20}$  and  $(\text{Pd}_{55}\text{Cu}_{45})_{80}\text{P}_{20}$

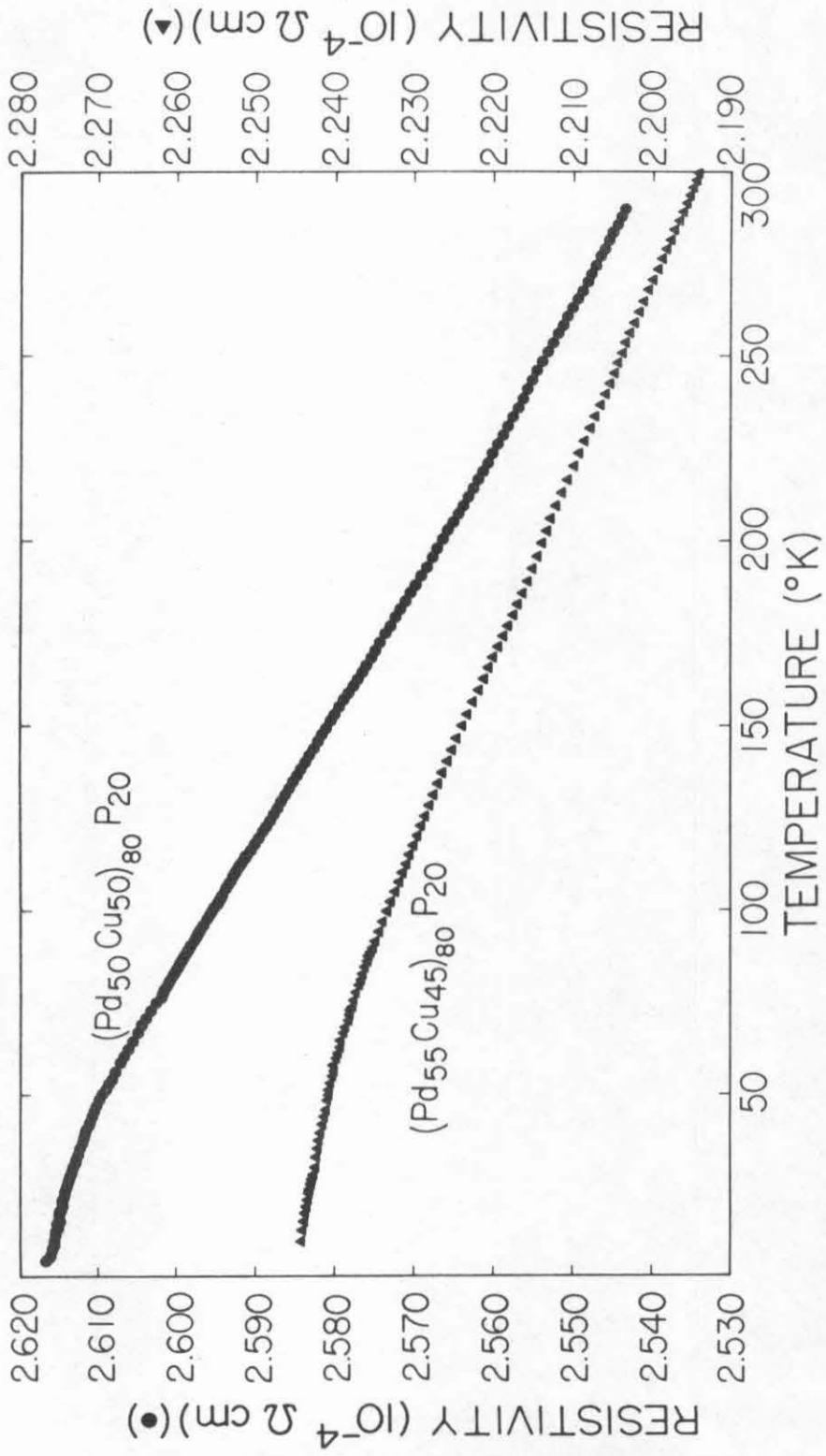


Fig. 26 Low Temperature Resistivity of (Pd<sub>55</sub>Cu<sub>45</sub>)<sub>80</sub>P<sub>20</sub> and (Pd<sub>50</sub>Cu<sub>50</sub>)<sub>80</sub>P<sub>20</sub>

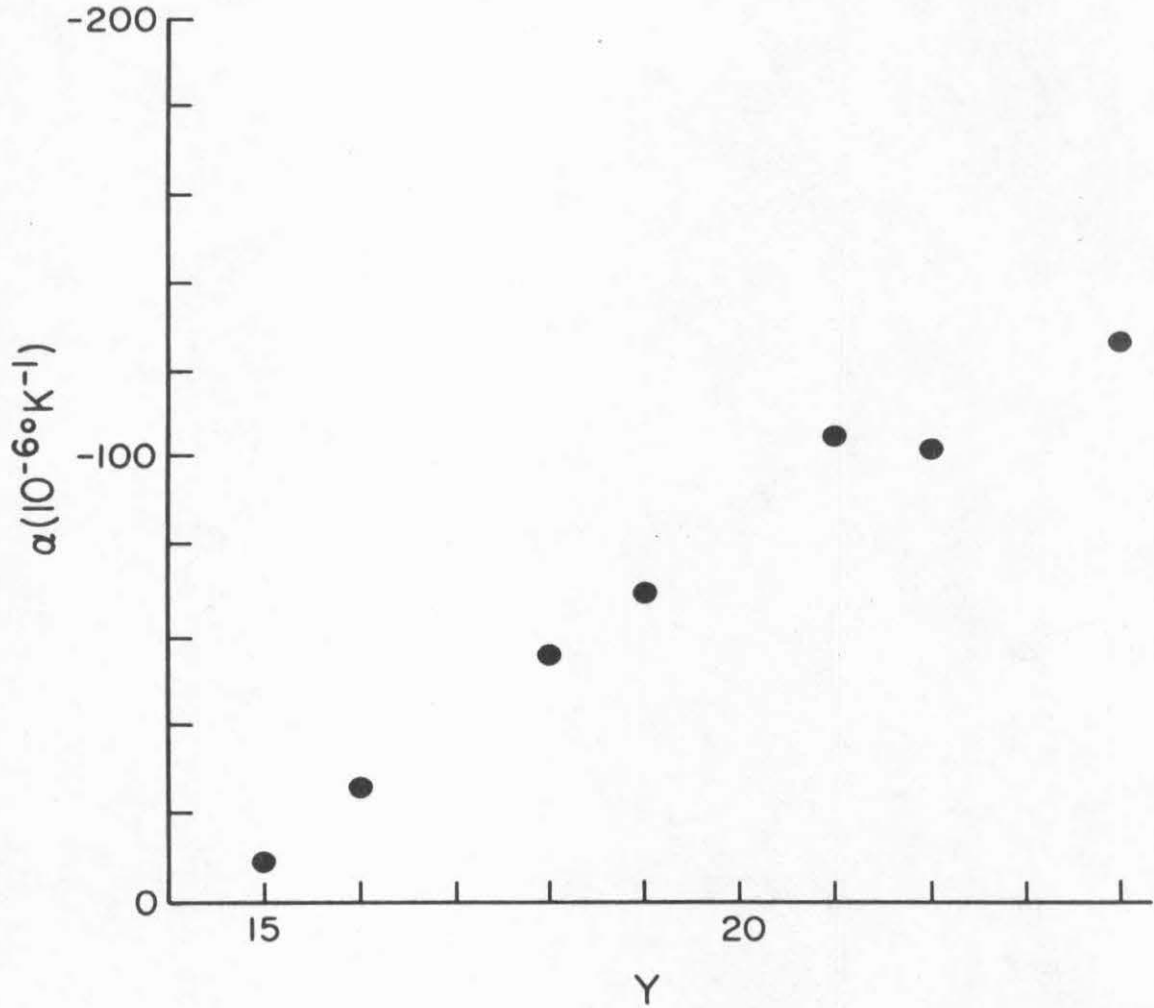


Fig. 27 Temperature Coefficients of Resistivity for  $(\text{Pd}_{65}\text{Cu}_{35})_{100-y}\text{P}_y$  Alloys

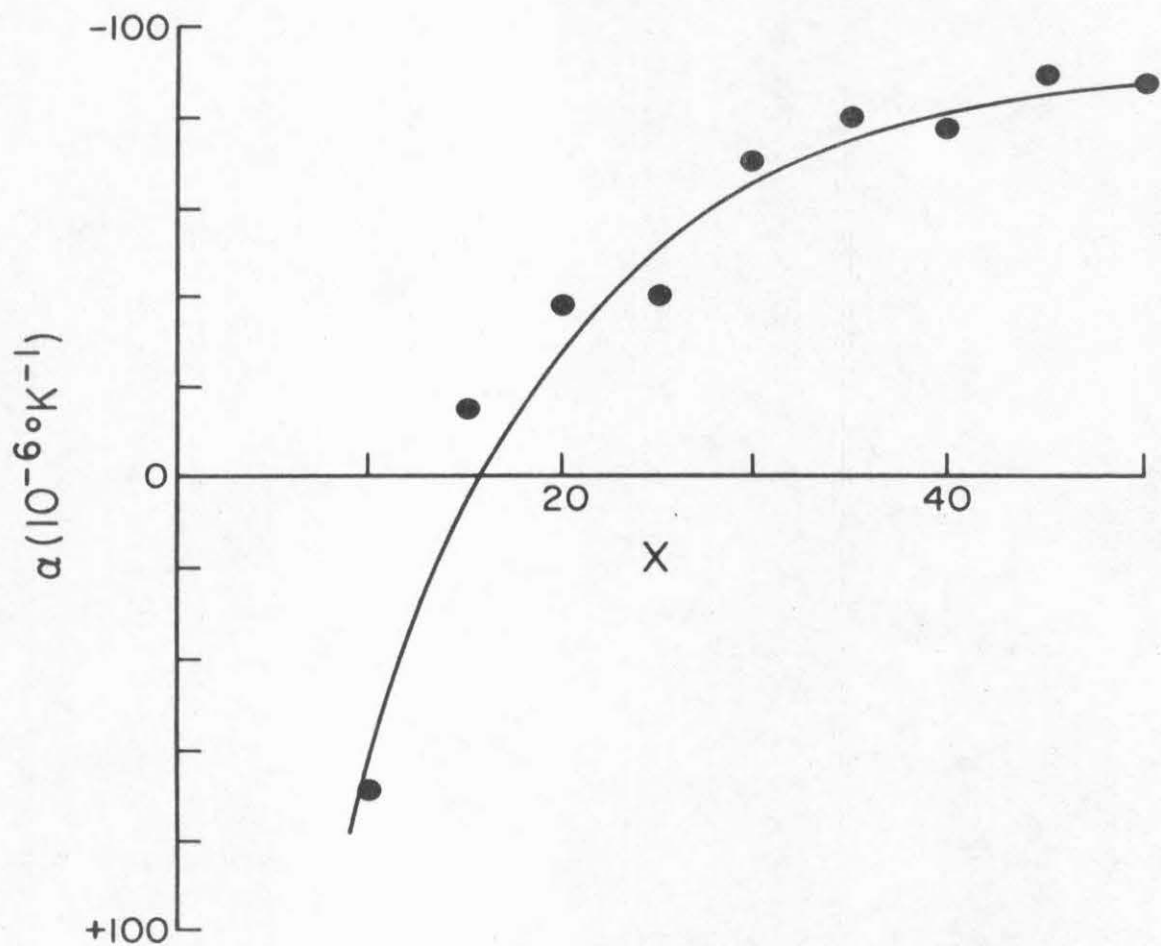


Fig. 28 Temperature Coefficients of Resistivity for  $(\text{Pd}_{100-x}\text{Cu}_x)_{80}\text{P}_{20}$  Alloys

In the following sections the results of the experimental measurements are compared to the results of previous studies on the Pd-Ni-P and Pt-Ni-P alloys. The different models for the electrical resistivity decrease with temperature proposed by Sinha<sup>(8)</sup> and Hasegawa<sup>(9)</sup> discussed in the light of the present results and objections are given based on theoretical results. Both models are found to be unsatisfactory and an alternate approach is given. This approach is based on the realization that the negative temperature coefficients observed in these alloys follow the Mooij correlation for numerous crystalline transition metal alloys, there being a commonality of behavior of these amorphous alloys with the crystalline alloys. The model of the phonon induced modification of the density of states discussed by Chen et al. and Brouers and Brauwiers is used to explain the origin of the negative temperature coefficient of resistivity.

The  $(\text{Ni}_x\text{Pt}_{1-x})_{75}\text{P}_{25}$  Alloys Studied by Sinha

Sinha has studied the structure and measured the electrical properties of the amorphous alloy having the composition  $(\text{Ni}_x\text{Pt}_{1-x})_{75}\text{P}_{25}$  where  $0.20 \leq x \leq 0.60$ . The x-ray diffraction measurements indicated a higher degree of structural disorder in these alloys and an atomic arrangement similar to the liquid metals, in that the RDF does not have a double peak beyond the first maximum as evidenced by the absence of a shoulder on the high angle side of the second peak of  $a(k)$ . At room

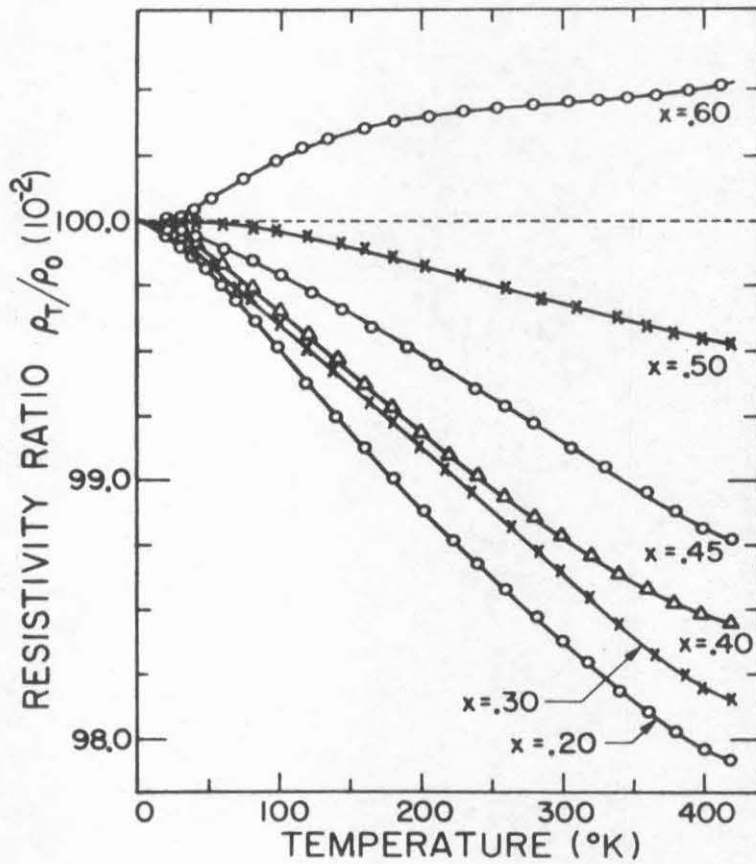


Fig. 29 Resistivity ratio  $\rho(T)/\rho(0)$  for  $(\text{Pt}_{1-x}\text{Ni}_x)_{75}\text{P}_{25}$  alloys (Sinha).

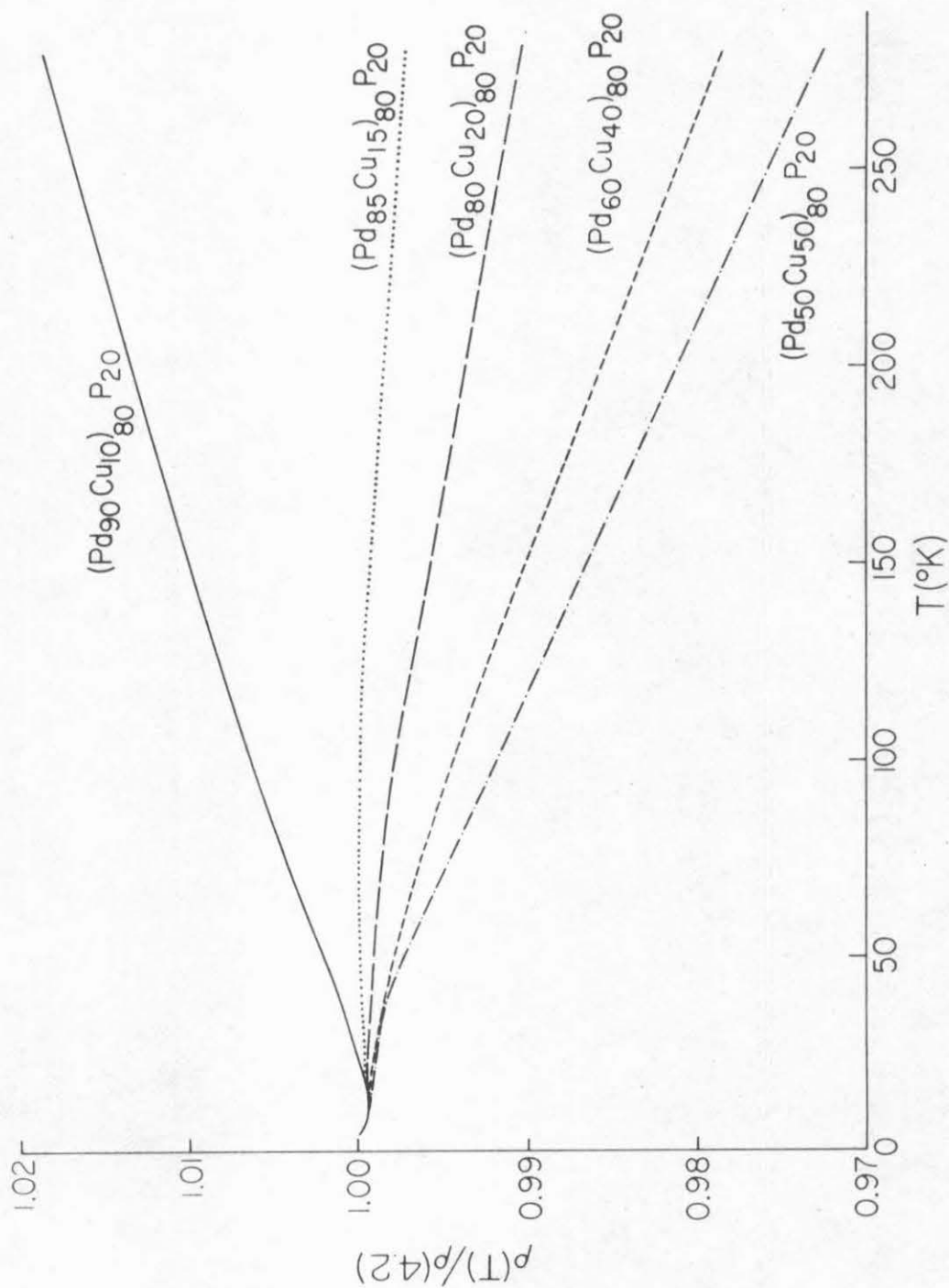


Fig. 30 Reduced Resistivity  $\rho(T)/\rho(4.2)$  for (Pd<sub>100-x</sub>Cu<sub>x</sub>)<sub>80</sub>P<sub>20</sub> Alloys

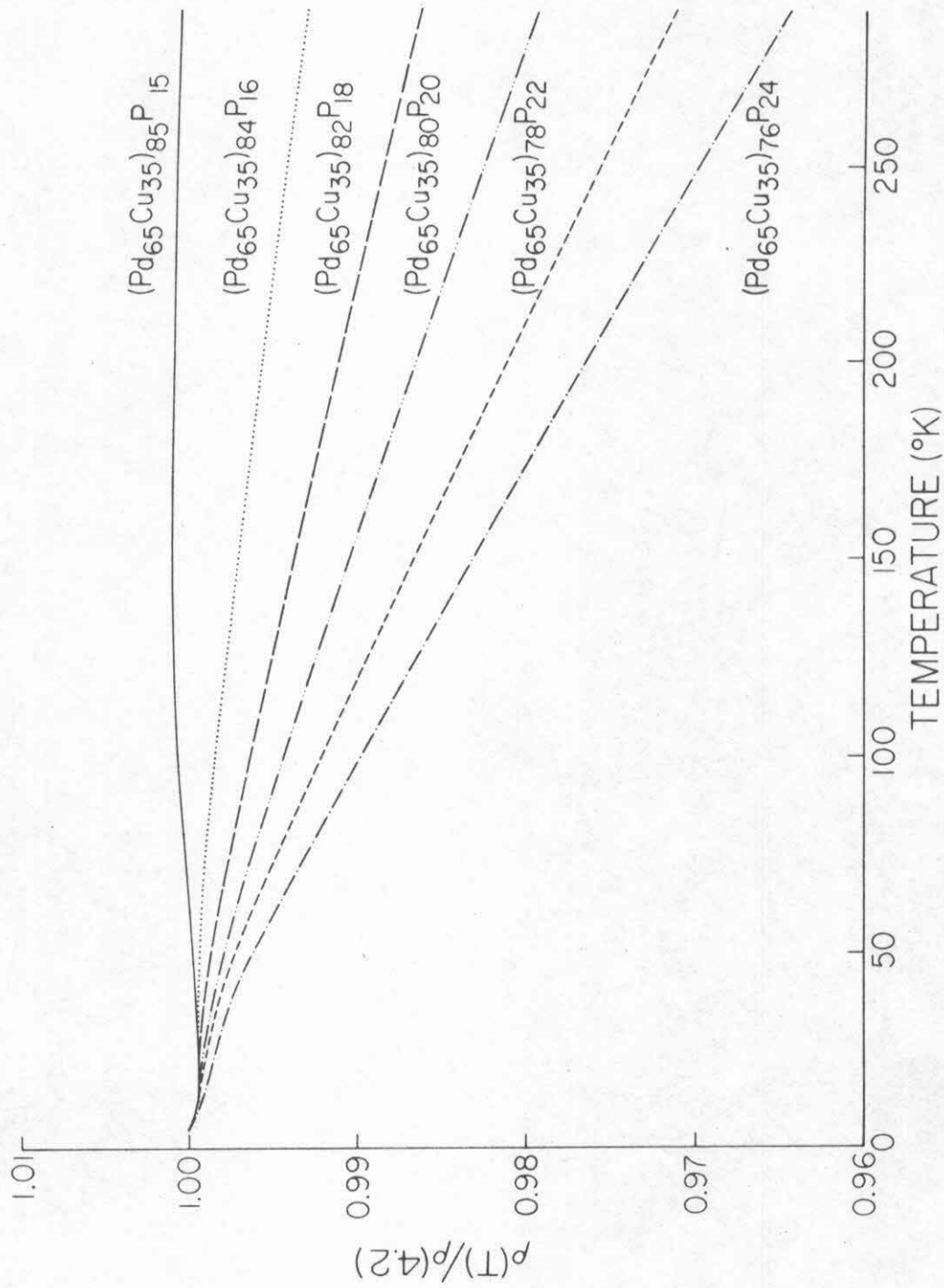


Fig. 31 Reduced Resistivity  $\rho(T)/\rho(4.2)$  for  $(Pd_{65}Cu_{35})_{100-y}P_y$  Alloys

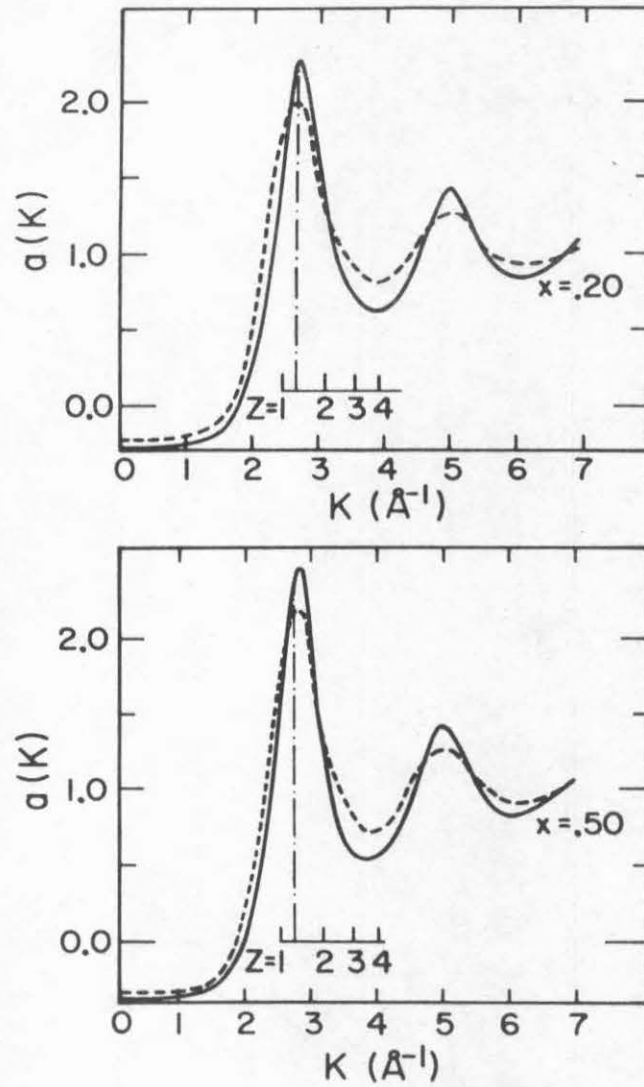


Fig. 32  $a(K)$  versus temperature and composition for  $(Pt_{1-x}Ni_x)_{75}P_{25}$  alloys. The dashed curve represents higher temperature  $a(K)$ . (Sinha)

temperature the electrical resistivity  $\rho$  in these alloys lies between 160 and 185  $\mu\Omega$  cm. On increasing  $x$ , no obvious trend in  $\rho$  at room temperature is seen over the  $0.20 < x < 0.60$  change in  $x$ , and the spread in the measured resistivity at room temperature is mostly experimental in origin due to the thickness uncertainty. On increasing the temperature from 4 to 420°K ( $T_g$ ) the resistivity of the alloys with  $x = 0.20$  decreases by about 2%; the value of  $\frac{1}{\rho} \frac{d\rho}{dT}$  progressively increases with increasing Ni content, becoming positive at  $0.50 < x < 60$ . The resistivity ratio  $\rho(T)/\rho(0)$  is shown in Fig. 29 for Pt-Ni-P alloys, the value  $\rho(0)$  being obtained by subtracting the Kondo-like portion of  $\rho$  at low temperatures and extrapolating to zero. For comparison the uncorrected values of  $\rho(T)/\rho(4.2)$  for Pd-Cu-P is shown in Figs. 30 and 31.

Sinha proposed that the electron scattering in the disordered structures may be treated in a manner analogous to Ziman's theory of electron transport in liquid metals. The Ziman theory predicts that negative temperature coefficients of resistivity occur for liquids with the average valency of  $z$  of  $1 < z < 2$  as shown in Fig. 32. Sinha asserts that the  $d\rho/dT$  of the Pt-Ni-P alloys is then qualitatively explained in terms of the temperature and composition dependence of the x-ray interference function  $a(k)$ , assuming an average number of 1.3 conduction electrons per atom in these alloys. For the alloy with  $x = 0.20$  this implies a Fermi energy of 6.9 eV, which for a free electron model positions  $2k_F$  at the first peak of  $a(k)$ . An increase in Ni content of the alloy causes a shift in the first peak in the  $a(k)$  toward higher  $k$  values. This fact is established from the increase in

density from  $0.063 \text{ atoms}/\text{A}^3$  to  $0.067 \text{ atoms}/\text{A}^3$  in going from  $x = 0.20$  to  $x = 0.50$ . This shift of the  $a(k)$  peak has the effect of shifting  $2k_F$  toward a region where  $a(k)$  increases with temperature as shown in Fig. 32, thus  $\frac{1}{\rho} \frac{d\rho}{dT}$  becomes more positive with increasing Ni concentration.

Several objections to Sinha's interpretation may be raised. The general question of the applicability of Ziman theory to an amorphous solid is worth discussion. The first peak of  $a(k)$  is presumed in liquid metals to decrease and broaden with increasing temperature enough to account for the decrease in  $\rho$  with temperature. Such a temperature dependence of  $a(k)$  has been experimentally established by Halder et al.<sup>(10)</sup> for liquid Cu-Sn alloys. The value of  $2k_F$  falls at the position of the peak of  $a(k)$  and the observed decrease of 18% of the peak height over a  $360^\circ\text{C}$  temperature increase is enough to explain the negative  $d\rho/dT$  in these alloys. Wingfield and Enderby<sup>(11)</sup> have performed neutron diffraction measurements on liquid zinc and have observed a decrease of  $a(q)$  with temperature which is too small to explain the  $-130 \times 10^{-6} \text{ }^\circ\text{K}^{-1}$  temperature coefficient of resistivity for liquid zinc. While the alloy  $(\text{Ni}_{0.20}\text{Pt}_{0.80})_{0.75}\text{P}_{0.25}$  has a rate of decrease of only  $-49 \times 10^{-6} \text{ }^\circ\text{K}^{-1}$ , it is difficult to envisage structural rearrangements of the frozen amorphous solid being in any way comparable in magnitude to that in liquid metals. More importantly, for the Pd-Cu-P,  $\alpha$ 's of up to  $-120 \times 10^{-6} \text{ }^\circ\text{K}^{-1}$  are observed, which must be explained. It is worth noting that in the Pt-Ni-P and Pd-Cu-P the resistivity is decreasing almost as rapidly at  $100^\circ\text{K}$  to  $150^\circ\text{K}$  as it is at the range of crystallization temperatures of  $400^\circ\text{K}$ - $550^\circ\text{K}$ . At

low temperatures the solid has hardly achieved the full degrees of freedom of the liquid, and yet the rates of decrease of resistivity with temperature are as high as the high temperature rates.

Further objections can be traced to the assumption of the valency of 1.3 conduction electrons per atom for these transition metal-rich alloys, where normally only  $\sim 0.5$  conduction electrons are expected. To achieve the 1.3 value of  $z$  for the Pt-Ni-P alloys, the phosphorus atoms must contribute up to 4 electrons per atom to the transition metal energy band states. The electronegativity values of Pd and P do not differ appreciably (Pd 2.2, and P 2.4), and yet, if the  $z = 1.3$  is admitted, a very large charge transfer must occur in these alloys.

#### Spin Fluctuation Model for Amorphous Metals

Following the study of  $(\text{Ni}_x\text{Pt}_{100-x})_{75}\text{P}_{25}$  alloys by Sinha, Boucher<sup>(12)</sup> and Maitrepierre<sup>(13)</sup> studied the amorphous alloys  $(\text{Pd}_x\text{Ni}_{1-x})_{1-y}\text{P}_y$ . In Maitrepierre's work on  $(\text{Pd}_{100-x}\text{Ni}_x)_{80}\text{P}_{20}$  alloys ( $16 \leq x \leq 91$ ) no systematic variation in the temperature coefficient of resistivity between 40°K and about 550°K was found within the rather large uncertainty range resulting from the variation in the average rate of quenching from specimen to specimen. In Fig. 33 is shown the result of Maitrepierre and Boucher's work for alloys of fixed phosphorus concentration; the data points due to Boucher's work

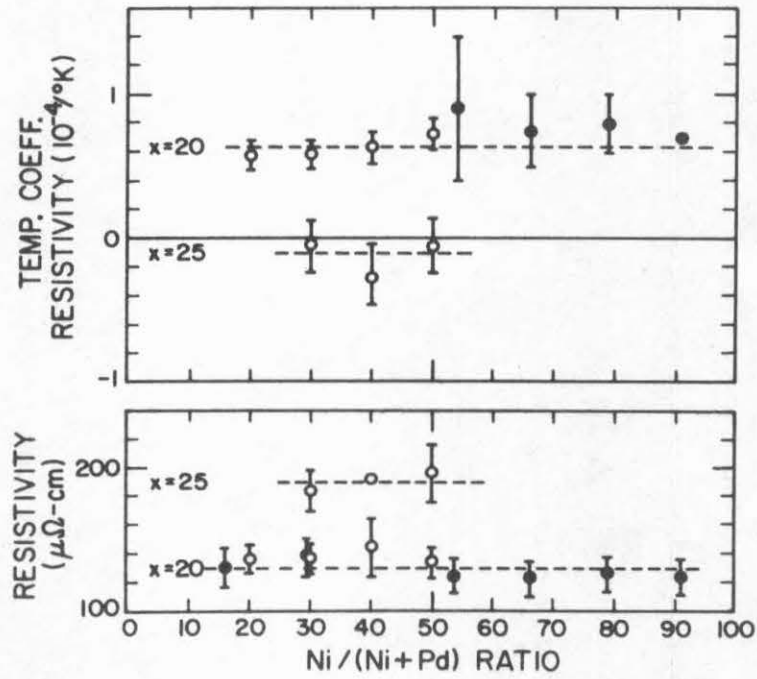


Fig. 33a Transition metal composition dependence of  $\rho$  and  $\alpha$  for  $(\text{Pd}_{100-y}\text{Ni}_y)_{100-x}\text{P}_x$  alloys (Boucher and Maitrepierre).

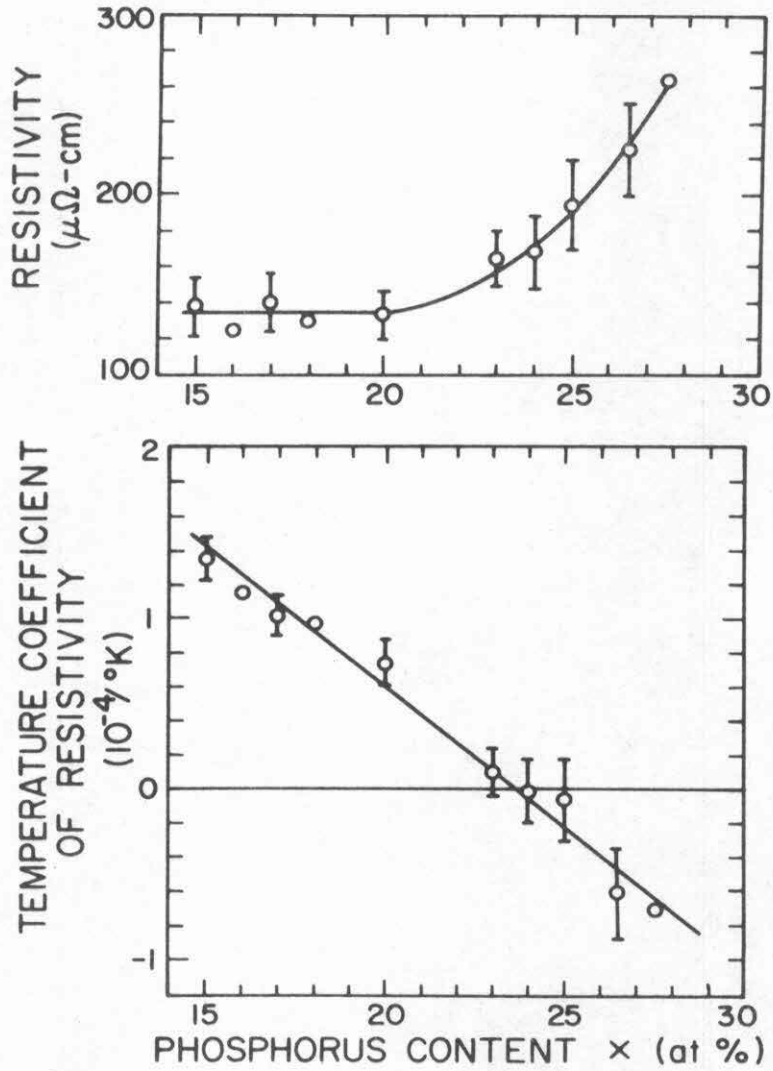


Fig. 33b Metalloid composition dependence of  $\rho$  and  $\alpha$  for  $(\text{Pd}_{50}\text{Ni}_{50})_{100-x}\text{P}_x$  alloys (Boucher).

are those with a phosphorus concentration of 25. For the alloys studied by Maitrepierre, the low temperature (4-20°K) resistivity behavior shows a Kondo minimum. The resistivity increases with increasing temperature at  $T^2$  up to about 40°K, after which a  $T$ -dependent increase of resistivity is observed up to  $T_g$ . The average temperature coefficient of resistivity of  $+60 \times 10^{-6} \text{ } ^\circ\text{K}^{-1}$  was attributed to the large disorder of the amorphous structure which makes the contribution of phonon scattering small. The main temperature dependence of the resistivity was interpreted as being due to the temperature dependence of  $a(k)$ , as discussed by Sinha. To explain the positive coefficient, an average valence of 0.5 to 1.0 electrons per atom was assumed by Maitrepierre. Boucher's measurement of the dependence of the resistivity behavior with phosphorus concentration is most interesting. The changes in P concentration have a strong effect on the temperature coefficient of resistivity with a change of sign from positive to negative at around 24% P, the phosphorus range for the  $(\text{Pd}_{50}\text{Ni}_{50})_{100-y}\text{P}_y$  alloys being  $17 \leq y \leq 26.5$ . In Fig. 33 are plotted the results of Boucher's measurements of the room temperature values of  $\rho$  and  $\alpha$ . This marked sensitivity of both  $\rho$  and  $\alpha$  to phosphorus concentration is in contrast to the insensitivity of both  $\rho$  and  $\alpha$  to changes in Ni concentration with  $\rho$  constant as found by Maitrepierre. The  $\rho(T)/\rho(293)$  plot for these alloys is given in Fig. 34.

Any interpretation of the Pd-Ni-P data along the lines of Sinha's structural scattering model must meet the same objections mentioned previously. Hasegawa<sup>(9)</sup> has attempted to explain the Pt-Ni-P

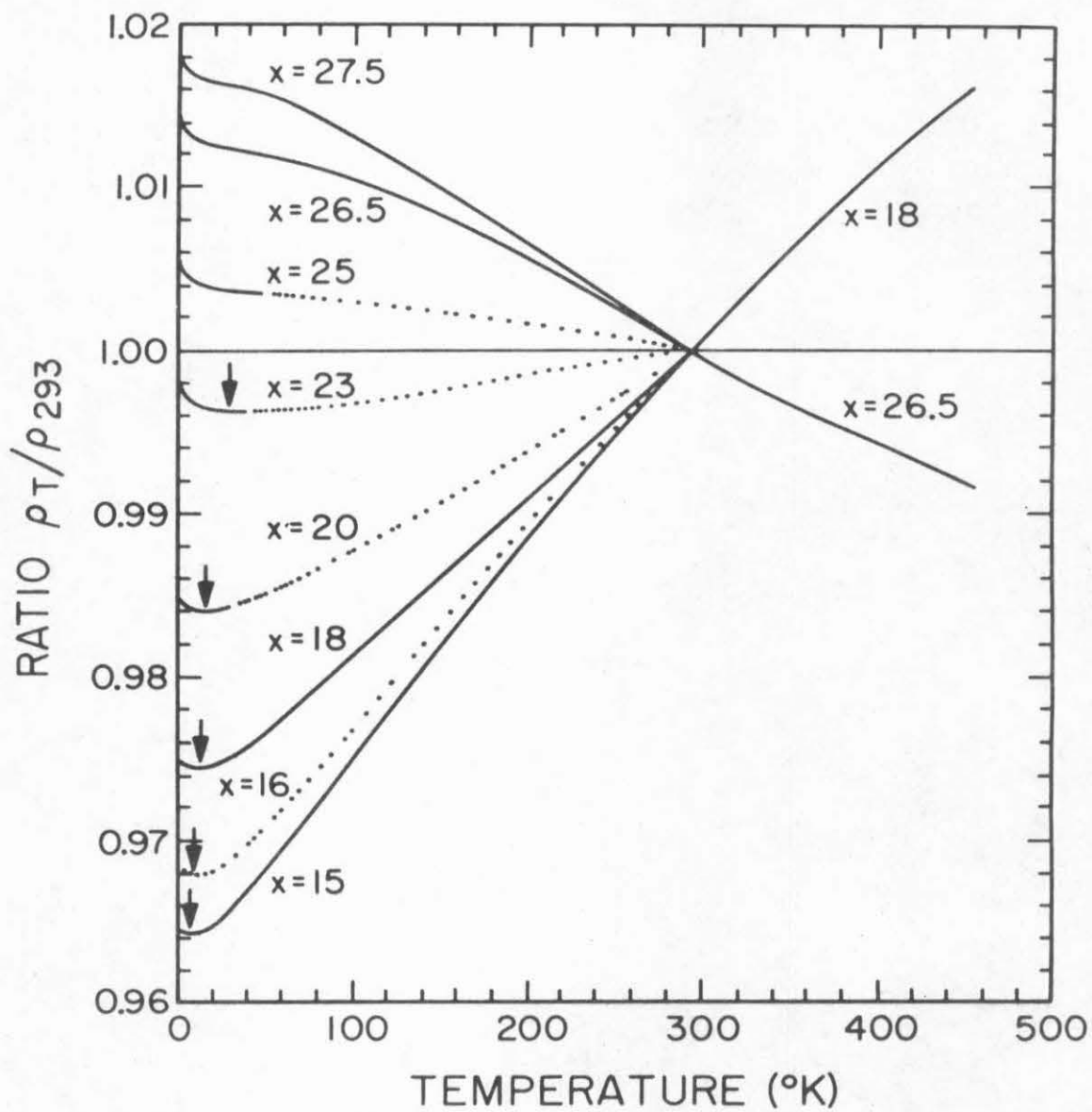


Fig. 34 Reduced Resistivity  $\rho(T)/\rho(293)$  for  $(\text{Pd}_{50}\text{Ni}_{50})_{100-x}\text{P}_x$  Alloys (Boucher).

and Pd-Ni-P results in terms of a spin fluctuation model discussed by Lederer and Mills<sup>(14)</sup> and Kaiser and Doniach.<sup>(15)</sup> The basic assumptions and results of this theory are discussed in this section along with their application to palladium-based amorphous alloys.

For a metal-like Pd, if we denote the density of states at the Fermi level in the d-band by  $N(0)$ , and the intra-atomic Coulomb interaction between two electrons in the same unit cell by  $V_0$ , then a simple Hartree-Fock theory<sup>(16)</sup> indicates that the susceptibility of the metal is larger than the Pauli free electron susceptibility by the factor  $[1 - V_0 N(0)]^{-1}$ . If  $V_0 N(0) > 1$  the theory predicts the system is unstable with respect to the ferromagnetic state. For Pd,  $V_0 N(0) \approx 0.9$ <sup>(17)</sup>, and because of this the repulsive intra-atomic Coulomb interactions are so strong that the d-band is near the threshold of instability. The addition of less than 2% Ni into the Pd matrix leaves the alloy nonmagnetic, while if the Ni concentration exceeds 2% the Ni sites acquire a moment and the spins order. With only such small concentration being involved, it is clear that the intra-atomic Coulomb interaction  $V_I$  associated with a Ni cell is very close to the critical value required for moment formation. If  $V_I > V_0$  then one can expect the region of space in the vicinity of the Ni cell to be much closer to the magnetic instability than in the Pd matrix. So it is plausible to expect the low frequency fluctuations in spin density in the d-band are enhanced considerably in the vicinity of the Ni cell. The s-electrons, which in Pd carry the major portion of the current, can scatter from these local spin fluctuations. Since the amplitude of

the fluctuations varies with the temperature. This can lead to a single-impurity contribution to the resistivity which is temperature dependent.

In dilute alloys like PdNi, AlMn, AlCr, PtCr, IrFe and RhFe, evidence for the occurrence of large amplitude spin fluctuations causing "anomalous" resistivity behavior has been given. For instance, in the AlCr and AlMn alloys studied by Caplin and Rizzuto<sup>(18)</sup> the low temperature resistance goes as  $\rho = \rho_0 [1 - (T/\theta)^2]$  where  $\theta = 530^\circ\text{K}$  and  $1200^\circ\text{K}$  for Mn and Cr, respectively. This behavior has been correlated with the enhanced Pauli susceptibility of these alloys for these nearly magnetic impurities. A clear prerequisite for large spin fluctuation contributions to the resistivity to be observed is that either the impurity is very nearly magnetic as discussed by Friedel<sup>(19)</sup> and Anderson<sup>(20)</sup>, or that the magnetic impurity enhances the local intra-atomic Coulomb interaction between two electrons of a nearly ferromagnetic matrix like Pd.

Hasegawa has fitted the Pt-Ni-P and Pd-Ni-P resistivity results to a temperature dependence of:

$$\begin{aligned}\rho_{\text{phonon}} &= A + BT^2 \quad \text{for low } T \\ &= C + DT \quad \text{for high } T\end{aligned}$$

$$\begin{aligned}\rho_{\text{spin}} &= E - FT^2 \quad \text{for low } T \\ \text{fluctuations} & \\ &= G - HT \quad \text{for high } T\end{aligned}$$

where all coefficients are positive. The calculations of Kaiser and Doniach<sup>(15)</sup> show that a universal curve for the spin fluctuation exhibits

resistivity in which the temperature dependence changes from  $T^2$  to  $T$  at temperatures of the order of 0.25 of the characteristic  $T_S$ , where  $K_B T_S$  is the energy of the peak of the localized spin fluctuation excitation spectrum. In the presence of resonance scattering, the effects of spin fluctuations is to force the scattering off resonance, and negative coefficients can occur. Hasegawa obtains for Pt-Ni-P,  $T_S = 120^\circ\text{K}$ , and for Pd-Ni-P,  $T_S = 450^\circ\text{K}$ , which agree somewhat with the observed results.

It is, however, very difficult to envisage that the spin fluctuation model holds true at all in the Pd-Cu-P alloys, and even its application to Pd-Ni-P and Pt-Ni-P alloys leaves unexplained certain experimental facts. The Pd-Ni-P and Pt-Ni-P alloys are weakly magnetic,  $\chi \approx 10^{-7}$  emu/g, and show no enhanced exchange susceptibility. The resistivity and the negative temperature coefficients of resistivity in these alloys are insensitive to the changes in Ni concentration. Only in dilute alloys have large spin fluctuation effects been observed. In fact for PdNi alloys the addition of more Ni (above 2%) has the effect of limiting the range of temperature over which the spin fluctuation component is dominant over the phonon scattering ( $T^5$ ).

For the Pd-Cu-P alloys the use of the spin fluctuation model meets an obvious difficulty: Cu cannot serve to enhance the local intra-atomic Coulomb interaction as Ni is presumed to do for Pd-Ni-P and Pt-Ni-P alloys. The non-magnetic nature of Cu certainly precludes this from happening. The experimental results on Pd-Cu-P indicate: the temperature coefficient of resistivity and the resistivity are quite sensitive to variations of Cu concentration; the temperature

coefficients of resistivity are all negative for alloys with  $x > 15$  and the temperature dependence of resistivity is quite similar in shape to the Pd-Ni-P and Pt-Ni-P alloys. These results are certainly difficult to explain using the spin fluctuation model.

It is worth noting that scattering off giant polarization clouds in crystalline  $\text{Ni}_{35}\text{Cu}_{65}$  alloys has been proposed by Houghton et al.<sup>(21)</sup> to explain the anomalous resistivity behavior of this alloy. Ahmad and Greig<sup>(22)</sup> have shown that an alloy of  $\text{Pd}_{60}\text{Ag}_{40}$ , which is certainly not even almost magnetic, has similar behavior. This situation is quite similar to that described here between the measured Pd-Cu-P data results and their similarity to the Pd-Ni-P and Pt-Ni-P data which are explained by a similar spin-fluctuation model also.

The comparison we have made of the Pd-Cu-P data with the systems Pt-Ni-P and Pd-Ni-P point out the relevance of this work to past studies of amorphous materials. Both the structural scattering model proposed by Sinha and the spin-fluctuation model proposed by Hasegawa have inherent difficulties when applied to the resistivity behavior of the amorphous alloys Pt-Ni-P, Pd-Ni-P and Pd-Cu-P and yet, in a general sense, the temperature dependence of the electrical is quite similar. This commonality of behavior of these amorphous materials will be shown to be shared with numerous crystalline transition metal alloys in the following section. Recognition of this fact leads quite naturally to an explanation of the electrical properties of these materials.

### Comparison with Crystalline Transition Metal Alloys

Metallic systems with high resistivity due to strong s-d scattering and low temperature coefficients of resistivity are of interest in the production of high-quality resistors. Perhaps best known for these applications are the  $\text{Ni}_x\text{Cr}_{1-x}$  alloys, for which the temperature coefficient of resistivity is far below that expected (for pure Ni  $\alpha$  is  $7 \times 10^{-3} \text{ }^\circ\text{K}^{-1}$ ). In the concentration range  $20 < x < 80$ ,  $\rho$  is about  $110 \mu\Omega \text{ cm}$  and  $\alpha$  is around  $100 \times 10^{-6} \text{ }^\circ\text{K}^{-1}$ , with this low  $\alpha$  persisting down to low temperatures ( $4^\circ\text{K}$ ). In thin films of NiCr, three different crystal structures have been observed: up to  $x = 50$  the fcc structure is found, between  $x = 25$  and  $x = 50$  an unidentified phase is found, and for  $x < 25$  the bcc structure is found. Despite these variations in structure, no influence of the phase changes on the measured resistivity is observable, and  $\alpha$  remains at  $100 \times 10^{-6} \text{ }^\circ\text{K}^{-1}$  for  $60 < x < 80$ . Several other materials with high  $\rho$  and low  $\alpha$  are known such as CuNi, FeCrAl and TaN, all having properties resembling NiCr. Mooij<sup>(23)</sup> has surveyed the literature and listed the systems for which  $\alpha < 100 \times 10^{-6} \text{ }^\circ\text{K}^{-1}$  is found for some composition range. In all the alloys listed the weak temperature dependence of the resistivity persists to low temperature, with exceptions for those systems with order-disorder transitions occurring. In Table 2 are listed the many systems which have  $\alpha < 100 \times 10^{-6} \text{ }^\circ\text{K}^{-1}$  in either bulk or thin film form. In all cases the low  $\alpha$  is found in concentrated alloys; usually at least 20% admixture is required. Ternary systems have also been studied and, in general,

Table 2. Crystalline Systems with  $\alpha < 100$  ppm/°K

BULK ALLOYS

AgPd  
AlFe  
AlTi  
AlV  
CrNi  
CuMn  
CuNi  
CuPd  
CuPt  
MnNi  
MnPd  
MoTi - *super*  
MoU - *super*  
NbTi - *super*  
PtW  
TiV  
UZr  
NbPdAl  
NiCrPd  
FeCrAl  
NiCrAl

THIN FILMS

AlNb  
AlTa  
AgMn  
AuCr  
NTa

the addition of a third element to a binary alloy with low  $\alpha$  has not been found to cause the disappearance of the low  $\alpha$ . The addition of a third element to a system with high  $\alpha$  causes  $\rho$  to increase or be constant, while  $\alpha$  may decrease markedly. In the FeCr system, the addition of 10% Al increases  $\rho$  (from  $50\mu\Omega$  cm to  $125\mu\Omega$  cm) and lowers  $\alpha$  from  $1000 \times 10^{-6}\text{K}^{-1}$  to  $100 \times 10^{-6}\text{K}^{-1}$ . Mooij also points out that negative  $\alpha$ 's occur in a number of alloys. For some, like CuNi alloys, above the Curie point, and  $\text{Ni}_{80}\text{Cr}_{20}$  around  $600^\circ\text{C}$  where short range orderings occur, negative  $\alpha$ 's occur over a restricted temperature range. For many systems a negative temperature dependence of resistance is found over a wide temperature range. In Fig. 35 is plotted the resistivity versus temperature for bulk  $\text{Ti}_{67}\text{Al}_{33}$  for which negative temperature coefficients of resistivity occur for the  $80^\circ\text{K}$  to  $1100^\circ\text{K}$  range. Similar results are found for  $\text{Ti}_{80}\text{V}_{20}$ <sup>(24)</sup>,  $\text{U}_{30}\text{Zr}_{70}$ <sup>(25)</sup>,  $\text{VA1}$ <sup>(26)</sup> in bulk alloys, and for  $\text{TaAl}$ <sup>(27)</sup>,  $\text{TaN}$ <sup>(28)</sup>, and  $\text{NiCrAl}$ <sup>(24)</sup> in thin film.

Most surprising is the existence of a correlation between  $\alpha$  and  $\rho$  (which we refer to as the Mooij correlation). In Fig. 36 are plotted the measured temperature coefficients of resistivity for bulk alloys and thin film alloys. It is clear that no negative  $\alpha$  is observed for resistivities below  $100\mu\Omega$  cm, while above  $150\mu\Omega$  cm hardly any positive  $\alpha$  is found.

Any explanation of this behavior based on the structural dependence of the d-band structure is certainly ruled out due to the varieties of structures involved in the Mooij correlation. The

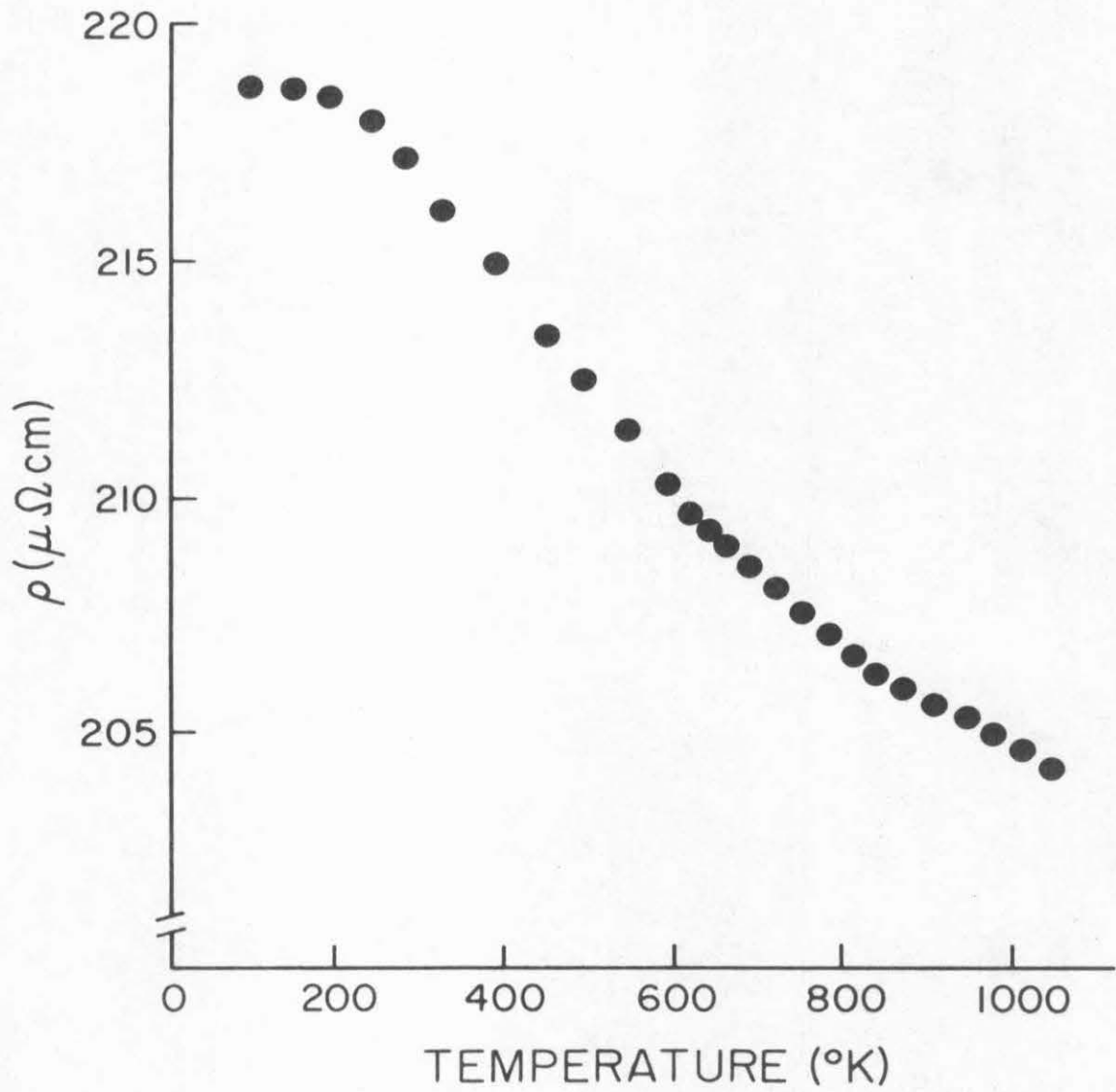


Fig. 35 Resistivity of Bulk  $\text{Ti}_{67}\text{Al}_{33}$  versus Temperature

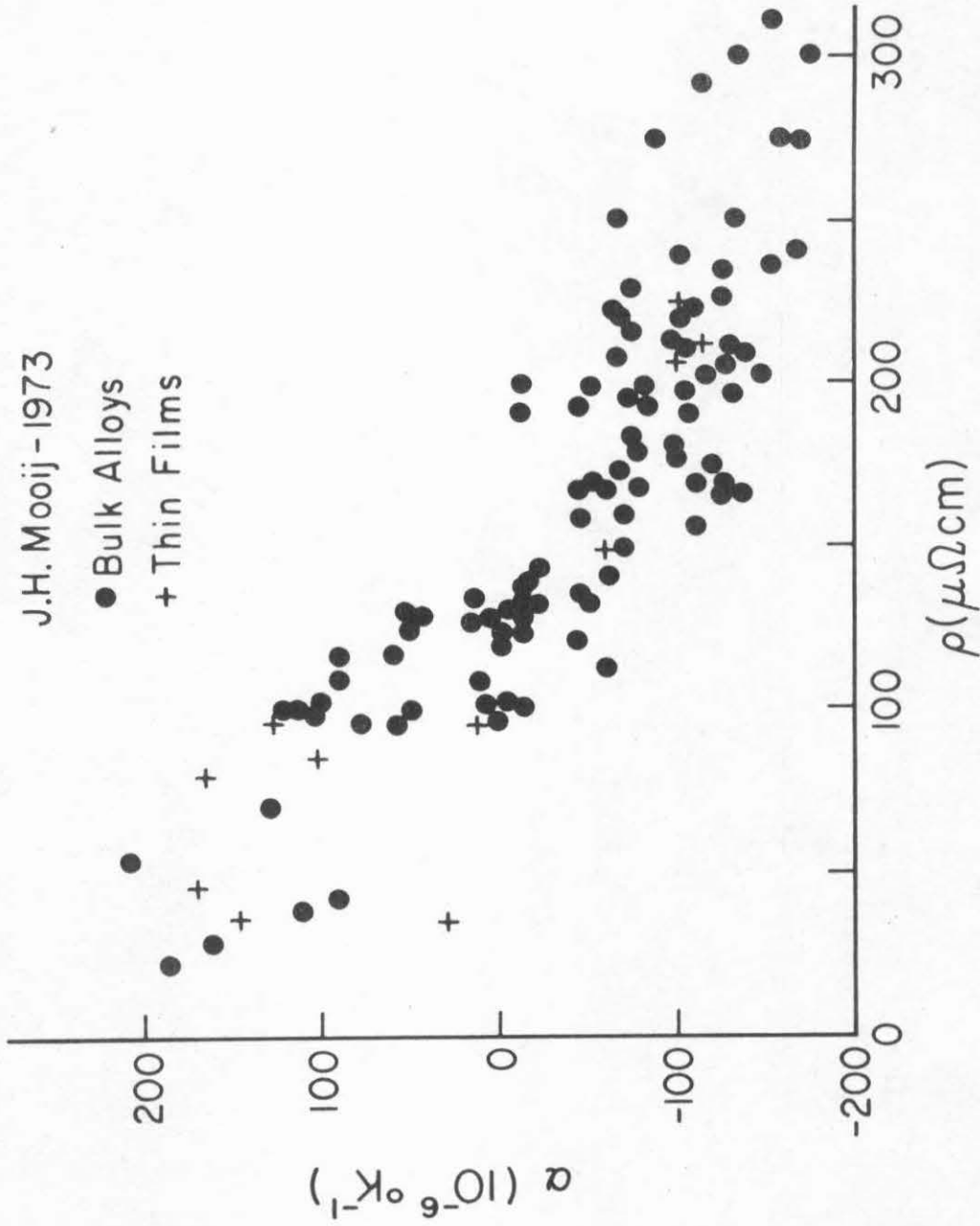


Fig. 36 Temperature Coefficient of Resistivity versus Resistivity for Bulk Alloys and Thin Films (Mooij).

occurrence of negative temperature coefficients of resistivity is a consequence of the same causes which yield low values of  $\alpha$ . The mean free path for these resistivity levels is small, and for NiCr alloys has been calculated to be approximately  $4\text{\AA}$  or slightly larger than the interatomic distance.<sup>(29)</sup> Certainly for these small values of the mean free path, differences of structural properties have a minimal effect on the temperature dependence of the resistivity.

In Fig. 37 the  $\alpha$  versus  $\rho$  plot for amorphous Pd-Ni-P, Pt-Ni-P and Pd-Cu-P alloys is shown. A comparison of these results with the Mooij correlation shown in Fig. 36 reveals a remarkable conformity of the data for amorphous alloys with those for the numerous crystalline transition metal alloys surveyed by Mooij. Thus the "anomalous" behavior of  $\rho(T)$  in these amorphous alloys is not due to the unique amorphous nature, as the explanation of Sinha suggests, and not due to their magnetic properties as the spin fluctuation model of Hasegawa suggests. The variety of structural and magnetic properties involved in the Mooij correlation of numerous alloys establishes this fact.

The observation of negative temperature coefficients of resistivity over large temperature ranges indicates that in these very strong scattering cases the role of lattice vibrations is actually to assist the conduction of electrons. Chen et al.<sup>(30)</sup> and very recently Brouers and Brauwers<sup>(31)</sup> have shown that the effect of phonons in modifying the d-density of states at the Fermi level through the electron-phonon interaction is significant and can cause the resistivity to decrease with temperature due to the blurring of the density of

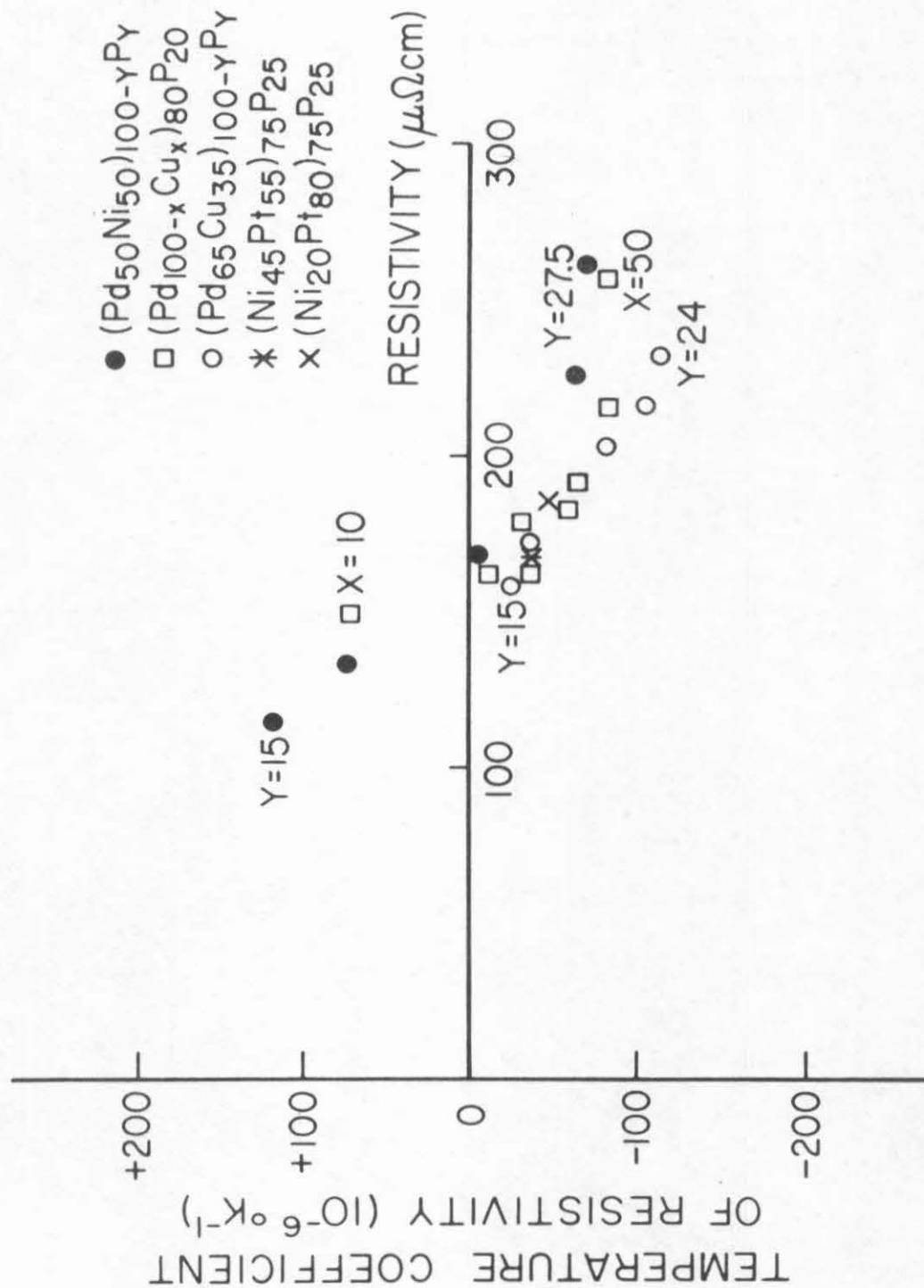


Fig. 37 Temperature Coefficients of Resistivity of Amorphous Pd-Ni-P, Pt-Ni-P and Pd-Cu-P Alloys

states with temperature. Details of these calculations will be given in a later section. It suffices to say that the comparison of the experimental results with crystalline systems leads to a natural re-interpretation of the "anomalous" resistivity behavior in the amorphous systems which emphasizes the commonality of this behavior of  $\rho(T)$  with disordered crystalline transition metal alloys.

### An Alternate Explanation of the Resistivity Behavior

An alternate explanation of the resistivity behavior of the amorphous alloy Pd-Cu-P, Pd-Ni-P and Pt-Ni-P is given along the following lines. First the order of magnitude of the resistivity for these alloys is explained using the Evans, Greenwood and Lloyd (EGL) formalism for the resistivity in liquid transition metal alloys. Second, the concentration dependence of  $\rho$  is discussed in the context of the EGL formalism to point out how the interplay of structural scattering and resonance scattering leads to the observed concentration dependencies in amorphous alloys. Lastly, the negative temperature coefficients of resistivity is explained along the lines of the modification of density of states at  $E_F$  through the thermal blurring of the d-state energies by the electron-phonon interaction.

#### The Magnitude of the Observed Resistivities

From the experimentally determined resistivities of the  $(Pd_{100-x}Cu_x)_{80}P_{20}$  and  $(Pd_{100-x}Ni_x)_{80}P_{20}$  alloys, an extrapolated value of  $\rho$  for an amorphous  $Pd_{80}P_{20}$  alloy of  $\approx 130 \mu\Omega$  is obtained. For  $(Pt_{100-x}Ni_x)_{75}P_{25}$  the resistivity for a  $Pt_{75}P_{25}$  alloy is  $\approx 175 \mu\Omega$  cm. It is of interest to ascertain whether a level of resistivity of  $\approx 150 \mu\Omega$  cm can be calculated from first principles using the theoretically derived formulas for the resistivity of liquid transition metals obtained by EGL. (32)

EGL extended Ziman's formula using physical arguments by replacing the pseudopotential by the t matrix of the muffin tin potential for one ion. An exact expression for the resistivity in terms of the phase shifts and the ion positions in agreement with Ziman's formula is derived:

$$\rho = \frac{3\pi\Omega_0}{4e^2\hbar V_F^2 K_F^4} \int_0^{2K_F} a(k) |t(k)|^2 k^3 dk$$

where  $\Omega_0$  is the atomic volume,  $V_F$  is the Fermi velocity, and  $t(k)$  is the single site t-matrix which is defined in the partial wave representation as

$$t(k) = \frac{-2\hbar^3}{m(2mE)^{1/2}} \sum_{\Omega_0 \ell} (2\ell+1) \sin \eta_\ell(E) \exp[i\eta_\ell(E)] P_\ell(\cos \theta)$$

where  $m$  is the electron mass,  $E_F$  is the Fermi energy (measured relative to the muffin tin zero), and the sum is over all the various partial waves contributing to the scattering.  $P_\ell(\cos \theta)$  is the Legendre polynomial of order  $\ell$  and the  $\eta_\ell$  are the partial wave phase shifts describing the scattering of the conduction electrons by the ion cores. If the  $\eta_2$  phase shift is dominant, as it is expected to be in transition metals, the electrical resistivity can be written in the following ways:

$$\rho = \frac{30\pi^2\hbar^3}{e^2 m K_F^2 \Omega_0 E_F} a(2K_F) \sin^2 \eta_2(E_F)$$

or

$$= \frac{30\pi^2\hbar^3}{e^2 m K_F^2 \Omega_0 E_F} a(2K_F) \frac{\Gamma^2}{\Gamma^2 + (E_0 - E_F)^2}$$

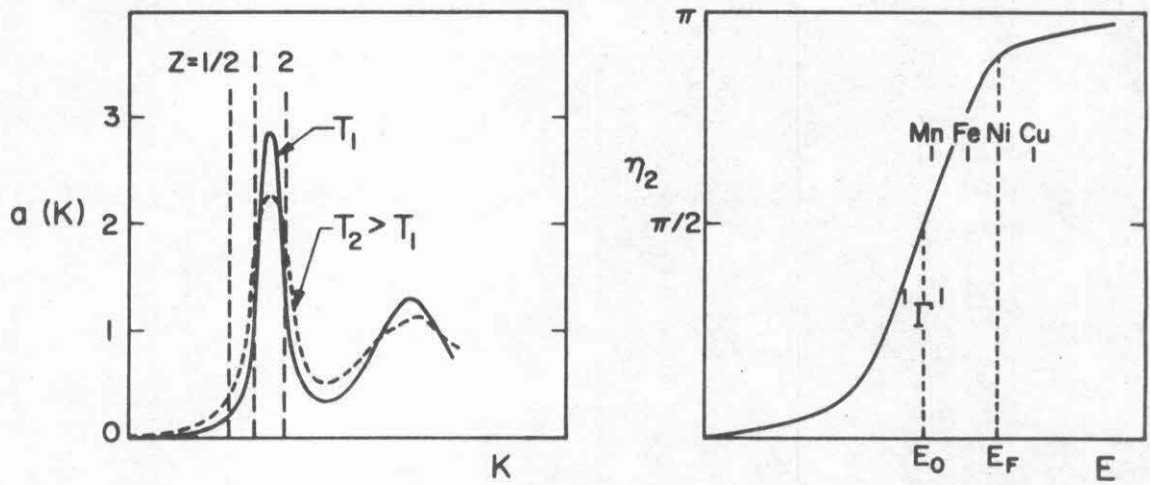


Fig. 38 Schematic diagram of the parameters  $a(K)$  and  $\eta_2$  involved in determining the electrical resistivity in liquid transition metals.

where  $\Gamma$  is the width and  $E_0$  is the position of the d resonance. A schematic diagram of the interplay between the structural scattering (as determined by the  $a(2K_F)$  factor) and the resonance scattering (as determined by  $\eta_2$ ) is shown in Fig.38. Clearly, the determination of  $\rho$  requires accurate structural data ( $a(k)$  and the density) and the determination of accurate values of  $\eta_2$ ,  $E_F$  and  $K_F$ . The major difficulty lies in the determining of the resonance parameters, since structural studies of reliable accuracy for amorphous alloys have for quite a while been available. In applying the EGL formulas for liquid transition metals and alloys, several authors<sup>(32,33,34)</sup> have used the phase shifts obtained by integrating the muffin-tin potentials derived from self-consistent band structure calculations. The Fermi energy has been calculated using the method given by Drierach et al<sup>(33)</sup>

$$E_F = E_0 + \frac{\hbar^2}{2m^*} K_F^2$$

where  $E_0$  is the bottom of the conduction band measured from the muffin tin zero. The Fermi wave number  $K_F$  is given by the free-electron formula

$$K_F = \left( \frac{3\pi z}{\Omega_0} \right)^{1/3}$$

where  $z$  is the valence of the liquid transition metal.

No  $\text{Pd}_{80}\text{P}_{20}$  or  $\text{Pt}_{75}\text{P}_{25}$  alloys have been obtained in the amorphous state, even though the  $a(k)$  for a similar system,  $\text{Pd}_{80}\text{Si}_{20}$ , may be used.<sup>(35)</sup> In the light of the strong similarities of the structural scattering of the amorphous alloys, this substitution is a good approximation. Using

the structural data  $a(k)$  and the density, a resistivity of  $150 \mu\Omega \text{ cm}$  for a  $\text{Pd}_{80}\text{P}_{20}$  alloy with  $E_F = 7.5 \text{ eV}$  and  $z = 0.50$  is found to correspond to  $\eta_2 = 3.02$ . These values are shown in Table 3, where other calculation results based on this  $\eta_2$  value are also shown. The choice of  $z = 0.50$  used here is consistent with the assumption of  $z = 0.36$  for Pd (the crystalline Pd value) and  $z = 1.00$  for the glass former. This is felt to be more suitable a value of  $z$  than the value of  $z = 1.3$  which is necessitated in Sinha's explanation of the high resistivity in these alloys as being due to the strong structural scattering ( $a(2K_F) = 2.2$ ). This large value of  $z$  requires that the glass former atoms exist in the amorphous alloys in highly ionized states, a requirement that makes the formation of a strong metal-metalloid bond and the stabilization of the amorphous phase highly unlikely. The calculated phase shift  $\eta_2 = 3.02$  can be compared with the values obtained by different authors for Pd metal: 3.06 from Kaga<sup>(36)</sup> and 2.80 from Evans et al.<sup>(37)</sup> Very recently Güntherodt and Ohtani<sup>(38)</sup> have measured the resistivity of liquid Pd and obtained  $\rho = 80 \mu\Omega \text{ cm}$ . Using  $\eta_2 = 3.02$  and the recent results of Waseda et al.<sup>(39)</sup> on the structure factor  $a(K)$  for  $z = 0.36$ , one obtains  $\rho = 95 \mu\Omega \text{ cm}$ , which is in reasonable agreement with the measured results. This agreement of  $\eta_2$  with the calculated values of  $\eta_2$  taken from muffin tin potentials used in actual band structure calculations on pure Pd metal should be understood as an indication that the EGL formalism for  $\rho$  gives reasonable phase shifts, an agreement which demonstrates the consistency of this approach when applied to calculating  $\rho$  for these amorphous alloys.

Table 3. THE CALCULATED RESISTIVITY FOR AN AMORPHOUS Pd<sub>80</sub>P<sub>20</sub> ALLOY

Z	$k_F(\text{\AA}^{-1})$	$a(2k_F)$	$\eta_2$	$E_F(\text{eV})$	$\rho(\mu\Omega \text{cm})$
0.36	.898	0.125	3.02	7.5	116
0.50	1.002	0.193	3.02	7.5	150
0.75	1.147	0.386	3.02	7.5	220
1.00	1.263	1.000	3.02	7.5	470

It is interesting to note that if this value of  $\eta_2 = 3.02$  is used to calculate the number of filled d-states below the energy  $E_F$ , using the formula  $z_d = (10/\pi)\eta_2$ , one obtains  $z_d = 9.6$ . Furthermore, according to Klein and Heeger,<sup>(40)</sup> the effective density of states at  $E_F$  can be obtained from the following formula:

$$N_d(E_F) = \frac{20}{\pi} \frac{\sin^2 \eta_2}{\Gamma}$$

For Pd the value  $\Gamma = 0.17$  eV is obtained by Kaga,<sup>(36)</sup> and this yields an effective density of states at the Fermi level of 0.55/eV-atom. This value of  $z_d$  is close to the 0.36 holes in the crystalline Pd d-band, while the density of states at  $E_F$  is significantly lower than the crystalline Pd value of  $2.2 \text{ eV}^{-1}$ .<sup>(41)</sup> This reduction of the effective density of states is in agreement with the present understanding of the band structure of fcc metals like Pd and Pt. In these metals the high density of states at  $E_F$  is due to a saddle point in the d-like part of the 5th band slightly below  $E_F$ ,<sup>(42)</sup> a property which is certainly not expected in the amorphous alloys. This reduced density of states is also consistent with the low value of the Pauli paramagnetism observed in the Pd-Cu-P, Pd-Ni-P and Pt-Ni-P alloys.

#### Concentration Dependence of $\rho$

The experimental results which must be explained are: the sensitivity of  $\rho$  in the  $(\text{Pd}_{100-x}\text{Cu}_x)_{80}\text{P}_{20}$  alloys, where a near doubling of  $\rho$  is observed for increasing  $x$  with  $10 \leq x \leq 50$ ; the insensitivity of  $\rho$  to changes in Ni concentration for both the  $(\text{Pd}_{100-x}\text{Ni}_x)_{80}\text{P}_{20}$  alloys,  $10 \leq x \leq 90$ , and the  $(\text{Pt}_{100-x}\text{Ni}_x)_{75}\text{P}_{25}$  alloys with  $20 \leq x \leq 50$ ; and the similar increase of  $\rho$  with phosphorus concentration in the  $(\text{Pd}_{65}\text{Cu}_{35})_{100-y}\text{P}_y$ ,  $15 \leq y \leq 24$  and the  $(\text{Pd}_{50}\text{Ni}_{50})_{100-y}\text{P}_y$ ,  $15 \leq y \leq 27.5$  alloys.

A proper explanation of the concentration dependence of  $\rho$  in these alloys necessitates a detailed understanding of the variation of the  $a(2K_F)$  factor with concentration as well as the effects of concentration on the resonance parameters  $E_0$ ,  $\Gamma$  and  $E_F$ . While the former can be given reasonable treatment, the latter requires considerable insight into the complexities of the formation of the transition metal-metalloid bonds. The concentration dependence of the Pd muffin-tin potential, the variation of the relative position of the d-band of states and the s-p conduction band are among other difficult problems. It is, however, possible to show, based on the assumption that the transition metal-glass former interactions fix the value of the  $\ell = 2$  phase shift  $\eta_2$ , that the variation of the  $a(2K_F)$  factor with concentration can explain the resistivity behavior of the  $(Pd_{100-x}Cu_x)_{80}P_{20}$ ,  $(Pd_{100-x}Ni_x)_{80}P_{20}$  and  $(Pt_{100-x}Ni_x)_{75}P_{25}$  alloys.

The results of the calculation of  $\rho$  for varying  $z$  with  $\eta_2 = 3.02$  are shown in Table 3. It is of interest to note that the variation of the Cu concentration  $x$  over  $10 \leq x \leq 50$  in the  $(Pd_{100-x}Cu_x)_{80}P_{20}$  alloys corresponds to variations of  $0.54 \leq z \leq 0.74$ , assuming  $z_{Pd} = 0.36$ ,  $z_{Cu} = 1.00$ ,  $z_P = 1.00$ . The increase of the calculated resistivity from  $144 \mu\Omega \text{ cm}$  to  $220 \mu\Omega \text{ cm}$  for  $z = 0.50$  and  $z = 0.75$  respectively is directly traceable to the doubling of the  $a(2K_F)$  factor (0.193 to 0.386). This behavior for the  $(Pd_{100-x}Cu_x)_{80}P_{20}$  alloys is in contrast to the  $(Pd_{100-x}Ni_x)_{80}P_{20}$  and  $(Pt_{100-x}Ni_x)_{75}P_{25}$  alloys, where there is little change in  $z$  due to the similarity of the  $z$  values for Pd, Ni and Pt (0.36, 0.46, 0.40, respectively). Thus the difference in the concentration dependence of the Pd-Cu-P alloys to changes in metal

concentration is due to the change in structural scattering through the increase of  $a(2K_F)$  as  $K_F$  is increased toward the first peak in the  $a(K)$  function.

The increase of  $\rho$  with phosphorus concentration in these alloys seems to indicate a marked sensitivity of the resonance parameters to the glass former concentration. This is due to the hybridization of the transition metal d states to form strong bonds with the glass former atoms. It is conceivable that the increase in the resistivity is then due to increase in the density of states at  $E_F$  as the transition metal d states tighten about  $E_d^{\text{hyb}}$ , the energy of the hybridized states, with increasing phosphorus concentration.

#### Temperature Dependence of $\rho$

Perhaps the most interesting aspect of this study is the observation that the negative temperature coefficients of resistivity in the amorphous Pd-Cu-P, Pd-Ni-P and Pt-Ni-P alloys is in accordance with the Mooij correlation found for concentrated substitutionally-disordered transition metal alloys as shown in Figs. 36 and 37. Metallic systems that exhibit a high resistivity and temperature independent resistivity are of great interest for producing high-quality resistors. The alloys NiCr, CuNi, FeCrAl and AgPd are examples of alloys for which low temperature coefficients of resistivity ( $\alpha < 100 \times 10^{-6} \text{ } ^\circ\text{K}^{-1}$ ) are observed for the concentrated alloys. Of note is the fact that the low  $\alpha$ 's are not observed in the pure metals but rather only in the concentrated alloys. Negative  $\alpha$ 's are observed in many alloys; in some cases over only temperature restricted ranges close to some magnetic or structural transition (like CuNi just above the ferromagnetic Curie point), in others (like TiV) the decrease of  $\rho$

with  $T$  is observed over large temperature ranges. The correlation between  $\alpha$  and the magnitude of the resistivity pointed out by Mooij (excluding the data on alloys where  $\alpha$  is affected by magnetic or structural transitions) for the crystalline alloys suggest that perhaps a common mechanism may be effective in assisting the conduction of electrons in these high scattering cases. An intuitive argument might lead one to conclude that since the mean free path should be limited to a distance on the order of the lattice spacing, when this condition is reached the temperature coefficient of resistivity should be zero; no further disorder could decrease the mean free path any more. The experimental facts are contrary to this point of view. In these transition metal alloys the calculated mean free paths are on the order of the interatomic distances and yet negative  $\alpha$ 's are the rule rather than the exception for  $\rho > 150 \mu\Omega \text{ cm}$ . So it has been suggested by Chen et al.<sup>(30)</sup> and Brouers and Brauwerts<sup>(31)</sup> that in these strong scattering cases the effect of thermal fluctuations is to assist the motion of these highly localized electrons, giving rise in certain circumstances to a decrease of the resistivity with temperature. Coles and Taylor<sup>(43)</sup> have suggested an alternative model, in that this effect might be due to the blurring of the Fermi level with temperature leading to a decrease in the effective density of states  $N_d(E) f(E)$ , where  $f(E)$  is the Fermi factor, which would yield a temperature modulation of the residual resistivity due to s-d scattering and therefore explain the negative temperature coefficients of resistivity in thin alloys. Seen in this perspective the explanations of the

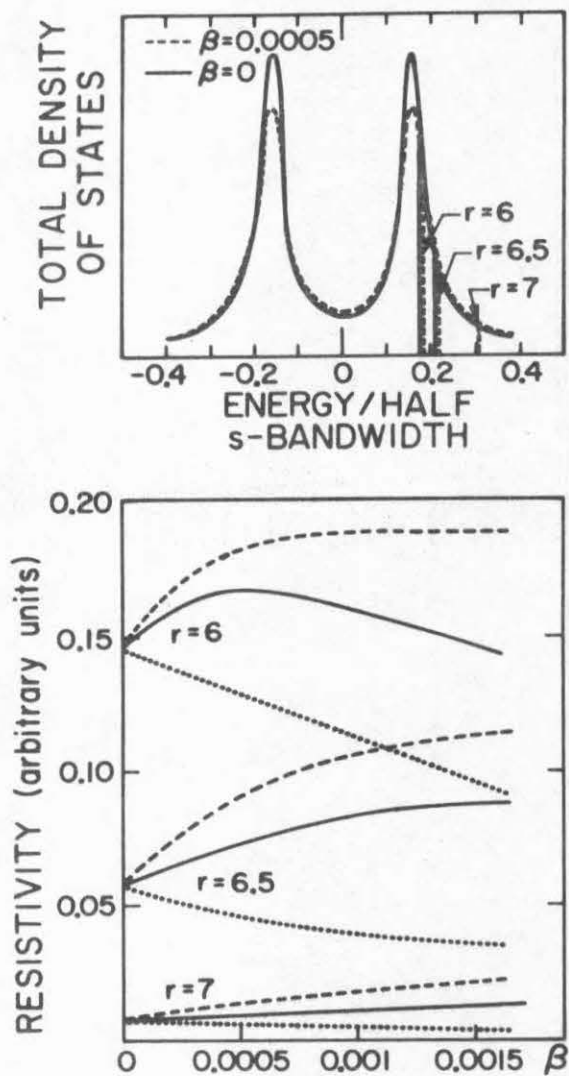


Fig. 39 Phonon induced modification of the density of states and the electrical resistivity. The dashed curve is for  $E_F$  fixed; dotted curve for  $E_F$  shifted to preserve occupancy; and solid curve for the total resistivity.

negative temperature coefficients of resistivity concentrate separately on the different factors in the effective density of states  $N_d(E) f(E)$ . Chen et al.<sup>(30)</sup> and Brouers and Brauwiers<sup>(31)</sup> show that the electron-phonon interaction can cause blurring of  $N_d(E)$  with temperature which is indeed significant; Coles and Taylor<sup>(43)</sup> among others<sup>(45)</sup> state that the blurring of the Fermi level with temperature accounts for the negative temperature coefficients.

While it is certainly true that the latter mechanism does hold, it is however difficult to conceive that such a mechanism should be effective in such a generally occurring phenomenon, since it is based on the fact that the density of states must vary considerably fast with respect to  $kT$  in each circumstance. On the contrary, the highly disordered nature of these alloys (structurally disordered too, since the amorphous alloys are in conformity with Mooij's correlation) suggest that the grosser effect--phonon modification of the density of states--is more effective in determining the temperature dependence of the resistivity.

The results of Brouers and Brauwiers<sup>(31)</sup> very recent calculations on the temperature dependence of the resistivity in concentrated disordered transition binary alloys are shown in Fig. 39. In the particular example shown the  $t_{2g}$  sub-band of a bcc alloy of 50-50 composition is simulated using the parameters shown. The combined effects on the resistivity of the blurring of the density of states by the electron-phonon interaction and the subsequent shift of  $E_F$  as a result of this blurring are clearly shown in Fig. 39. A direct comparison of these results with an experimental study requires

considerable information about the nature of the d states, the d-d interactions which are neglected here, and the s-d hybridization parameters. These results must then be understood as indications that such a general mechanism as the blurring of the density of states by electron-phonon interactions can be significant and may account for the Mooij correlation more satisfactorily than the simple blurring of  $E_F$  as proposed by Coles and Taylor and others. (44)

Considering the amorphous alloys in particular, it has been shown that the level of the resistivity can be explained by considering the interplay of structural scattering and resonance scattering according to the EGL formulation. The role of the glass former in determining the resonance scattering factor has been recognized as being quite significant due to the strong transition metal-glass former interactions which stabilize the amorphous structure. In these amorphous structures the glass former atoms are surrounded by metal atoms with no glass former nearest neighbors. The environment about a glass former atom may be thought of as being similar to a tetrakaidecahedron formed of a triangular prism with six metal atoms at the corners and three metal atoms situated above the rectangular faces of the prism in half-octahedral positions. The modification of this environmental arrangement by phonons which may compress or expand the metal-glass former distance must be given special theoretical emphasis to determine the effects of temperature on the resonance characteristics, and therefore the electrical resistivity.

#### IV MAGNETIC SUSCEPTIBILITY RESULTS AND DISCUSSION

The magnetic susceptibility of four alloys,  $(\text{Pd}_{80}\text{Cu}_{20})_{80}\text{P}_{20}$ ,  $(\text{Pd}_{50}\text{Cu}_{50})_{80}\text{P}_{20}$ ,  $(\text{Pd}_{65}\text{Cu}_{35})_{84}\text{P}_{16}$  and  $(\text{Pd}_{65}\text{Cu}_{35})_{78}\text{P}_{22}$ , was studied using the superconducting magnetometer described previously. In Fig. 40 and Fig. 41 the results are given for these alloys taken at  $H = 50 \text{ kG}$  and  $dH/dx = 1 \text{ kG/cm}$ . The weak susceptibility of these alloys presented several experimental difficulties which had to be overcome, the high field and high field gradient capability of this apparatus facilitating the meeting of these difficulties. A sample of  $\chi \approx 0.5 \times 10^{-7} \text{ emu/gm}$  of 250 mg exhibits a change in mass of 0.625 mg which is almost canceled by the diamagnetic signal from a quartz holder ( $\chi \approx 0.5 \times 10^{-6} \text{ emu/gm}$ ) of 30 mg. Under these circumstances accurate measurements of the sample susceptibility is very difficult. To avert these difficulties the quenched foils were carefully cut into 4 mm x 4 mm squares and a small hole was drilled in each foil. A pure Cu wire of .27 mm diameter was threaded through a stack of squares and looped, with the total mass of wire being less than 4 mg. Thus the sample holder correction was minimized ( $\chi_{\text{Cu}} = -0.8 \times 10^{-7} \text{ emu/gm}$ ) to less than 3% of the total signal.

The magnetic susceptibility of these materials may be considered to be the net result of a Pauli-like paramagnetic susceptibility which is dominant at temperatures above 100°K and a "Curie tail" due to the presence of impurities (presumably Fe). The measured susceptibility over 4 to 300°K is shown in Fig. 40 for the four alloys studied. To exhibit the weak temperature dependence of the Pauli paramagnetism as

measured, the susceptibility is plotted on an expanded scale in Fig. 41. From the low temperature portion of  $\chi(T)$  a concentration of 70 to 100 ppm Fe was deduced (using  $g = 2$  and  $s = 5/2$ ).

The level of the observed susceptibility of these alloys can be contrasted with the strong paramagnetism of crystalline Pd ( $\chi = 5.3 \times 10^{-6}$  emu/gm). To discuss this difference correctly, it is important to review the reasons for the large susceptibility of Pd. If the measured static susceptibility of Pd is compared with the value computed from the band structure density of states, according to

$$\chi = 2\mu_B^2 N(E)_{E=E_F}$$

with  $N(E_F) = 1.99/\text{eV}\cdot\text{atom}$ , the calculated value of  $\chi$  is found to be  $0.6 \times 10^{-6}$  emu/gm, which is considerably smaller than the measured susceptibility. It is believed that short-range, intra-atomic Coulomb interactions between the d electrons strongly enhance the susceptibility of Pd. Denoting the intra-atomic Coulomb interaction between two electrons in the same unit cell by  $U_0$ , the enhancement factor is

$$[1 - U_0 N_d(E_F)]^{-1}$$

If  $U_0 N_d(E_F) > 1$ , the system is unstable with respect to the ferromagnetic state. If  $N_d(E)$  is deduced from the specific heat data where the mass-renormalization effects are included,  $U_0 N_d(E_F)$  is found to be  $\approx 0.9$  for Pd. This situation is further complicated by the observation of Shimizu et al.<sup>(45)</sup> who showed that there exists in Ni, Pd and Pt additional paramagnetic components due to orbital paramagnetism and the spin-orbit paramagnetism which make significant contributions to the

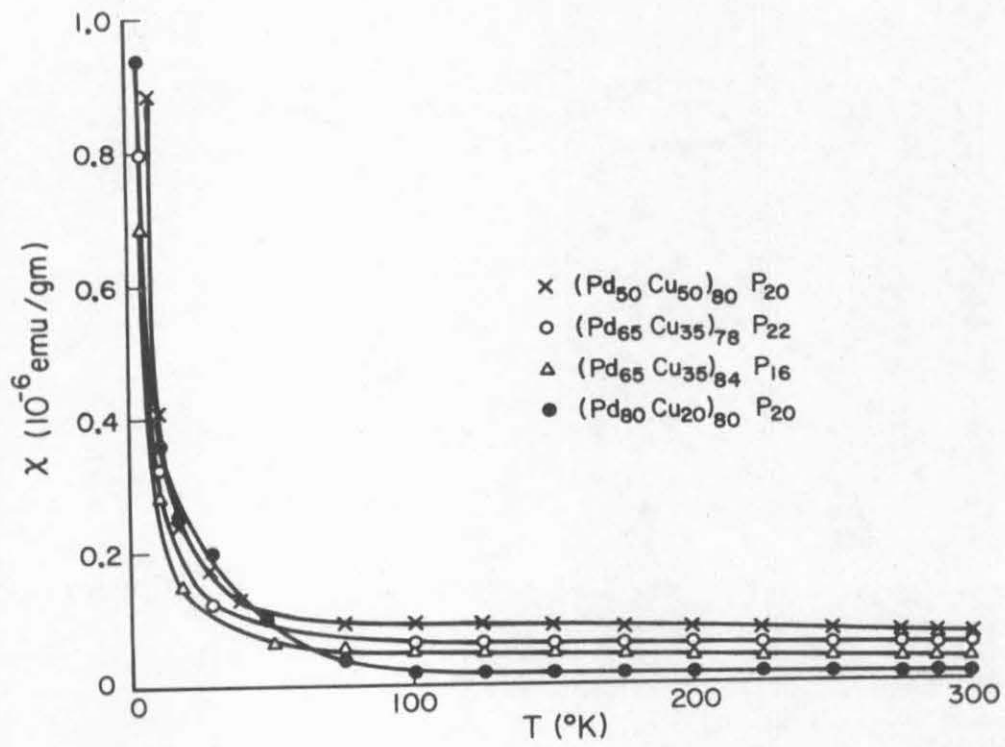


Fig. 40 Measured Magnetic Susceptibility of Pd-Cu-P Alloys

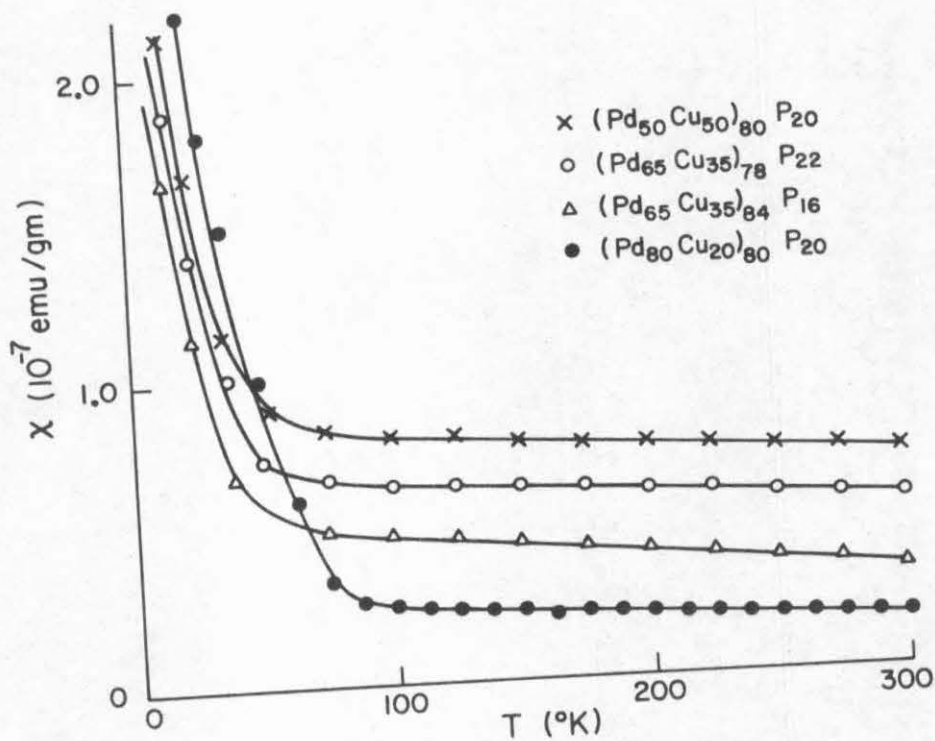


Fig. 41 Measured Magnetic Susceptibility of Pd-Cu-P Alloys on Expanded Scale

total susceptibility. Mori<sup>(46)</sup> has calculated the total susceptibility of these elements and shows in the case of Pd that the spin susceptibility and the orbital susceptibility are approximately equal, and the spin-orbit susceptibility makes up 20% of the total susceptibility.

It is important to note that the amorphous alloys Pd-Ni-P and Pt-Ni-P have magnetic susceptibilities estimated to be in the  $10^{-7}$ - $10^{-8}$  emu/gm range,<sup>(8,13)</sup> so it is not simply the addition of the noble metal Cu to the Pd matrix in Pd-Cu-P alloys which causes the reduced susceptibility. Perhaps the most relevant works on crystalline transition metal phosphides are those of Gambino et al.<sup>(47)</sup> and Albert et al.<sup>(48)</sup> on the Ni-P system. Gambino et al. studied the compound  $Ni_3P$  and found a Pauli-type paramagnetism with  $\chi = 8 \times 10^{-6}$  emu/gm. Albert et al. have investigated the disappearance of ferromagnetism in Ni-P alloys in the 0 to 14 atomic % range and concluded that the electron transfer model sufficiently explains the disappearance of ferromagnetism with the assumption of 0.5 holes in the Ni d-band and an effective transfer of up to 5 phosphorus valence electrons to the Ni d-band. Maitrepierre<sup>(13)</sup> has used this electron transfer model to explain the low value of the Pauli-type paramagnetism in amorphous Pd-Ni-P; here again two or more electrons must be transferred to the Pd d-states.

Clearly the validity of the use of electron transfer model for this circumstance rests on whether it is indeed true that no major change in the band structure occurs upon alloying with the glass former and the retention of a local ordering considerably different from the fcc environment of the pure transition element for both

situations of the  $\text{Ni}_3\text{P}$  crystalline compound and the amorphous Pd-Cu-P, Pd-Ni-P and Pt-Ni-P alloys. Furthermore, the large transfer of electrons from phosphorus to the transition metal d-states necessitates that the crystalline  $\text{Ni}_3\text{P}$  structure and the amorphous structure are stabilized by having the glass former atoms in highly ionized states. There are at present numerous indications that the rigid band model of the density of states is not valid from photo-emission studies on transition metal-nonmetal systems,<sup>(49)</sup> magnetic studies on amorphous transition metal-noble metal systems,<sup>(50)</sup> as well as theoretical studies on the band structure of these systems<sup>(51,52)</sup>. With respect to the large electron transfer from phosphorus to the transition metal, the electronegativities of Ni, Pd, and Pt are 1.8, 2.2, and 2.2, respectively, while that of P is 2.1. For transition metal-metalloid alloys when the metalloids are boron, carbon or nitrogen and the ratio of the radius of the metalloid to the transition metal is less than about 0.6, interstitial structures occur in which the metal atoms form a close-packed cubic or hexagonal array. When it is greater (when Si or P are the metalloids, for instance) much more complex structures occur in which there is evidence of directed chemical bonds.<sup>(53)</sup> This rule is probably due to the fact that when the metalloids are small enough the transition metal band structure still obtains, but when they are larger so that the transition metals are too far separated, it breaks down and structures with directed bonds from the metalloids occur. The metal-metal distances for the  $\text{Pd}_3\text{P}$  and  $\text{Ni}_3\text{P}$  compounds are in excess of the fcc metal-metal distance

by 7% and 17% respectively, and for the "amorphous"  $\text{Pd}_4\text{P}$  and  $\text{Ni}_4\text{P}$  alloys<sup>(13)</sup> these are in excess by 9% and 14% respectively. These indications make the use of the electron transfer model for explaining the reduced susceptibility in the Pd-Ni-P, Pt-Ni-P and Pd-Cu-P amorphous alloys difficult to justify.

Instead the effects of the complex process of the formation of strong covalent bonds between transition metal elements and the metalloids on the exchange enhancement as well as the orbital and spin-orbit contributions must be investigated. The extreme difficulties of this approach preclude, at the present time, any detailed presentation along these lines.

## V. SUMMARY AND CONCLUSIONS

The electrical resistivity and magnetic susceptibility of Pd-Cu-P amorphous alloys obtained by the rapid quenching technique have been measured. The observed resistivity behavior is found to be similar to the Pd-Ni-P and Pt-Ni-P systems in that  $\rho$  decreases linearly with increasing temperature from 120°K to 550°K ( $T_g$ ), while at lower temperatures  $\rho$  decreases as  $T^2$  with increasing temperature. The proposed explanations for this behavior, the structural scattering model of Sinha and the spin fluctuation scattering model of Hasegawa, have been re-examined in the light of these results and found to be unsatisfactory for a number of reasons. An alternate explanation of the level of resistivity, the concentration dependence of resistivity, and the observed negative temperature coefficients of resistivity has been given. The approach is based on the Evans, Greenwood and Lloyd formulation for the electrical resistivity of liquid transition metals and alloys and the phonon induced modification of the density of states in transition metal alloys. The weak Pauli paramagnetism observed for the Pd-Cu-P system is interpreted as being due to the effects of covalent bond formation in these amorphous systems and not to a large transfer of electrons from the metalloid to the transition metal d-band.

REFERENCES

1. P. Duwez and S. Lin, J. Appl. Phys. 38, 4096 (1967).
2. W. L. Johnson, S. J. Poon and P. Duwez, Phys. Rev. B 11, 150 (1975).
3. J. J. Gilman, Physics Today 28, 46 (1975).
4. W. Klement, Jr., R. Willens and P. Duwez, Nature 187, 869 (1960).
5. P. Duwez and R. H. Willens, Trans. AIME (Met), 227,326 (1962);  
P. Pietrokowsky, Rev. Sci. Instr. 34, 445 (1962).
6. D. Harbur, J. Anderson and W. Maraman, Rapid Quenching Drop Smasher, Los Alamos Scientific Laboratory of the University of California, Report No. LA-3584 (1966).
7. W. Y-K. Chen, Ph.D. thesis, California Institute of Technology (1975).
8. A. K. Sinha, Phys. Rev. B 1, 4541 (1970).
9. R. Hasegawa, Phys. Lett. 38, 5 (1972).
10. N. C. Halder, D. M. North and C.N.J. Wagner, Phys. Rev. 177, 47 (1969).
11. B. F. Wingfield and J. E. Enderby, Phys. Lett. 27A, 704 (1968).
12. B. Y. Boucher, J. Non-Crystalline Solids 7, 113 (1972).
13. P. L. Maitrepierre, J. Appl. Phys. 41, 498 (1970).
14. P. Lederer and D. L. Mills, Phys. Rev. 165, 837 (1968).
15. A. B. Kaiser and Doniach, Int. J. Magn. 1, 11 (1970).
16. E. C. Stoner, Proc. Roy. Soc. A 154, 656 (1936).
17. A. I. Schindler and M. J. Rice, Phys. Rev. 164, 759 (1967).
18. A. D. Caplin and C. Rizzuto, Phys. Rev. Lett. 21, 746 (1968).
19. J. Friedel, J. Phys. Chem. Solids 1, 175 (1956).
20. P. W. Anderson, Phys. Rev. 109, 1492 (1958); *ibid* 164, 352 (1967).

21. R. W. Houghton, M. P. Sarachik and J. S. Kouvel, Phys. Rev. Lett. 25, 238 (1970).
22. H. M. Ahmad and D. Greig, Phys. Rev. Lett. 32, 833 (1974)
23. J. H. Mooij, Phys. Stat. Sol.(a) 17, 521 (1973).
24. F. R. Brotzen, E. L. Harmon, Jr. and A. R. Troiano, J. Metals 7, 413 (1955).
25. R. G. Loasby, Proc. Phys. Soc. 72, 425 (1958).
26. C. A. Steidel, J. Vac. Sci. Technol. 6, 694 (1969).
27. D. Gerstenberg and C. J. Calbick, J. Appl. Phys. 35, 402 (1964).
28. J. H. Mooij and M. de Jong, J. Vac. Sci. Technol. 9, 446 (1972).
29. J. M. Ziman, Electrons and Phonons, Clarendon Press, Oxford, 1960.
30. A. B. Chen, G. Weisz, A. Sher, Phys. Rev. B 5, 2897 (1972).
31. F. Brouers and M. Brauwers, J. de Physique Lett. 36, L-17 (1975).
32. R. Evans, D. A. Greenwood and P. Lloyd, Phys. Lett. A 35, 57 (1971).
33. O. Drierach, R. Evans, H. J. Gündtherodt and H. U. Kunzi, J. Phys. F: Metals Phys. 2, 709 (1972).
34. J. S. Brown, J. Phys. F: Metal Phys. 3, 1003 (1972).
35. R. C. Crewdson, Ph.D. thesis, California Institute of Technology (1966).
36. H. Kaga, Phys. Lett. 37A, 373 (1971).
37. R. Evans, G. D. Gaspari and B. L. Gyorffy, J. Phys. F: Metals Phys. 3, 39 (1973).
38. H. J. Güntherodt, E. Hauser, H. U. Kunzi, R. Müller, Phys. Lett. 54A, 291 (1975).
39. Y. Waseda and M. Ohtani, Z. Physik B 21, 229 (1975).
40. A. P. Klein and T. J. Heeger, Phys. Rev. 144, 458 (1966).

41. F. M. Mueller, A. J. Freeman, J. O. Dimmock and A. M. Furdyna, Phys. Rev. B 1, 4617 (1970).
42. F. M. Mueller, Phys. Rev. 153, 659 (1967).
43. B. R. Coles and J. C. Taylor, Proc. Roy Soc. A 267, 139 (1962).
44. N. F. Mott, Phil. Mag. 26, 1249 (1972).
45. M. Shimizu, A. Katzuki and K. Ohmari, J. Phys. Soc. Japan 21, 1922 (1966).
46. N. Mori, J. Phys. Soc. Japan 20, 1383 (1965).
47. R. J. Gambino, T. R. McGuire and Y. Nakamura, J. Appl. Phys. 38, 1253 (1967).
48. P. A. Albert, Z. Kovac, H. R. Lilienthal, T. R. McGuire and Y. Nakamura, J. Appl. Phys. 38, 1258 (1967).
49. D. H. Seib and W. E. Spicer, Phys. Rev. Lett. 20, 1441 (1968).
50. J. J. Hauser, to be published in Physical Review (1975).
51. N. D. Lang and H. Ehrenreich, Phys. Rev. 168, 605 (1968).
52. A. C. Switendick, Solid State Commun. 8, 1463 (1970).
53. W. B. Pearson, in Treatise on Solid State Chemistry (N. B. Hannay, ed.), Plenum Press, New York (1973), p. 115.